DECREASING THE ALKYL BRANCH FREQUENCY IN PRECISION POLYETHYLENE

By

BORA INCI

A DISSERTATION PRESENTED TO THE GRADUATE SCHOOL
OF THE UNIVERSITY OF FLORIDA IN PARTIAL FULFILLMENT
OF THE REQUIREMENTS FOR THE DEGREE OF
DOCTOR OF PHILOSOPHY

UNIVERSITY OF FLORIDA

2011

To my parents

ACKNOWLEDGMENTS

I would like to acknowledge my advisor, Professor Kenneth Wagener, for all the guidance and friendship over these many years. His door was always open and whenever I talked with him, I always felt encouraged, with my motivation to work hard revitalized. He has given me a wealth of advice and guidance for things both inside and outside the laboratory. I have never seen him angry, as he always deals with situations in a calm manner. He is a true role model for any graduate student`s professional career. I will forever be thankful for his presence in my life.

I would like to thank Professor Fabio Zuluaga for his endless help and guidance especially during my first summer in Gainesville. I had great fun working, drinking, playing soccer, talking politics and singing Venceremos with him. I should also thank to him and Marialena Zuluaga for taking care of me during my visit to Cali, Colombia.

I want to thank my committee members (Professors John Reynolds, Ronald Castellano, Tony Brennan and Benjamin Smith) for their time, effort and advice. Furthermore, I want to thank Dr. Kathryn Williams for her helpful discussions and for editing my manuscripts.

The stay at Florida would not be complete without thanking and acknowledging former and present Wagener group members who made the graduate school a pleasure. I would like to thank Dr. Giovanni Rojas, Dr. Erik Berda, Dr. Yuying Wei and especially Dr. James Leonard for their endless help during my first year in the lab. I would like to thank Brian Aitken and Sam Popwell for their friendship and nice discussions during the last four years. Special thanks to Paula Delgado for her endless help and great friendship. Without her, I could not be able to finish my manuscripts and dissertation. Special thanks to Michael Schulz for reading my dissertation. I would like to

thank Ashlyn Dennis for making delicious peach cobbler for me. I want to thank Pascale Attallah and Chip Few for being a great friend. It was a lot of fun sharing my hood with Chip. I would like to thank former undergraduate student Adam Garland for his help and friendship. Further, I would like to thank Luke Fischer, Chet Simocco, Donovan Thompson, Nicolas Sauty, Thomas Young and Sotaro Inomata for their friendship.

I was very lucky for having opportunity to work in Butler Polymer Research Laboratory. I would like to thank Dr. and Mrs. Butler for their support to polymer research. Special thanks to Mrs. Sara Klossner, and Mrs. Gena Borrero for their endless help. I think this laboratory is a great place to do research and have fun at the same time. I would like to thank Dr. Dan Patel for his invaluable help, guidance and friendship. I had a lot of fun working and discussing science with him. I should thank Dr. Jiango Mei for his guidance and advices. He was extremely helpful during my stay in Gainesville. I would like to thank Laura Moody, Coralie Richard, Stefan Ellinger, Mike Craig, Romain Stalder, Dr. David Liu, Frank Arroyave and Egle Puodziukynaite for their help and friendship. I would like to thank Alexander Pemba for his endless help and great friendship.

As part of my graduate study, I spent three months in Max Planck Institute for Polymer Research at Mainz, Germany. I would like to thank International Max Planck Research School for Polymer Materials for financial support of this trip. Special thanks to Dr. Ingo Lieberwirth for his endless help and guidance in TEM analysis during my stay in Mainz. I would like to thank Prof. Dr. Katharina Landfester for making this research experience possible. I also want to thank Dr. Markus Mezger, Dr. Werner Steffen and Michael Bach for their help in WAXS measurements. I would like to thank

Dr. Robert Graf for his help in solid state NMR measurements. Special thanks to Sandra Seywald for her help with GPC measurements. I would like to thank Dr. Robert Haschick and Dr. Katja Niles for taking care of me during my stay in Mainz and for their friendship. I also would like to thank Samet Varol for his great friendship and help in Mainz, Germany.

Finally, I would like to thank all former and present members of “Isotopes” soccer team for making the life in Florida enjoyable.

TABLE OF CONTENTS

page

LIST OF TABLES

LIST OF FIGURES

Figure page

LIST OF ABBREVIATIONS

ADMET	Acyclic diene metathesis
CCD	Charged Coupled Device
DSC	Differential scanning calorimetry
DART	Direct Analysis in Real Time
GIF	Gatan Imaging Filter
GPC	Gel permeation chromatography
HDPE	High density polyethylene
HRMS	High Resolution Mass Spectrometry
NMR	Nuclear magnetic resonance
IR	Infrared spectroscopy
LCB	Long chain branching
LDPE	Low density polyethylene
LLDPE	Linear low density polyethylene
RID	Refractive Index Detector
SCB	Short chain branching
TEM	Transmission electron microscopy
TREF	Temperature rising elution fractionation
UHMWPE	Ultra high molecular weight polyethylene
VLDPE	Very low density polyethylene
WAXD	Wide angle X-ray diffraction

Abstract of Dissertation Presented to the Graduate School
of the University of Florida in Partial Fulfillment of the
Requirements for the Degree of Doctor of Philosophy

DECREASING THE ALKYL BRANCH FREQUENCY IN PRECISION POLYETHYLENE

By

Bora Inci

December 2011

Chair: Kenneth B. Wagener
Major: Chemistry

Metathesis polycondensation chemistry has been employed to control the crystalline morphology of Linear Low Density Polyethylene (LLDPE) by precisely introducing the alkyl branches along the polymer backbone. These polymers, while structurally akin to copolymers made via chain copolymerization of ethylene and vinyl comonomers, have unique properties, because use of symmetrical α, ω diene monomers ensures precise spacing of the chain branches. An important limitation in this work was the synthesis of the symmetrical diene monomers required in this chemistry. Spacing in the symmetrical monomer directly determines the precision run lengths in the polymer: Prior monomer synthetic schemes have limited the maximum run lengths between branch points along the polymer to 20 methylene carbons (ie, a branch placed on each and every 21st carbon).

The present work describes the systematic increase of precision run lengths to 38 and 74 methylene carbons. Successful preparation of symmetrical α,ω-dienes for both run lengths is presented. For the case of 38 run lengths, the synthesis and characterization of precisely sequenced polyethylenes containing thirteen different branches allowed systematic examination of the effect of branching on polyethylene

properties. A clear change in morphology is observed for these polymers from a situation where the methyl branch is included in the polymer's unit cell, to one where branches of greater mass are excluded from the unit cell. The precision LLDPE model polymers were characterized with Differential Scanning Calorimetry (DSC), Infrared Spectroscopy, Solid State Nuclear Magnetic Resonance Spectroscopy, Wide Angle X-ray Scattering (WAXS) and Transmission Electron Microscopy (TEM).

Precision polymer with butyl branches on every 75^{th} carbon was successfully prepared, and X-ray investigation of this polymer displayed an orthorhombic unit cell structure with the absence of metastable phase formation. Increasing the distance between the two consecutive branches from 38 carbons (5.26 mole% branch concentration) to 74 carbons (2.70 mole% branch concentration) fully expels the butyl branches from the crystal lattice to the amorphous phase. This precision polymer with butyl branches on every 75^{th} carbon represents the first realistic model of commercial LLDPE reported so far in precision polyolefin research.

CHAPTER 1
INTRODUCTION

Since it was first produced in large scale in 1936, industrial polyethylene has been the most manufactured polymer worldwide. Depending on the synthetic methodology and polymer processing, polyethylene can be classified as various types, such as high density polyethylene (HDPE), low density polyethylene (LDPE), linear low density polyethylene (LLDPE), ultra high molecular polyethylene (UHMPE), etc. Each type exhibits distinct macroscopic properties, and consequently has found various broad applications based on performance. To understand the structure-property-performance relationships of these materials, precision polyolefins are used as model structures for commercial polyethylenes. In precision polyethylene, the branch identity and branch frequency can be precisely controlled, while in commercial polyethylene, there are many variables, including the branch size, branch spacer, and branch distribution. By limiting the freedom of the system, a better understanding of branching in PE can be achieved.

An important limitation in this research relates to the concentration of incorporated branches in the final material. So far, the developed monomer synthetic schemes provide the maximum run lengths between branch points along the polymer to 20 methylene carbons, which corresponds to 10 mole% of comonomer incorporation. This document describes the systematic decrease of the comonomer incorporation below 10 mole%.

This dissertation is organized as follows: In Chapter 2, polyethylene and crystallization phenomena are briefly reviewed. The historical significance of polyethylene and different polyethylene structures are discussed. Chain folding as well as commonly observed unit cell structures are also discussed.

Chapter 3 describes different branch structures in chain polymerized polyethylene and introduces the precision polyethylene structures. Limitations in monomer synthesis are discussed.

In Chapter 4, increasing the branch run length in monomer synthesis is described. Successful preparation of precise polyethylenes possessing alkyl branches on every 39^{th} carbon is presented. Various alkyl branches ranging from methyl to pentadecyl are incorporated in the polymer backbone. Primary structure delineation of these polymers is discussed.

In Chapter 5, morphological characterization of precise polymers is presented. Differential scanning calorimetry (DSC), wide angle X-ray scattering (WAXS), transmission electron microscopy (TEM) and solid state nuclear magnetic resonance spectroscopy (ssNMR) investigation results are presented.

In Chapter 6, systematic increase of alkyl branch run length in precision polyethylene to yield precision polymer possessing butyl branches at every 75^{th} carbon is presented. Primary structure characterization and morphological examination of this polymer is also described.

Chapter 7 presents a summary of the dissertation and suggestions for future work.

CHAPTER 2
POLYETHYLENE AND CRYSTALLIZATION PHENOMENA

2.1 Historic Importance of Polyethylene

The term “polyethylene” was first mentioned during the Chemical Society meeting on April 27, 1863 by M. P. E. Berthelot[1]. Incidental synthesis of polyethylene from decomposition of diazomethane was reported by von Pechman[2] in 1898 and shortly thereafter by Bamberger and Tschirner[3]. They described the unexpected product as “a white flocculant material” and were disappointed about this product because it was not what they had expected to find in their experiments. In a 1930 paper[4], Friedrich and Marvel reported formation of the “non-gaseous product” during the investigation of the reaction between alkali metal alkyls and quaternary arsonium compounds. The rapid polymerization reaction was attributed to the presence of alkyl lithium species in the reaction flask and the significance of “non-gaseous product” was not realized. In the early 1930s, W. H. Carothers from Du Pont De Nemours Chemical Company was interested in the preparation of “giant individuals” by employing the Wurtz reaction with alkyl dibromides[5]. He was able to isolate various long hydrocarbons, such as *n*-eicosane, *n*-triacontane, *n*-tetracontane, *n*-pentacontane, *n*-hexacontane and *n*-heptacontane, by fractional distillation and crystallization.

Imperial Chemical Industries in the early 1930s initiated a research program to investigate the high pressure reactivity of selected organic compounds. The existence of polyethylene was recognized for the first time in 1933 by R. Gibbon and E. Fawcett. They correctly identified the recovered white waxy solid from the reaction of ethylene and benzaldehyde, but the reaction was not reproducible. In December 1935, M. Perrin optimized the polymerization conditions to consistently produce polyethylene and this

procedure was patented in 1936[6]. The success in reproducible polymer synthesis came from the trace amount of oxygen contamination that leads to the formation of free radicals to initiate the polymerization. The first set of experimental conditions gave highly ductile material having a melting point of about 110^{o}C in a gram scale. This material is now known as low density polyethylene and was utilized in insulation applications for submarine communication cables and telecommunication cables linking France and England during World War II. The superior advantages of polyethylene over the conventional insulators were recognized by Union Carbide and du Pont, and both companies obtained licenses from Imperial Chemical Industries to produce polyethylene in the United States.

The war-related demand for polyethylene diminished in the years following World War II, and companies in the United States and Britain shifted their focus to consumer development. In the United States, the use of polyethylene was expanded into the packaging industry, while in Britain applications for molded items attracted more interest. Despite the desirable properties and various applications of polyethylene available after World War II, a number of characteristics limited its general usage, such as its low tensile strength, flexibility and its low softening temperature. In addition to its material properties, the extremely harsh polymerization conditions (1000 to 2000 atm, 200 ^{o}C) required for its the commercial production also hindered the further exploitation of polyethylene.

2.2 Discovery of High Density Polyethylene

Investigation of new catalyst systems to polymerize ethylene under milder temperature and pressure conditions was an emerging field after the World War II. The most noticeable achievement in catalyst research was made by the German chemist

Karl Ziegler, who was heading a research group at the Max Planck Institute for Coal Research at Mulheim/Ruhr. As a pure synthetic chemist, Ziegler was interested in preparation and reactivity of metal alkyl compounds in his early career at the University of Heidelberg[7]. There, he observed the addition of butadiene and styrene to the alkali alkyls at room temperature[8-10]. Based on this observation, he proposed the “stepwise organometallic synthesis” of high molecular weight products. In 1943, Ziegler moved to the Max Planck Institute for Coal Research at Mulheim/Ruhr. He attempted to transfer his “stepwise organometallic synthesis” approach from butadiene to ethylene mainly because of the availability of ethylene in the Mulheim/Ruhr area from coke manufacture. However, unlike butadiene, the addition product of ethylene and Li alkyls readily decomposed to give lithium hydride and olefin without any molecular weight increase.

After a couple of years of preliminary research, the dimerized product (1-butene) was detected when ethylene addition to the recently discovered lithium aluminum hydride was examined[11-13]. Triethyl aluminum was identified as an intermediate for the ethylene addition, and E. Holzkamp, a graduate student in the Ziegler group, focused on the possible mechanisms of 1-butene formation[14]. The trace amount of nickel from the stainless steel reaction vessel was identified to be the reason for the observed chain termination giving 1-butene. The potential for ethylene polymerization was then realized, and different transition metals were investigated to control the chain termination. Chromium complexes were found to catalyze ethylene polymerization to yield a mixture of oligomers and high polymer. In 1953, H. Breil, another graduate student in the Ziegler group, employed a zirconium complex catalyst to form mainly high molecular weight polyethylene[15]. H. Martin, a senior staff member in the group, successfully polymerized

ethylene with a titanium complex at low pressure. This improvement made it possible to conduct the ethylene polymerization in a glass vessel[16].

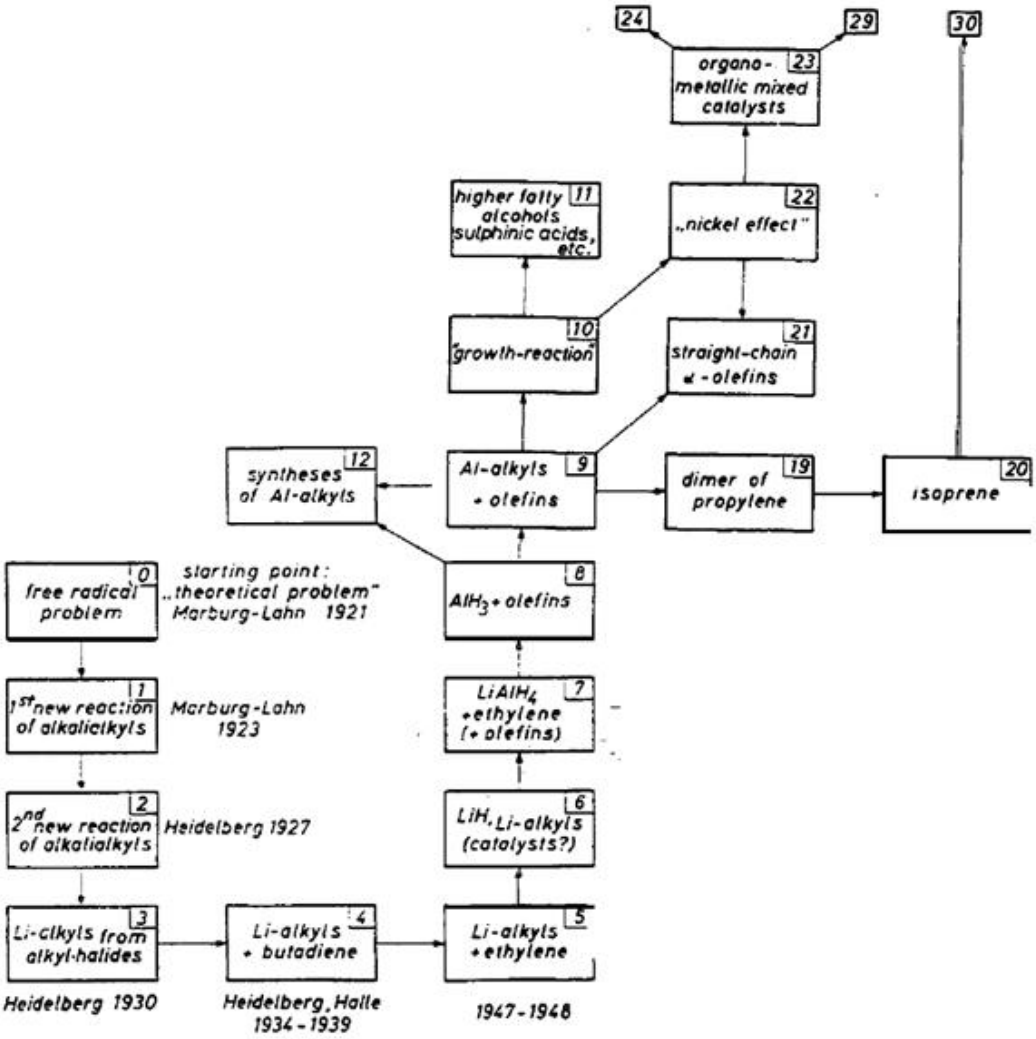

Figure 2-1. Timeline and the significant steps for the development of the “Mulheim” catalyst. Reproduced from Karl Ziegler Nobel Lecture, 1963. © The Nobel Foundation.

The development of the Mulheim catalyst, as Karl Ziegler describes, is illustrated in Figure 2-1. The new form of polyethylene made with this catalyst displayed superior properties, including higher melting point, better mechanical response and easier producibility at lower pressures. A variety of structures[17-25] have been proposed for the

active species of the Mulheim catalyst. The generally accepted mechanism for ethylene polymerization is depicted in Figure 2-2.

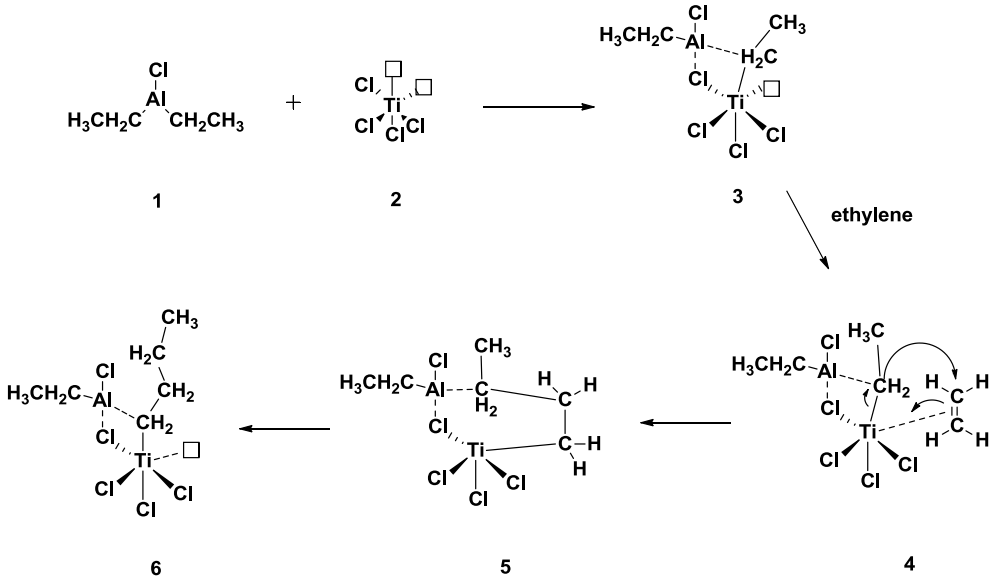

Figure 2-2. Mechanism for the Mulheim catalyst used in ethylene polymerization. Adapted from Arlman, E. J. et. al[18]

As shown in Figure 2-2, $TiCl_3$ is activated with alkyl aluminum to form complex **3**. The activated octahedral titanium complex on the surface of a $TiCl_3$ crystal has an unoccupied site where the ethylene insertion takes place. After the insertion, a new chemical bond forms between the inserted ethylene and the titanium coordinated alkyl. Reorganization of complex **5** generates the active species for the next ethylene insertion to yield linear polyethylene.

In 1953, K. Ziegler and coworkers began filing patents around the world including in Germany[26] and the US[27]. The improved properties and low production costs of this new polymer attracted considerable attention from several chemical companies around the world. In less than 10 years of its discovery, Mulheim catalyst was utilized in commercial production of high density polyethylene in Europe, the US, Russia and Japan, as shown in Figure 2-3.

Figure 2-3. Location of industrial applications of the Mulheim process in the world (as of 1963). Numbers indicate the number of chemical plants. Reproduced from Karl Ziegler Nobel Lecture, 1963. © The Nobel Foundation.

The significance of this discovery was recognized by the Nobel Prize Committee in 1963, when it awarded the Nobel Prize to Karl Ziegler for his work in the field of ethylene polymerization.

2.3 Towards More Specialized Polyethylene

The development of the Mulheim catalyst expanded the range of material properties of polyethylene, and it became the world's leading synthetic macromolecule. However, one of the shortcomings of this highly crystalline polymer was related to processing methodologies. High density polyethylene tends to shrink upon cooling, and uneven cooling conditions yield warped molded items. Research had been directed toward the suppression of crystallization by incorporating pendent side chains into the polymer backbone. Copolymerization of ethylene with various α-olefins was the prevailing methodology to modify polymer properties. This new class of polymers is now known as linear low density polyethylene (LLDPE) and was first commercialized in 1960 by Du Pont. The typical comonomers used for copolymerization are 1-butene, 1-hexene

and 1-octene to introduce ethyl, butyl and hexyl branches, respectively. The heterogeneous nature of the Mulheim catalyst generates nonuniform distribution of branches in linear low density polyethylenes. In addition to a broad composition distribution, molecular the weight distribution is also generally broad ($\overline{M}_w / \overline{M}_n \approx 3.5 - 4.5$).

A breakthrough observation by Kaminsky and Sinn had an enormous impact on the development of new polymerization catalysts and reactions[28,29]. They combined titanium and zirconium metallocenes with a hydrated form of trimethyl aluminum, methylaluminoxane (MAO), to afford an extremely active metallocene catalyst. The idea of converting cheap starting materials to specialized polymers led to an explosion of research into the development of metallocene catalysts involving numerous metals and ligands[30-33]. The homogeneous nature of these catalysts provides active polymerization sites for every molecule in solution and demonstrates very high activity. In some cases[34], there is a 100-fold activity enhancement compared to the heterogeneous Mulheim catalyst, resulting in the production of 300 metric tons of polyethylene per gram quantity of catalyst in one hour. In addition to high activity, metallocene catalysts can produce polyolefins with narrow molecular weight distributions ($\overline{M}_w / \overline{M}_n \approx 2.0$). For the case of LLDPEs, incorporation of α-olefins can be controlled to yield homogeneous distributions of pendent branches in the polyethylene backbone.

Homo and copolymerization of ethylene with late transition metals became an active field of research in the mid 1990s with a family of new cationic Pd(II) and Ni(II) α-diimine catalysts introduced by Maurice Brookhart and his coworkers at DuPont[35-45]. Late transition metal complexes are known to have lower olefin insertion rates

compared to early transition metal catalysts, and β-hydride elimination typically competes with chain growth yielding dimers and oligomers. Brookhart`s catalysts were designed to have highly electrophilic cationic metal centers resulting in rapid rates of olefin insertion. Moreover, sterically bulky α-diimine ligands favor insertion over chain transfer. Alterations of the ligand structure resulted in control of branching to obtain a variety of materials ranging from highly crystalline HDPE to hyperbranched oils from the same feedstock. Functional group tolerance is another important feature of these types of catalysts, where some of the late transition metals, especially cationic palladium α-diimine complexes, polymerize ethylene in the presence of ethers, organic esters and acids[46]. Brookhart and others employed this catalyst system for the copolymerization of ethylene and/or α-olefins with commercially important acrylates[37,40,47,48] and carboxylates[37,49] to yield high molecular weight and random copolymers. Aqueous emulsion and suspension polymerizations have also been developed[50-52] as a route to microspheres of polymer for adhesives, proving the possibility of insertion into the catalyst and chain growth in the presence of water.

2.4 Polyethylene Classifications

As mentioned above, many types of polyethylene exist. The versatility of polyethylene based materials arises mainly from branching, which can be directly related to the material behavior. Branches, like any other “defects” in the polymer, limit the packing ability of chains, and polyethylene samples that have few branches exhibit a higher degree of crystallinity than those that have many. Since the packing of crystalline regions is better than that of noncrystalline regions, the overall density of polyethylene will increase as the degree of crystallinity increases. The degree of branching varies the density and morphology of polyethylene from purely crystalline (1.00 g/cm^3) to totally

amorphous (0.850 g/cm^3). Based on its density and branching, polyethylene is traditionally classified into three categories: low density polyethylene (LDPE), high density polyethylene (HDPE), and linear low density polyethylene (LLDPE). Recent advances in the area of metallocene catalysts have expanded the nomenclature to include ultra-high molecular weight polyethylene (UHMWPE) and very low density polyethylene (VLDPE).

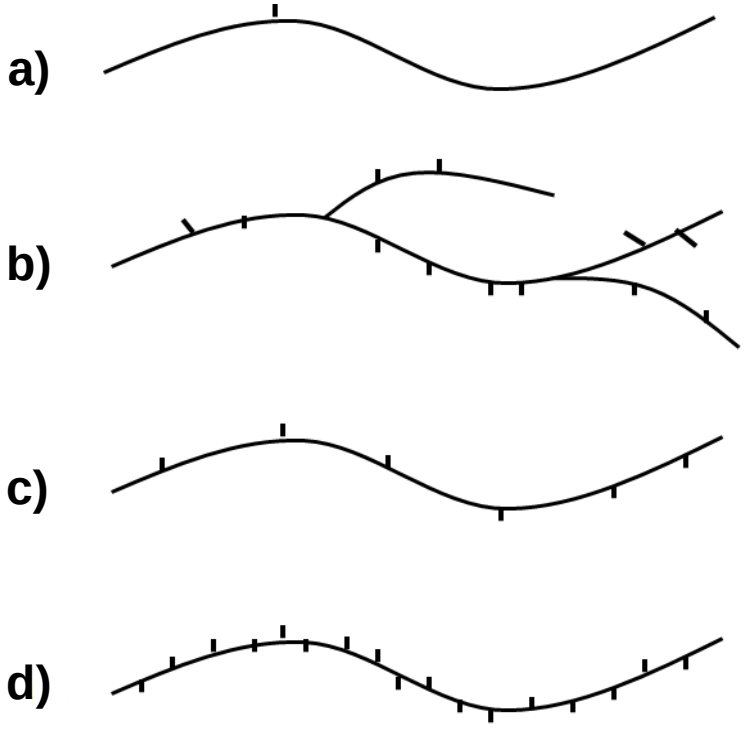

Figure 2-4. Types of polyethylenes: A) high density polyethylene, B) low density polyethylene, C) linear low density polyethylene, D) very low density polyethylene.

High density polyethylene (HDPE), as depicted in of Figure2-4A, has a typical density range of 0.94–0.97 g/cm^3. It exhibits an extremely low level of branches and high degree of crystallinity. Since HDPE has negligible branching in its backbone, the chemical structure of this polymer is the closest to pure polyethylene and is often

referred to as linear polyethylene. In most cases, HDPE shows 60-80% crystallinity and good mechanical strength (Table 2-1). HDPE is a stiff and opaque material and is used widely in grocery bags, pipes, bottles and toys, etc. Global HDPE demand was estimated at 32 million tons in 2009 and corresponds to 45 % of total polyethylene production[53]. Low density polyethylene (LDPE), or high pressure polyethylene, is named due to its relatively low density caused by substantial concentrations of branches. Formation of branches decreases the density of polyethylene to the range of 0.90–0.94 g/cm^3.

The most commonly observed branches are ethyl and butyl groups, as well as long chains. High pressure polymerization conditions and radical chemistry randomly distribute long chain and short chain branches along the backbone. As shown in Figure 2-4B, long chain branches can themselves be branched to give a soft and flexible material. It displays lower melting transition than HPDE and is mostly used in the packaging industry. The number of LDPE production sites decreases annually, mainly because of the high production costs. Global LDPE demand was estimated at 18 million tons in 2009 and corresponds to 27 % of total polyethylene production[53].

Linear low density polyethylene (LLDPE) is a linear version of polyethylene possessing short alkyl chains at random intervals, shown in Figure 2-4C. This type of polymer is produced by the copolymerization of ethylene and α-olefins. The most common monomers used for copolymerization are 1-butene, 1-hexene and 1-octene to give ethyl, butyl and hexyl branches, respectively. LLDPE resins may also contain small levels of long chain branches. Metallocene catalysts are most commonly used to produce LLDPE, yielding narrower molecular weight distributions compared to HDPE

and LDPE. Linear low density polyethylene is predominantly used in the packaging industry, due to its good mechanical properties and relative transparency. Global LLDPE demand was estimated at 19 million tons in 2009, exceeding the use of LDPE and corresponding to 28% of total polyethylene production[53].

Table 2-1. General properties for various commercial polyethylenes

Property	HDPE	LDPE	LLDPE	VLDPE
Density (g/cm^3)	0.94-0.97	0.91-0.94	0.90-0.94	0.86-0.90
Crystallinity (% from density)	62-82	42-62	34-62	4-34
Crystallinity (% form calorimetry)	55-77	30-54	22-55	0-22
Tensile modulus (kpsi)	155-200	25-50	38-130	<38
Tensile strength (kpsi)	3.2-4.5	1.2-4.5	1.9-4.5	2.5-4.5
Melting temperature (^{0}C)	125-132	98-115	100-125	60-90
Industrial production	low pressure Ziegler	high pressure radical	metallocene Ziegler	metallocene
Number of branches per 1000 carbons	5-7	20-30	10-25	numerous

Data adapted from *Handbook of polyethylene: structures, properties and applications*[2].

Very low density polyethylene (VLDPE) is a specialized form of linear low density polyethylene having a much higher concentration of short chain branches, as illustrated in Figure 2-4D. This level of branching suppresses crystalline structure to yield materials with very low crystallinity. In some extreme cases, totally amorphous materials can also be obtained (Table 2-1). Similar to linear low density polyethylene, VLDPE is also produced by a metallocene catalyst. These specialty polymers are mainly utilized in tubing, food containers and packaging applications.

Ultra high molecular weight polyethylene (UHMWPE) is a special type of high density polyethylene with extremely long chains. Typical molecular weights are in the order of millions, usually between 2 and 6 million. UHMWPE fibers, commercialized in the late 1970s by DSM, are widely used in defense applications, ballistics protection and hip replacement.

2.5 Polyethylene Morphology

2.5.1 Chain Folding and Lamella Formation

The term “morphology” is used to define the structural organization of polymer chains in the solid or molten state. Solid polyethylene exhibits a three-phase morphology, as illustrated schematically in Figure 2-5.

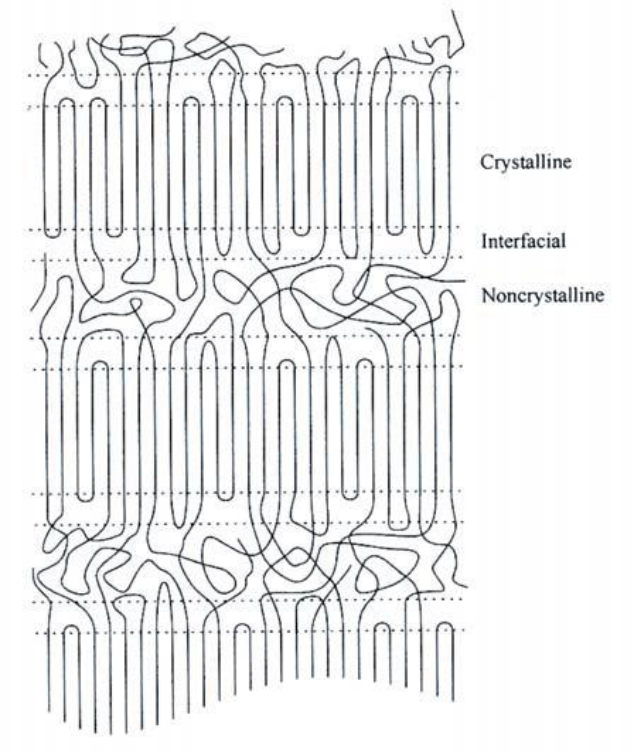

Figure 2-5. Schematic representation of three-phase morphology.

In this typical semi-crystalline morphological model, ordered polyethylene chains (crystalline phase) are surrounded by a disordered, noncrystalline phase. The boundary between these two phases is composed of a partially ordered interfacial layer.

The nature of the crystalline phase was clarified by the discovery of chain folding and lamellae in 1957, independently by Till[54], Fischer[55] and Keller[56,57]. Thickness measurements on polymer single crystals grown from dilute solution revealed the existence of chain folding and ruled out the previously accepted[58-60] fringed-micelle

model. The typical single crystal thicknesses (10-12 nm) reported by Keller and others is much smaller than the length of a polymer chain (100 nm).

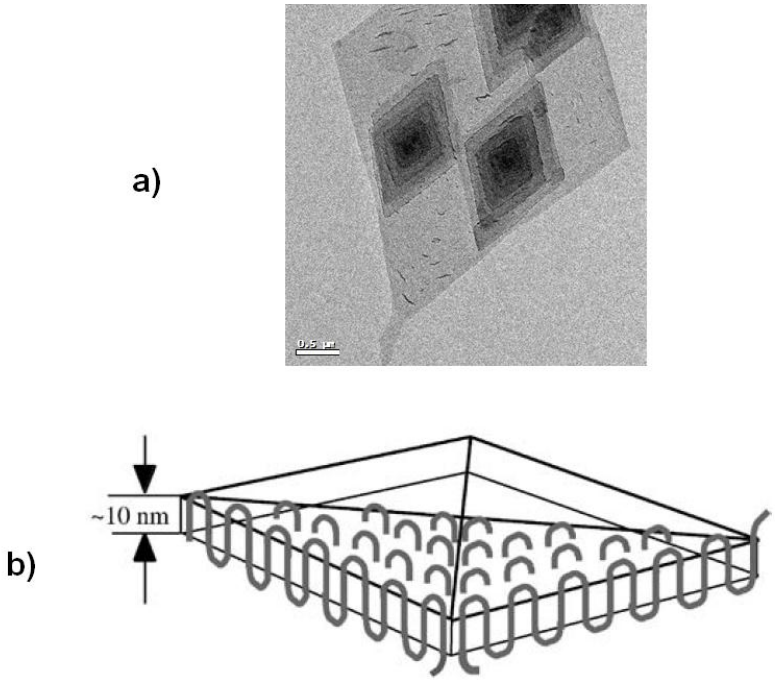

Figure 2-6. A) Transmission electron microscopy bright field image of HDPE single crystal grown from 0.03 % C_2Cl_4 solution, B) Schematic drawing of polyethylene single crystal with regular chain folding[61].

The strong evidence for chain folding and lamella formation was the birth of the modern crystalline polymer morphology. The transmission electron microscopy (TEM) image of an HDPE single crystal grown from dilute tetrachloroethylene solution is illustrated in Figure 2-6A. The single crystal observed in this TEM image is schematically reproduced in Figure 2-6B to better show the lamella formation and chain folding.

Sufficiently long monodisperse *n*-alkanes showing chain folding were independently synthesized by Whiting[62] and Wegner[63]. Long *n*-alkanes ranging from $C_{102}H_{206}$ to $C_{390}H_{782}$ were prepared, and crystals from both solution and the melt were

systematically analyzed. While *n*-alkane $C_{102}H_{206}$ could only be obtained in chain-extended form, chain folding was found in all *n*-alkanes longer than $C_{150}H_{302}$ and many orders of small angle X-ray diffractions were observed due to the high regularity of lamella stacking[64]. Preparation of sufficiently long *n*-alkanes allowed the first accurate calculation of lamella spacing.

2.5.2 Unit Cell Structure

The crystal structure of a polymer is built up from many periodic repeating entities called unit cells, each having representative information about the structure. A specific unit cell can be described by lengths (a, b, c) and angles (α, β, ɣ) parameters as illustrated in Figure 2-7A.

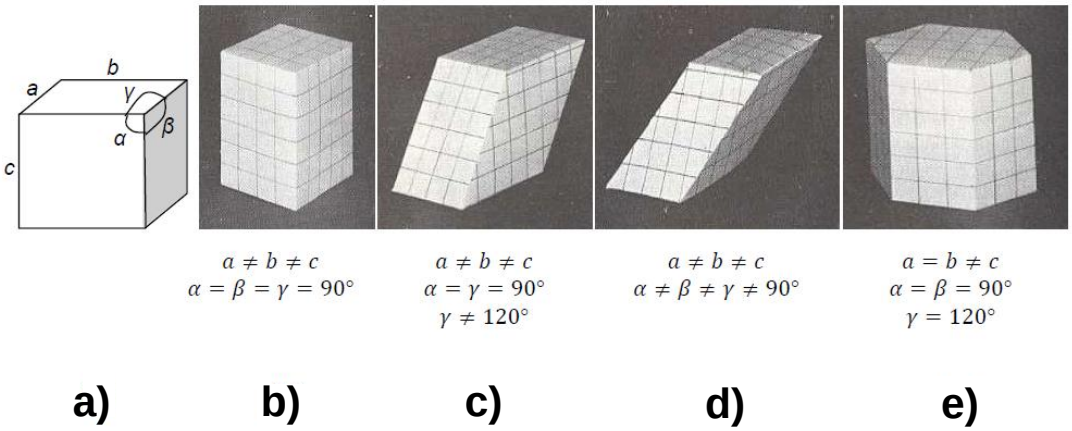

Figure 2-7. The observed unit cell structures in *n*-alkanes and polyethylene: A) schematic representation of a typical unit cell, B) orthorhombic unit cell, C) monoclinic unit cell, D) triclinic unit cell, E) hexagonal unit cell (Figure adapted from ref. 2)

Crystal structure and unit cell analysis of *n*-alkanes and polyethylene started with the development of X-ray crystallography in the early 20th century. The first crystallographic investigation of long hydrocarbons (in this case $C_{29}H_{60}$) was performed by Muller[65] in 1928. Methylene units in $C_{29}H_{60}$ form a zig-zag pattern (all-*trans* configuration) and the C-C bond length is found to be 1.52 Å. Crystalline *n*-alkanes have

been examined for decades and their properties were extrapolated to represent the crystalline phase of polyethylene. The crystal structure[66-68], crystal growth and morphology[69,70], melting temperature[71,72] and chain mobility[73-75] of *n*-alkanes have been evaluated and extensively reviewed[76,77].

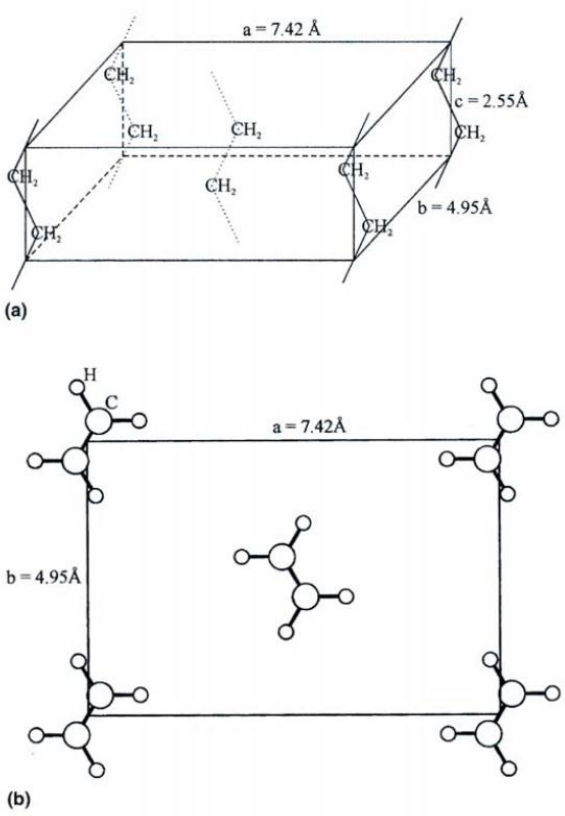

Figure 2-8. Polyethylene orthorhombic unit cell with *Pnam*-D_{2h} space group. A) orthogonal view, B) view along the c axis (Figure adapted from ref. 2).

A complete unit cell and space group determination study for the long paraffin $C_{60}H_{122}$ was first reported in 1939 by Bunn[78]. The orthorhombic unit cell with the space group *Pnam*-D_{2h} contains 4 CH_2 groups, and the all-*trans* chains are parallel as shown in Figure 2-8. The same crystal structure is also observed[79] for HDPE with the unit cell parameters: a=7.4069 Å, b=4.9491 Å and c=2.5511 Å, giving a crystal density of 0.996 g/cm^{-3}.

The dimensions of the orthorhombic unit cell are not constant. Due to the effect of branching, LDPE and LLDPE exhibit larger a and b axis dimensions than HDPE. The introduction of branches into polyethylene backbone not only affects the unit cell dimensions, but also generates metastable crystal forms. The commonly observed metastable phases are shown in Figure 2-9. According to Seto[81] et al., the dimensions of the monoclinic unit cell of linear polyethylene are found to be a=8.09 Å, b=2.53 Å and c=4.79 Å, giving a crystal density of 0.998 g/cm^{-3}. A monoclinic crystal form was also observed for ethylene/α-olefin copolymers in the absence of mechanical stress[82].

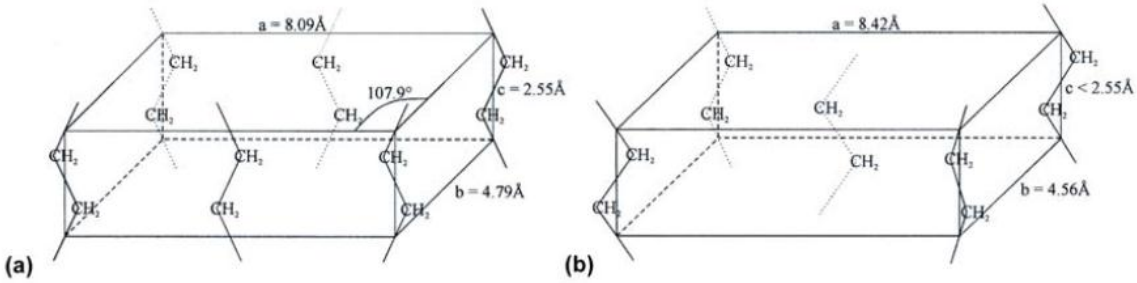

Figure 2-9. Metastable polyethylene unit cells. A) Monoclinic unit cell and B) Hexagonal unit cell (Figure adapted from ref. 2).

The hexagonal form of polyethylene, shown in Figure 2-9B, is generated under high temperature and pressure conditions and was first observed by Bassett[83] et al. The hexagonal phase has very special translational chain mobility characteristics which allow polyethylene to be easily processed under these conditions. Ethylene/1-propene copolymers having propylene content higher than 20 mol % exhibit a hexagonal crystal structure at room temperature and under normal pressure conditions[84]. It is important to note that the metastable unit cells shown in Figure 2-9 both feature a higher distance between neighboring chains (extended a axis) compared to an orthorhombic unit cell.

CHAPTER 3
ALKYL BRANCHED PRECISION POLYETYLENE[1]

3.1 Branching in Polyethylenes

The presence of branching in polyethylene has significant effects on material properties, such as density, degree of crystallinity, mechanical strength and processability[2]. Predictable alterations on the performance of polyethylene can be achieved by controlling the amount and the distribution of branching on the polyethylene backbone. Depending on the mode of polymerization, catalyst type, pressure and temperature, the nature of the branch varies and is classified as short chain branching (SCB) or long chain branching (LCB).

3.1.1 Short Chain Branching

Regardless of the conditions, short chain branching (SCB) inevitably forms during the chain growth polymerization of polyethylene. Intramolecular chain transfer of the reactive center results in SCB for radical and metal mediated polymerizations[85]. The generally accepted mechanism for the formation of various SCBs in LDPE is illustrated in Figure 3-1. Propagating radical species **3-1** abstracts hydrogens from the fifth, sixth and seventh methylene groups to yield *n*-butyl, *n*-pentyl and *n*-hexyl branches, respectively. *n*-Butyl branches are more abundant than others due to the formation of a six-membered transition state (five carbons and the hydrogen being abstracted) during the hydrogen abstraction[86]. Reactive radical species **3-2** can take up another available ethylene monomer to give species **3-5**, which can either propagate linearly to form an *n*-butyl branch or abstract another intramolecular hydrogen through different pathways to

[1] Part of this chapter is adapted with permission from (Rojas, G.; Inci, B.; Wei, Y.; Wagener, K. B. *Journal of American Chemical Society*, **2009**, 131, 17376). Copyright (2009) American Chemical Society.

yield 2-ethylhexyl and 1,3-diethyl branches. Short chain branches in LDPE have significant effects on chain packing where the maximum crystallinity of 60-70% can be achieved by free radical polymerization of ethylene.

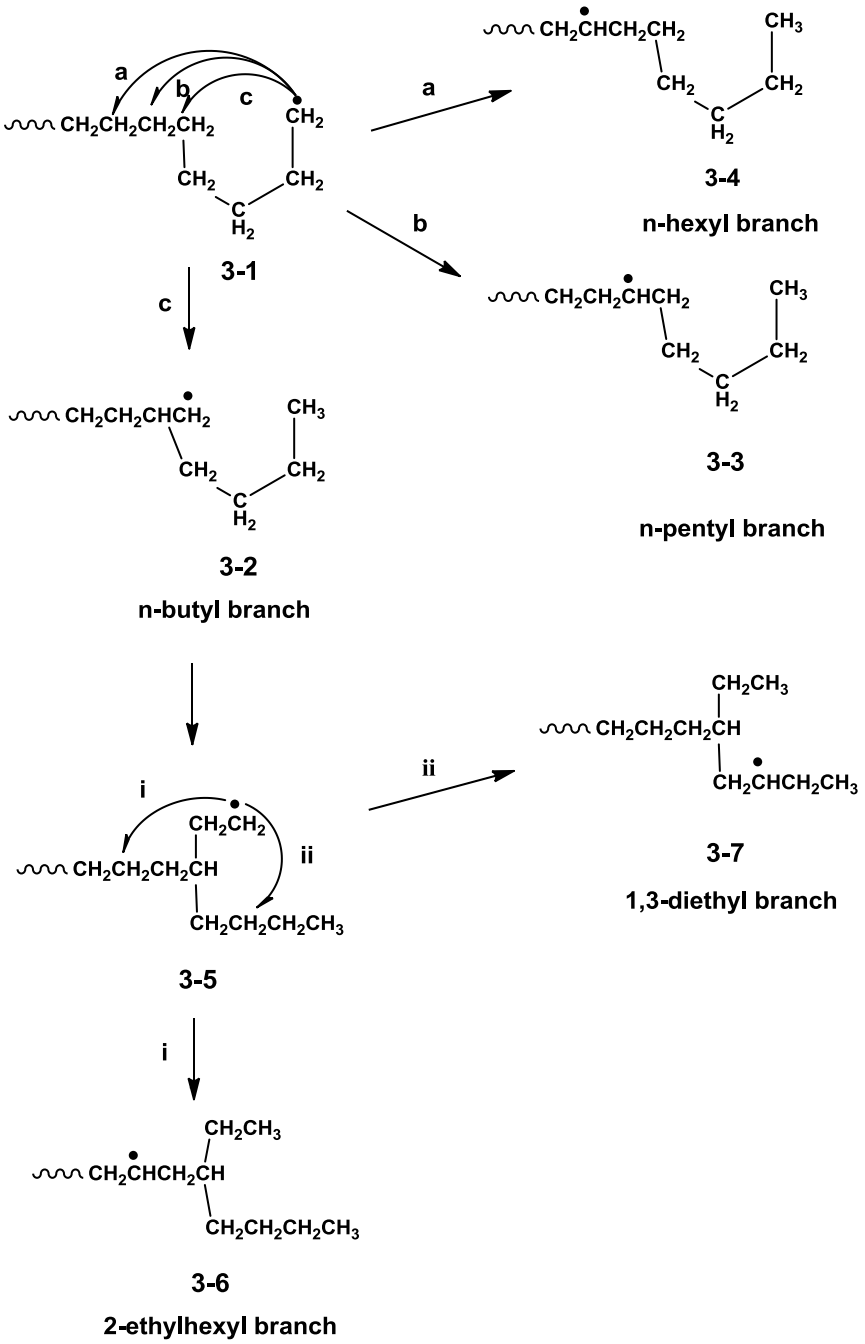

Figure 3-1. Generally accepted mechanism for the formation of n-butyl, n-pentyl, n-hexyl, 1,3-diethyl and 2-ethylhexyl branches in LDPE (Figure adapted from ref. 86).

Small concentrations of the undesired SCB can also be observed in HDPE prepared by Ziegler and metallocene chemistry. For example, ethyl branches up to 2 mol% are reported in the polymerization of ethylene by metallocene catalysts[87]. The situation is somewhat different for late transition metal mediated ethylene polymerization. Compared to early transition metal based catalyst (e.g. Ziegler and metallocene), late transition metal catalysis exhibit reduced activities for olefin insertion and β-hydride elimination, which typically compete with chain growth[44].

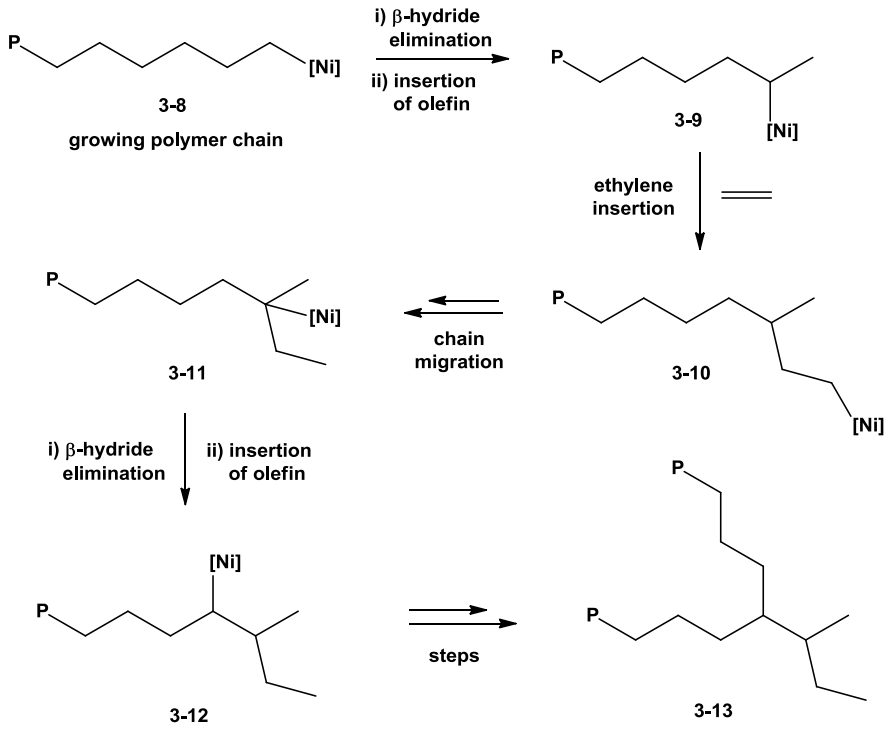

Figure 3-2. Suggested mechanism for *sec*-butyl branch formation[44].

For example, elucidation of highly branched nickel catalyzed polyethylene with ^{13}C NMR techniques revealed the formation of methyl, ethyl, *n*-butyl, *n*-pentyl, *n*-hexyl and *sec*-butyl branches in the polymer backbone[88].

The existence of short chain branching is not always an undesired phenomenon. For the case of linear low density polyethylene, SCBs are intentionally incorporated along the polyethylene chain to tune the properties. LLDPE resins exhibit high film tear strength, relatively high clarity and ease of processability. Because of these attractive properties, LLDPE films are extensively used in the packaging industry. Commercial LLDPE is prepared by chain-growth polymerization using Mulheim or metallocene chemistry[2], although recently late transition metal mediated copolymerization is also becoming more popular[35,36]. The absence of multisite initiation in single-site metallocene and late transition metal systems results in the synthesis of copolymers possessing narrower molecular weight distributions and higher levels of α-olefin comonomer incorporation[33,34,44].

3.1.2 Long Chain Branching

The presence of long chain branching (LCB) in LDPE has been known for decades[89-92]. Intermolecular chain transfer of a radical propagating center results in formation of LCBs, which significantly affect the rheological behavior of LDPE and improve its processability[93-95]. Even though most of the properties of LDPE are generally inferior to those of LLDPE, the former still has a large market share due to its greater processability. The term “long” describes a branch longer than ~70 methylene units, corresponding to the critical entanglement molecular weight of polyethylene (i.e ~1000 g/mol)[96].

The concept of long chain branching was revisited in the 1990s for its possible application in the field of metallocene polyethylene. Metallocene catalysts generate polymers of narrow molecular weight distribution with superior thermal and mechanical properties[31]. However, these polymers suffer from poor processability (e.g., high

susceptibility to melt fracture), mostly due to the narrow molecular weight distribution. Recent advances in catalyst technology have resulted in metallocene polymers containing small amounts of LCB to ease the processability, while still maintaining superior properties[97,98]. The constrained geometry catalyst developed at Dow Chemical was the first single site catalyst discovered to generate long chain branched polyethylene[99,100]. The LCB is believed to be incorporated into the polymer backbone via the insertion of vinyl terminated macromonomers into the catalyst[31].

3.1.3 Quantification of Branching in Polyethylene

By their nature, both radical and metal mediated chain propagation chemistries generate branches through uncontrolled intramolecular and intermolecular chain transfer. Inevitable chain transfer and chain walking processes produce alkyl branches of varying lengths randomly spaced along the polyethylene backbone[101]. Several methods have been developed to identify the branches and quantify their distribution in the main chain[102-106]. Gel permeation chromatography (GPC), nuclear magnetic resonance spectroscopy (NMR), light scattering and rheological measurements are frequently used to elucidate branching. GPC is ineffective in measuring low levels of branching, and rheological examination only provides indirect evidence for branching. NMR can quantify only linear branches from methyl to pentyl, as it cannot effectively distinguish short chain and long chain branches once the branch length exceeds six carbon atoms in length[107].

For the case of LLDPE, quantification of branches becomes even more challenging. In addition to intentionally incorporated branches from copolymerization with α-olefins, undesired branching also occurs, resulting in more complex systems. Analytical and preparative scale Temperature Rising Elution Fractionation (TREF) was

developed to prepare components with narrower distributions of molecular weight and branching[108-110]. TREF is a technique that fractionates polymer chains based on their individual crystallinity. Since branching directly affects the crystallinity of polyethylene, TREF can fractionate LLDPE chains based on branch concentration[111].

3.2 Structure of Precision Branched Polyethylene

As described in the previous section, conventional ethylene polymerization methodologies generate branches of varying lengths randomly spaced along the polyethylene backbone. The uncontrolled nature of branching in these polymer systems prevents the comprehensive primary structure delineation and possible tertiary structure correlations.

Recently, precise polyethylene structures were introduced to better understand the influence of branching on macroscopic properties[112-120]. A representative structure of these polymers is illustrated in Figure 3-3, where the identity of the branch and its position along the polyethylene chain is known without equivocation.

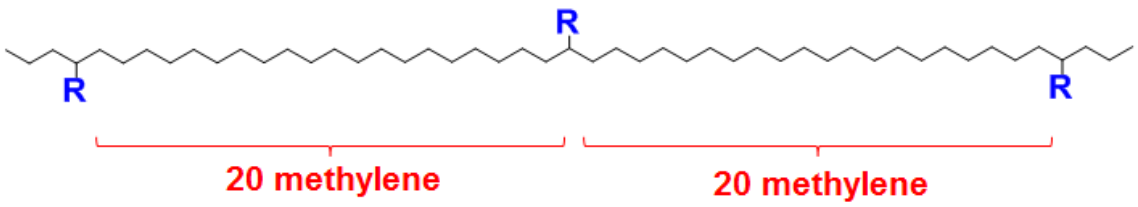

Figure 3-3. General chemical structure of precision polyethylene. Branches with known identity are incorporated regularly (in this case 20 methylene units between branches) along the polyethylene backbone.

Acyclic Diene Metathesis (ADMET) Polymerization is employed to generate these precisely branched polyethylenes[121,122]. A wide variety of branches such as, alkyl[112-114,116-120], halide[123-128], acid[129-133], siloxane[134-137] and biologically active[138-144] groups can

be precisely incorporated into the polyethylene backbone with this mild polymerization chemistry.

3.3 Synthesis and Properties of Precision Branched Polyethylenes

The historic background and utility of ADMET has recently been reviewed in detail[145-147]. Thus, only its application in the field of precision alkyl branched polyethylene will be discussed herein. The general synthetic scheme for this chemistry is illustrated in Figure 3-4. Symmetrical α,ω-diene monomers are condensed into unsaturated polymers which upon hydrogenation generate what we call “precision branched polyethylene”.

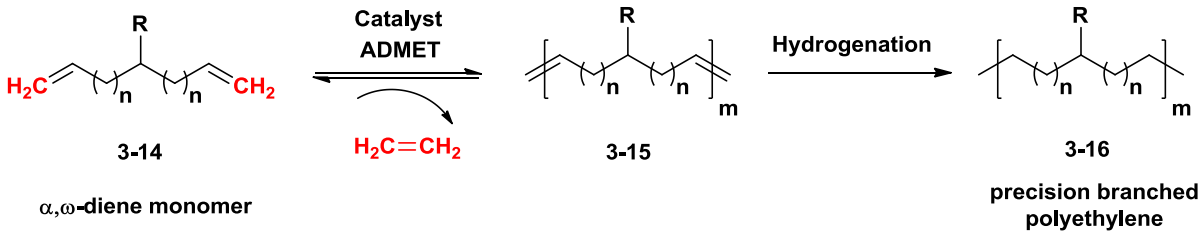

Figure 3-4. General two-step synthetic scheme for the preparation of precision branched polyethylene.

Typical polymerizations are performed in bulk, and ethylene is removed under vacuum to yield high conversion, which is necessary for any step growth polymerization. Monomers are required to be highly pure (>99%) and only one mechanism (metathesis) should be operating during the polymerization to ensure the precise placement of branches. Well defined metathesis catalysts are utilized to fulfill these requirements. As shown in Figure 3-4, monomer synthesis is the key in this research, because the branch identity and the distance between the branches are set in this step. Several synthetic

routes have been developed to incorporate alkyl branches with various lengths along the precision branched polyethylene.

3.3.1 Methyl Branch

Symmetrical α,ω-diene monomers possessing methyl branches were first prepared by alkylating ethyl acetoacetate[112-114] with alkenyl bromide to give compound **3-18**. As illustrated in Figure 3-5, retro-Claisen condensation yields deacylated product, compound **3-19**, which is subsequently reduced to a primary alcohol. Compound **3-20** is tosylated, and subsequent hydride displacement generates monomer **3-22**. Depending on the run length, the overall yield varies in the range of 25-30%.

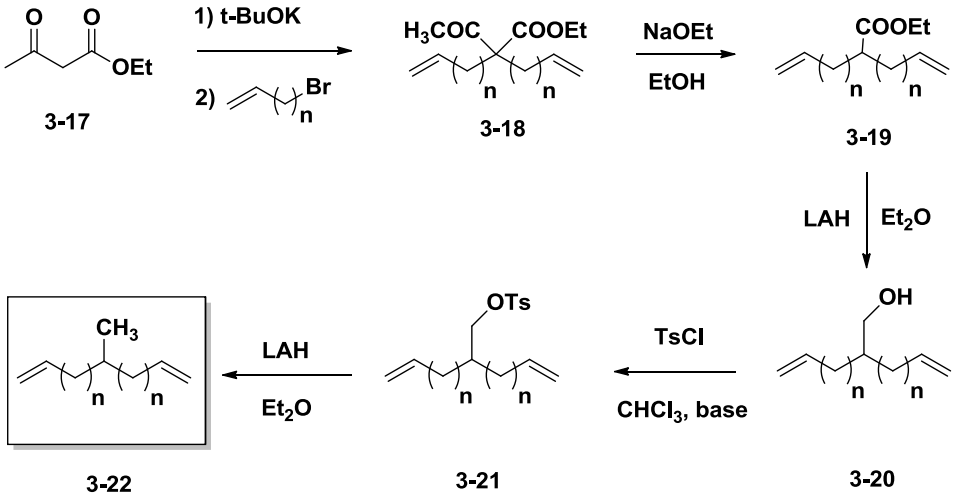

Figure 3-5. Synthesis of methyl branched monomers[112-114].

Alkenyl bromides of different sizes are utilized in the alkylation step to give methyl branches on every 9th, 11th, 15th, 19th and 21st carbons in the polyethylene backbone. Synthesis of the more frequent methyl branch placement in the polymer chain was also attempted with shorter alkenyl bromide run lengths. Although the monomers were successfully prepared, high molecular weight polymers could not be isolated due to cyclization. An alternative synthetic route was utilized to generate polymers with methyl

branches on every 5th and 7th carbons[117]. This synthetic approach is depicted in Figure 3-6 where diethyl malonate chemistry is applied for the preparation of both monomers **3-30** and **3-33**.

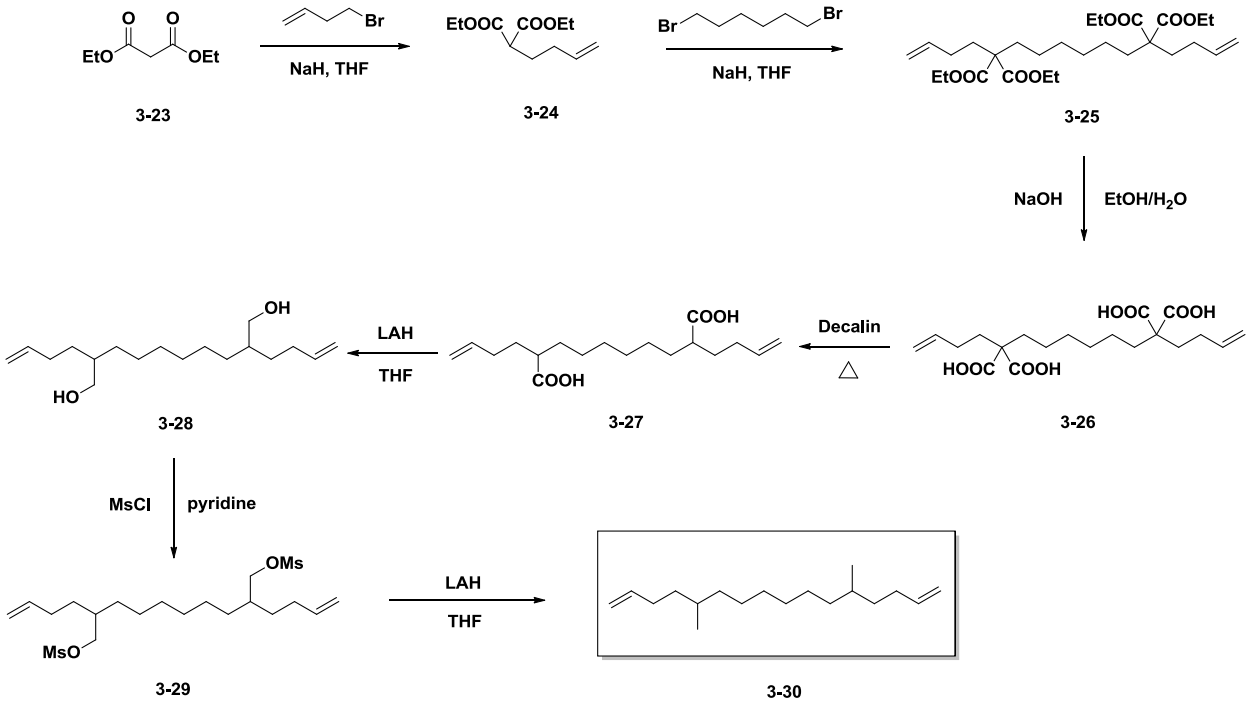

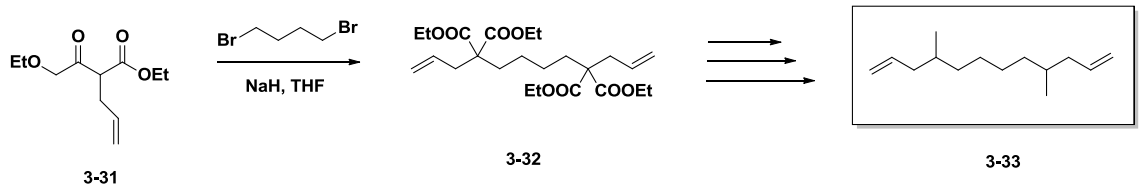

Figure 3-6. Synthesis of methyl branched monomers with short ethylene run length[117].

In this scheme, dialkylation of either 1,6-dibromohexane or 1,4-dibromobutane with diethyl alkenyl malonate generates a tetraester diene, which is then converted to the tetraacid diene after saponification and decarboxylation. Reduction to a diol and subsequent mesylation and reductive cleavage with hydride gives the desired

monomers **3-30** and **3-33**. Polymerization and hydrogenation of these monomers yield polyethylenes possessing a methyl branch on every 7th and 5th carbons.

Thermal and molecular weight data for the series of polyethylenes having methyl branches with various run lengths are presented in Table 3-1. In contrast to chain polymerized ethylene/propylene copolymers[108], precise polymers exhibit sharp and well defined thermal transitions as a result of control of branch identity and placement.

Table 3-1. Effect of precise methyl branch placement on thermal properties

Methyl branch on every *n*th carbon	1-propene comonomer content (mole%)	T_m(^{o}C) (peak)	ΔH_m(J/g)	$\overline{M}_n$ (kg/mol)
no branch	0	134	204	25.8
21	10.0	62	103	20.2
19	11.1	57	96	72.0
15	14.3	39	82	17.1
11	20.0	11	66	8.50
9	25.0	-14	28	17.5
7	33.3	-60	19	12.9
5	50.0	amorphous	--	28.4

It is also interesting to compare the thermal behavior of these precise polymers with unbranched polyethylene prepared with ADMET polymerization of 1,9-decadiene. ADMET polyethylene compares well with chain polymerized commercial polyethylene. (Both preparations melt at 134^{o}C and form orthorhombic unit cells.) Introduction of methyl groups onto the polyethylene backbone disrupts the crystallinity. As the concentration of methyl branches increases, both the melting point and heat of fusion gradually decrease, and amorphous polymer forms when the methyl branches are placed six carbons apart in the polymer backbone. As shown in Table 3-1, preparation of model polymers with this precision approach gives the opportunity to tune the melting point of polyethylene over a range of 200^{o}C.

Symmetrical α,ω-diene monomers are also copolymerized with 1,9-decadiene to produce a series of polymers whose thermal behavior and spectroscopic features begin to mirror those of commercial linear low density polyethylene (LLDPE). In addition to intentionally introduced SCBs with ethylene copolymerization of α-olefins, commercial LLDPEs possess undesired branches which prevent the primary structure elucidation. The situation is quite different in irregularly spaced methyl branched ADMET polymers. Copolymerization of α,ω-diene monomers with 1,9-decadiene yields polymers having only methyl branches and their concentration can be systematically be varied by the changing feed ratio of the monomers.

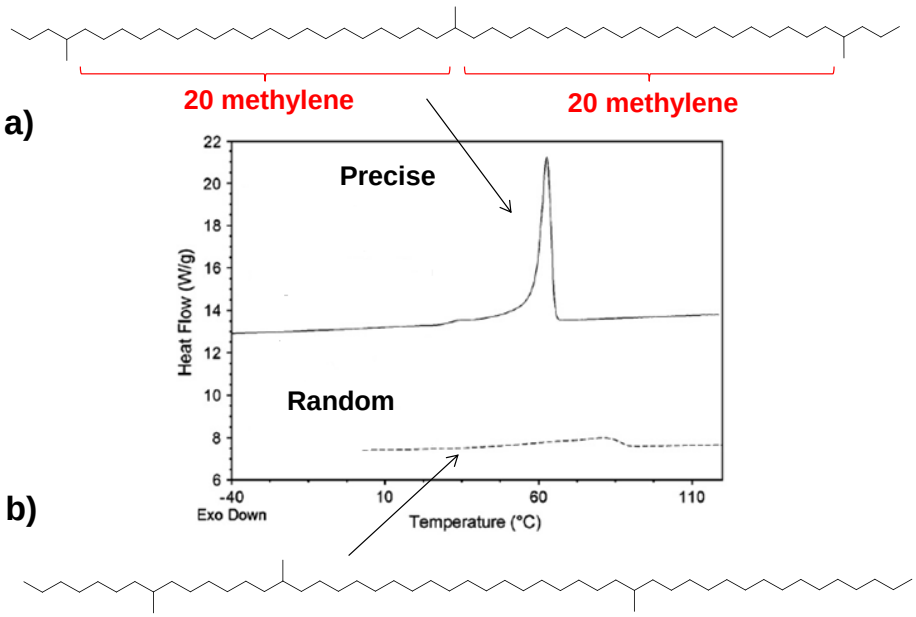

Figure 3-7. Thermal behavior of polyethylene having A) precisely spaced methyl branches and B) randomly spaced methyl branches.

The DSC thermogram of irregularly spaced methyl branched polyethylene (Figure 3-7) exhibits a broad melting transition consistent with its commercial analogues. In contrast, precise placement of methyl branches on every 21st carbon results in a well-defined thermal transition. The effect of methyl branch inclusion into the polyethylene

backbone on the crystal structure was also investigated[115]. For example, introducing methyl branches on every 21st carbon shifts the unit cell from orthorhombic to triclinic.

3.3.2 Ethyl and Hexyl Branches

Successful preparation of precisely placed methyl branches in polyethylene with ADMET stimulated efforts to model mainstream LLDPEs, such as ethylene/1-butene and ethylene/1-octene. The synthetic scheme for the preparation of ethyl and hexyl branched monomers is illustrated in Figure 3-8.

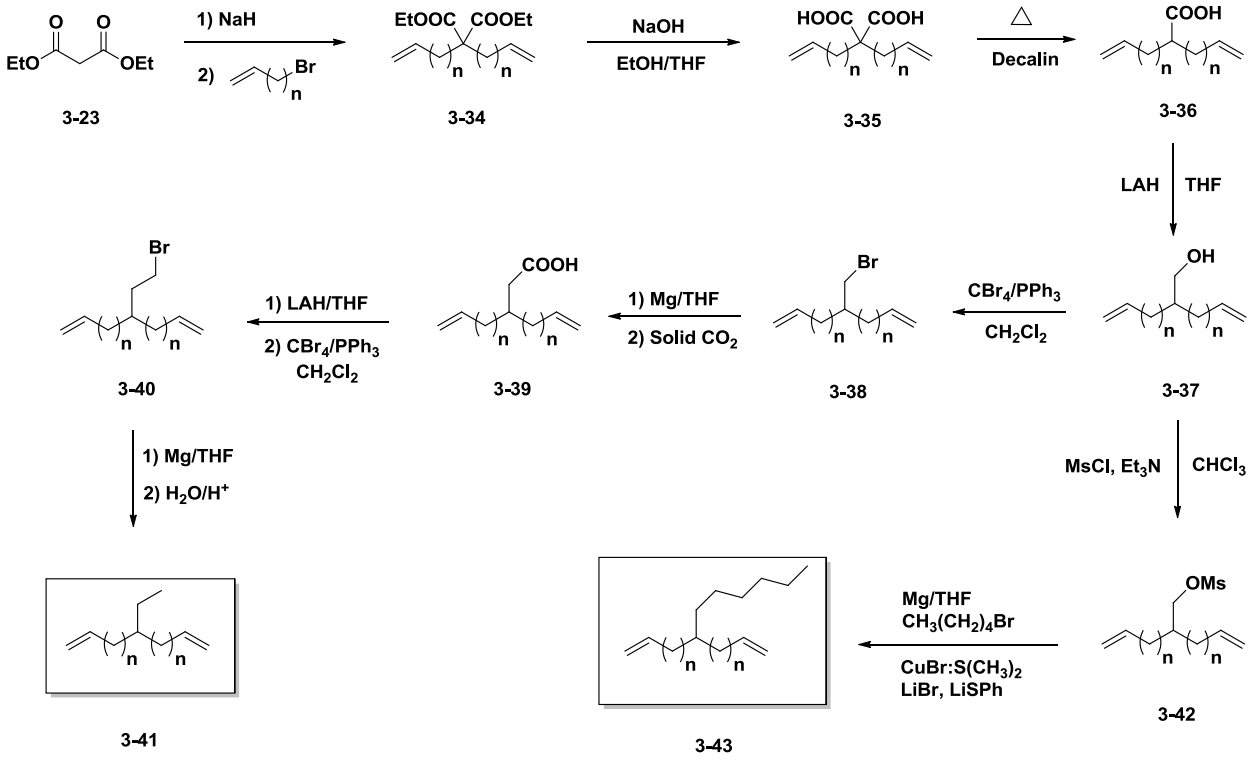

Figure 3-8. Synthesis of ethyl[116] and hexyl[118] branched monomers.

As shown in Figure 3-8, the key alcohol intermediate (compound **3-37**) for the synthesis of both monomers is generated through dialkylation of diethyl malonate (**3-23**), saponification, decarboxylation and reduction steps. Bromination of the primary alcohol and subsequent addition of solid CO_2 to the Grignard intermediate gives an acid

diene (**3-39**). After reduction of the acid and bromination steps, another Grignard reagent forms and is quenched with H_2O to yield the ethyl branched symmetrical monomer (**3-41**). The overall yields for this multistep synthetic route are in the range of 20-25%.

For the synthesis of hexyl branched monomer, primary alcohol (**3-37**) is first converted to the sulfonic acid ester (compound **3-42**) intermediate using mesyl chloride. A modified Grignard/Gilman reaction was developed to install hexyl branches in the presence of 1-bromopentane. Hexyl branched monomer **3-43** is recovered with overall yields within the range of 15-20%.

Monomers were polymerized and hydrogenated to yield precision branched polymers. The thermal data for ethyl branched polymers presented in Table 3-2. Similar to the methyl branched polymers, introduction of branch defects into the polymer backbone decreases both the melting point and the heat of fusion. Incorporation of an ethyl branch on every 21st carbon disrupts the crystallinity of linear ADMET polyethylene as indicated by the decrease in T_m and ΔH_m from 134^{o}C to 35^{o}C and 204 J/g to 57 J/g, respectively.

Table 3-2. Effect of precise ethyl branch placement on thermal properties

Ethyl branch on every *n*th carbon	1-butene comonomer content (mole%)	T_m(^{o}C) (peak)	ΔH_m(J/g)	$\overline{M}_n$ (kg/mol)
no branch	0	134	204	25.8
21	10.0	35	57	28.0
15	14.3	-33 & -6	NA	27.9
9	25.0	amorphous	--	31.4

Model ethylene/1-butene copolymers synthesized using either metallocene[148,149] or hydrogenated butadienes[150,151] with similar net concentrations of ethyl branches

display very ill-defined melting endotherms. The reduction of methylene sequence length to 15 causes the melting point to drop well below room temperature and the melting endotherm becomes less defined, as shown by the bimodal transition.

Table 3-3. Effect of precise hexyl branch placement on thermal properties

Hexyl branch on every *n*th carbon	1-octene comonomer content (mole%)	T_m(^{o}C) (peak)	ΔH_m(J/g)	$\overline{M}_n$ (kg/mol)
no branch	0	134	204	25.8
21	10.0	16	53	28.0
15	14.3	-48	19	24.7
9	25.0	amorphous	--	24.8

Ethylene/1-octene copolymers constitute approximately 25% of the LLDPE market and their thermal and material behavior has been well studied[152-155]. As shown in Table 3-3, incorporation of larger hexyl branches at precisely spaced run lengths disrupts the crystallinity of linear ADMET polyethylene to a higher degree than methyl and ethyl branches in precision polymers.

3.3.3 Universal Synthesis Route to Symmetrical α,ω-diene Monomers

As mentioned in previous sections and illustrated in Figure 3-4, preparation of symmetrical α,ω-diene monomers is the key in this research. So far, alkylation of malonate derivatives has been successfully employed to yield pure diene monomers[114,116-118]. One of the limitations in this chemistry relates to the required multistep transformations specific to each monomer. The relatively low (15-30%) overall yields of malonate route changed the direction of precision research towards the nitrile chemistry.

This new approach is based on the double alkenylation of the primary nitrile[156], followed by the reductive elimination of the nitrile moiety[157]. Figure 3-9 shows the

synthetic scheme for the preparation of symmetrical α,ω-diene monomer (compound **3-46**) in two steps with reasonably high (>80%) overall yield.

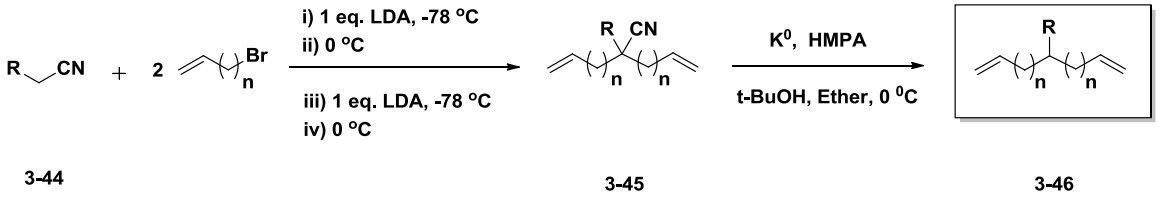

Figure 3-9. Alkylation/decyanation route for symmetrical α,ω-diene monomer synthesis[156,157].

Alkenylation of primary nitrile **3-44** in the presence of lithium diisopropyl amide (LDA) and alkenyl bromide produces the alkylcyano α,ω-diene **3-45** in high yield. Decyanation of nitrile **3-45** is achieved with potassium metal via radical chemistry. The resulting tertiary radical after decyanation is further quenched by abstraction of hydrogen from *t*-BuOH to give symmetrical α,ω-diene monomer **3-46** in quantitative yield.

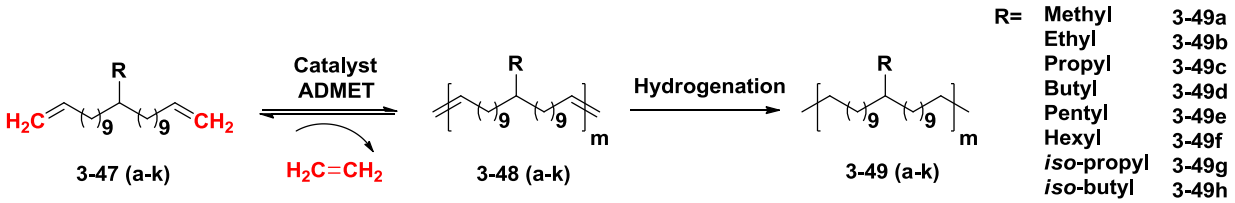

Figure 3-10. Incorporation of branches from methyl to adamantyl on every 21st carbon.

The ease of monomer synthesis has significantly expanded the scope of precision polyethylene studies. For example, a series of branches from methyl to adamantly were incorporated (Figure 3-10) in the polyethylene chain on every 21st carbon to examine the effect of branch identity on thermal and morphological behavior[158]. Previously discussed methyl and ethyl branched polymers were regenerated utilizing the

alkylation/decyanation route and essentially the same thermal behavior was observed for both, as shown in Table 3-4.

Table 3-4. Molecular weights and thermal data for precision polymers

Branch identity on every 21st carbon	T_m (°C) (peak)	ΔH_m (J/g)	M_w (kg/mol)(PDI) Unsaturated	M_w (kg/mol)(PDI) Saturated
No branch	134	204	70.2 (2.7)	70.2 (2.7)
Methyl	63	104	20.2 (1.7)	20.2 (1.7)
Ethyl	35	65	50.2 (1.9)	50.7 (1.9)
Propyl	12	60	41.2 (1.7)	41.4 (1.7)
Butyl	12	57	41.5 (1.8)	40.3 (1.7)
Pentyl	14	58	45.1 (1.8)	45.8 (1.8)
Hexyl	12	49	44.6 (1.8)	46.1 (1.7)
iso-propyl	11	37	45.5 (1.7)	46.0 (1.7)
iso-butyl	9	43	43.0 (1.6)	42.6 (1.9)
tert-butyl	13	50	30.6 (1.7)	32.1 (1.7)
Cyclohexyl	9	37	32.5 (1.6)	33.6 (1.6)
Adamantyl	-8 & 17	2 & 8	64.7 (1.7)	70.8 (1.3)

The data in Table 3-4 show that the incorporation of methyl and ethyl branches reduces the melting point of linear ADMET polyethylene in a progressing manner; on the other hand, all further branches, from propyl to adamantyl produce polymers that have essentially the same melting point. There is a clear change in the morphology of these polymers from a situation where the branch (methyl or ethyl) is included in the polymer's unit cell, to one where branches of greater mass are excluded from the unit cell as evidenced by wide angle X-ray diffraction (WAXD) (Figure 3-11).

ADMET polyethylene exhibits the typical orthorhombic crystal structure with two characteristic crystalline peaks superimposed with the amorphous halo, exactly the same as for high density polyethylene made by chain propagation chemistry. The more intense peak at scattering angle 21.5° and the less intense one at 24.0° correspond to reflection planes (110) and (200), respectively. Upon introducing precisely placed

branches of known identity, the crystal structure loses its symmetry with the unit cell shifting from orthorhombic to triclinic.

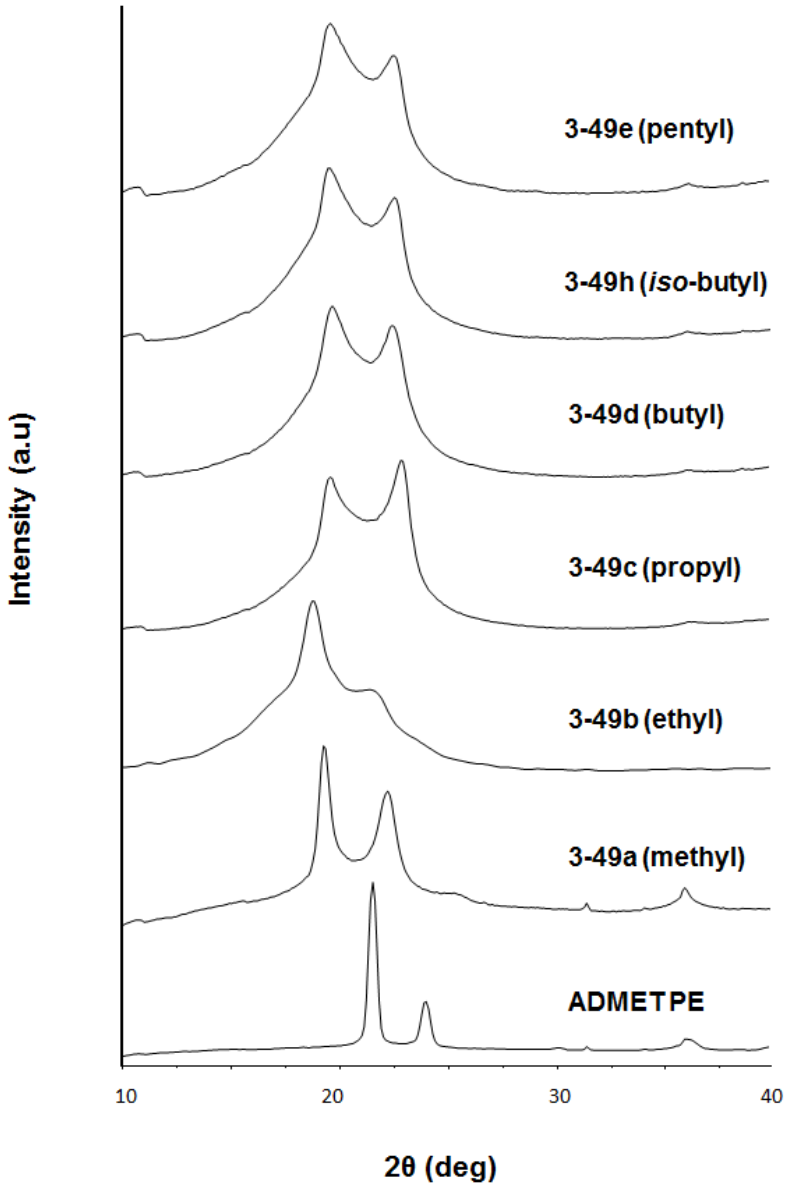

Figure 3-11. Wide angle X-ray diffraction patterns for seven precision polymers: **ADMET PE** at 27°C (no branch, T_m= 134°C), **3-49a-(methyl)** at 27°C (methyl branch, T_m= 63°C), **3-49b-(ethyl)** at room temperature (ethyl branch, T_m= 35°C), **3-49c-(propyl)** at 0°C (propyl branch, T_m= 12°C), **3-49d-(butyl)** at 0°C (butyl branch, T_m= 12°C), **3-49h-(*iso*-butyl)** at 0°C (*iso*-butyl branch, T_m= 9°C), **3-49e-(pentyl)** at 0°C (pentyl branch, T_m= 14°C). Prior to measurements, all samples were heated to above the melting temperature in order to remove thermal history, and then cooled to a specific temperature at a rate of 1°C/min.

Moreover, in contrast to linear polyethylene, scattering occurs at relatively lower scattering angles and with broader reflections being displayed, suggesting the increase of crystallite size and a decrease of crystallinity. In the case of the methyl branched polymers **3-49a-(methyl)**, two reflections representing a triclinic crystal orientation occur at scattering angles of 19.0^{o} with Miller index (100) and 22^{o} with Miller index (010).

Similar changes in the crystalline unit cell identity were observed in the ethyl branched polymer, **3-49b-(ethyl)**. Two strong reflections shift to lower scattering angles (18.0^{o} and 21.0^{o}), compared to the methyl branched polymer (19.0^{o} and 22.0^{o}). According to Bragg`s Law, the lower scattering angles correspond to larger d-spacings, indicating that the ethyl branch is incorporated in the crystalline region.

For the polymers possessing bulkier branches (propyl or larger), the WAXD diffractograms (the top four graphs in Figure 3-11) show nearly identical scattering patterns, indicating the crystal structure is independent on the branch identity. Moreover, these patterns are obviously different from those of polymers possessing smaller branches like methyl or ethyl, because they exhibit larger scattering angles and even broader reflections.

3.4 Dissertation Purpose

Alkyl branched precision polymers prepared by ADMET are excellent candidates for modeling commercial LLDPEs. This approach generates polymers where both the identity of the branch and its position along the chain are known without ambiguity. However, the monomer synthetic schemes developed so far provide maximum run lengths between branch points to 20 methylene carbons, which corresponds to 10 mole% of comonomer incorporation. This is considerably greater than the comonomer

concentrations in commercial LLDPEs (2-5 mole%), which produces materials with melting points in the range of 100 to 125^{o}C as shown in Table 2-1.

The remaining chapters in this dissertation describe the systematic increase of run lengths between branch points to 39 and 75 carbons. This level of advancement in monomer synthesis generates polymers that provide realistic models for commercial LLDPE.

CHAPTER 4
SYNTHESIS OF PRECISION POLYETHYLENE WITH BRANCHES ON EVERY 39TH CARBON[2]

4.1 Monomer Synthesis

Preparation of a symmetrical α,ω-diene monomer is vital to success in precision polyethylene research, because the built-in branch run length strictly dictates the spacing between the two consecutive branch points in the final polymer, as shown in Figure 4-1).

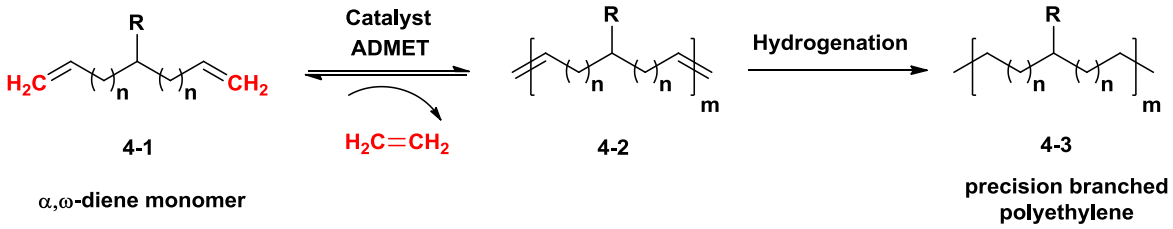

Figure 4-1. General two-step synthetic scheme for the preparation of precision branched polyethylene.

Increasing the run length in monomer **4-1** requires reproducible synthesis of the alkylating agent. Both the malonate[114,116,118] and nitrile[119,120,156] synthetic routes reported so far utilize alkenyl bromides with a maximum of 9 methylene run lengths (Figure 4-2).

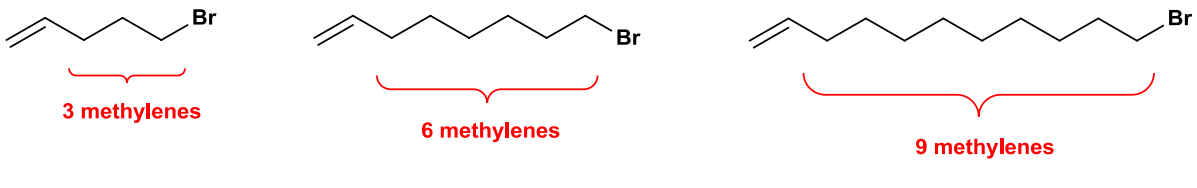

Figure 4-2. Alkenyl bromides with different run lengths used in precision research so far.

All of the three alkylating agents shown in Figure 4-2 are commercially available and introduction of these alkenyl bromides into the monomers generates polyethylenes

[2] Part of this chapter is adapted with permission from (Zuluaga, F.; Inci, B.; Nozue, Y.; Hosoda, S.; Wagener, K. B. *Macromolecules*, **2009**, 42, 4953). Copyright (2009) American Chemical Society.

with a branch on every 9th, 15th and 21st carbons in the polymer backbone, respectively. Alkenyl bromides with higher methylene run lengths are not commercially available and preparation of these compounds is required. Encouraged by the success of the previously reported[156,157] alkylation/decyanation synthetic route in monomer preparation, synthesis of compound **4-13** was attempted from commercially available starting material 11-bromo-undec-1-ene **4-6**.

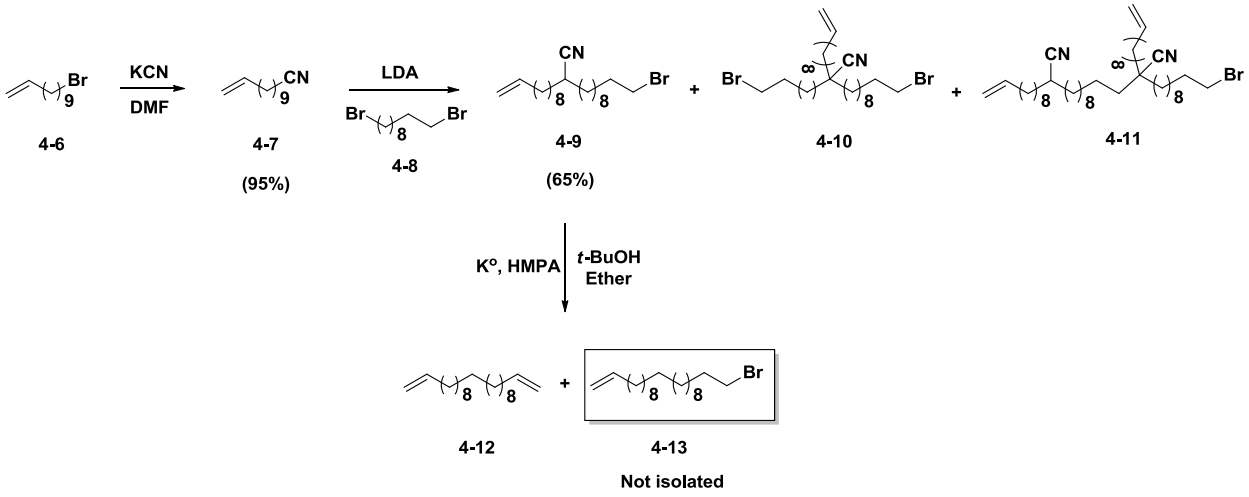

Figure 4-3. Synthetic attempt for the preparation of alkenyl bromide with 19 methylene run length.

As shown in Figure 4-3, alkenyl bromide **4-6** was converted into alkenyl cyanide, which was subsequently alkylated with 1 equivalent of commercially available 1,10-dibromodecane **4-8**. In addition to the desired mono-alkylated product **4-9**, di-alkylated compounds **4-10** and **4-11** were recovered in the crude product. Compound **4-9** was purified by column chromatography and recovered in moderate yield (65%). The same decyanation conditions developed for the monomer synthesis[157] were applied to compound **4-9** to yield alkylating agent **4-13** with 19 methylene run lengths. Two different products were identified by thin layer chromatography (TLC) analysis, and the presence of elimination product **4-12** was confirmed by ^{1}H nuclear magnetic resonance

(NMR) spectroscopy. Because of the nearly unnoticeable polarity difference between these species, column chromatography purification was not performed and the desired product **4-13** could not be isolated. The low overall yield, the use of highly toxic KCN and the required tedious purification for the synthesis changed our focus towards a malononitrile route.

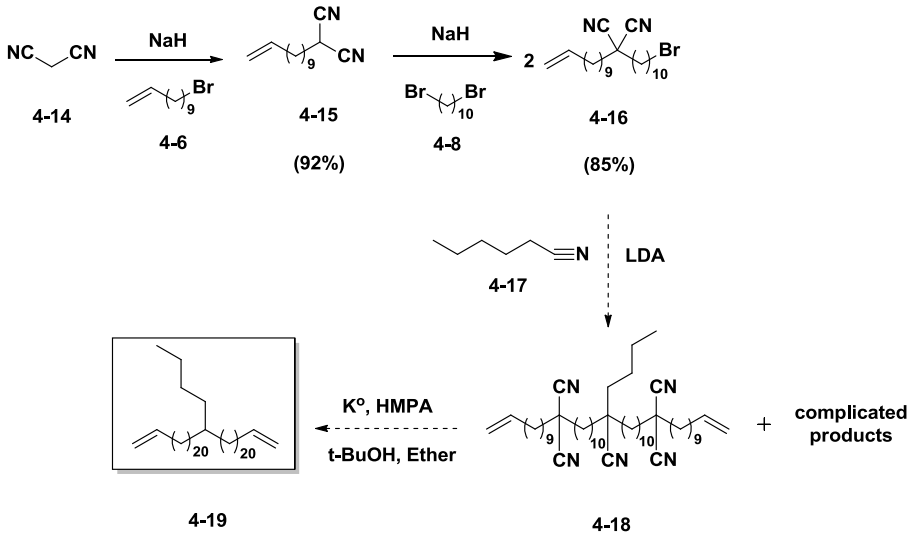

Figure 4-4. Synthetic attempt for the preparation of butyl branched monomer **4-19**.

The synthetic scheme shown in Figure 4-4 eliminates preparation of the alkenyl bromide and targets the direct synthesis of monomer **4-19**, which will generate a precision polymer with a butyl branch on every 42nd carbon. In this route, consecutive alkylation of malononitrile **4-14** with commercially available 11-bromo-undec-1-ene **4-6** and 1,10-dibromodecane **4-8** gives compound **4-16** in relatively high yield (two steps 78%). Then hexanenitrile **4-17** is alkylated by 2 equivalents of compound **4-16** in the presence of lithium diisopropyl amide (LDA) using the same alkylation conditions reported before[156]. Spots for both di-alkylated malononitrile **4-16** and hexanenitrile **4-17** disappeared on the TLC plate within 2 hours, but many other spots formed. Changing the reaction conditions did not decrease the number of spots and the desired product **4-**

18 could not be isolated. The difficulties in the alkylation step of this synthetic scheme decreased the motivation to pursue this route further.

The successful synthesis of an alkenyl bromide with a longer methylene run length is shown in Figure 4-5. The synthesis includes self-metathesis of 11-bromo-undec-1-ene **4-6** in the presence of first generation Grubb`s metathesis catalyst and subsequent hydrogenation of unsaturated dibromide **4-21** with Wilkinson`s catalyst to gives 1,20-dibromoeicosane, **4-22**.

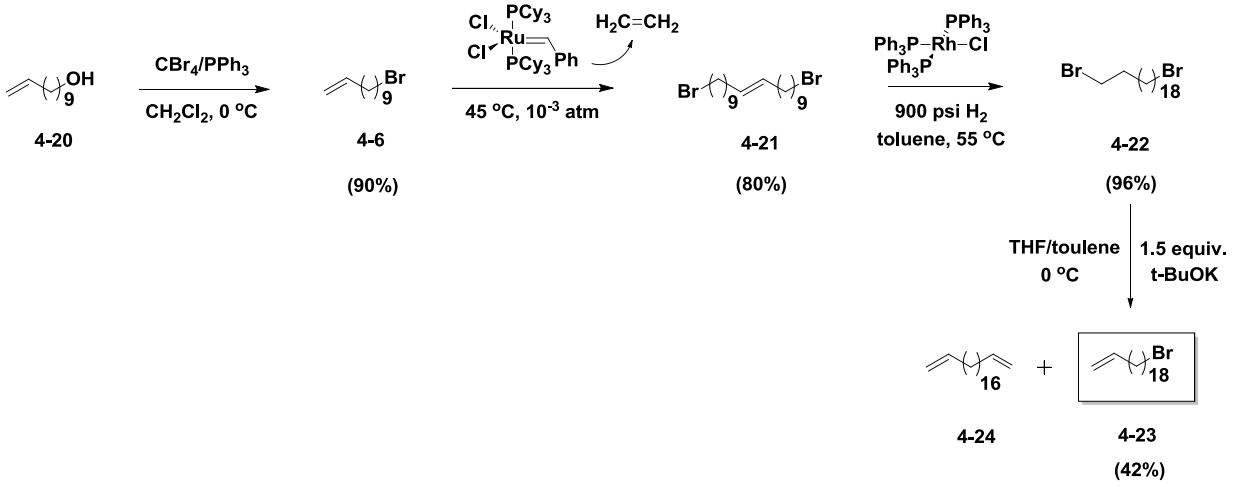

Figure 4-5. Successful synthesis of alkenyl bromide 20-bromo-eicos-1-ene, **4-23**.

For dehydrohalogenation of alkyl dibromide **4-22**, 1.5 equivalence of *t*-BuOK suppressed (but did not eliminate entirely) the formation of the di-elimination product **4-24**. The crude mixture contained the desired alkenyl bromide, 20-bromoicos-1-ene **4-23**, the di-elimination product and unreacted starting material, all having close retention factors by TLC. Due to the similar polarities of these three species and the relatively low room temperature solubility of the crude mixture in hexane, a special purification procedure is followed. The crude mixture was first dissolved in toluene and mixed with small amount of silica gel to form a slurry. Toluene was slowly evaporated and the

resulting silica particles with adsorbed crude mixture were added to a freshly packed column to form a uniform layer using hexane. Then, another uniform layer of pristine silica gel was added on top of the crude layer. Hexane was slowly added to the column without disturbing either layer. The flow rate of the column was also adjusted to obtain the most efficient separation. After two column chromatography passes, the desired alkenyl bromide **4-23** was recovered in moderate yield (42%).

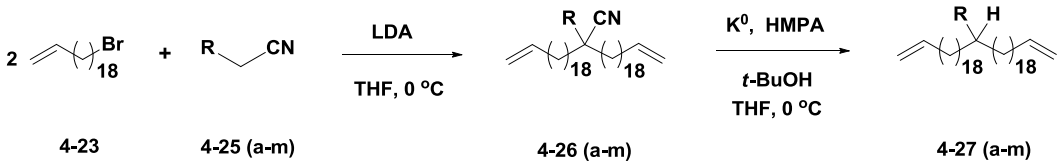

R = Methyl	**(4-27a)**
Ethyl	**(4-27b)**
Propyl	**(4-27c)**
iso-propyl	**(4-27d)**
Butyl	**(4-27e)**
iso-butyl	**(4-27f)**
Pentyl	**(4-27g)**
Hexyl	**(4-27h)**
Heptyl	**(4-27i)**
Octyl	**(4-27j)**
Nonyl	**(4-27k)**
Decyl	**(4-27l)**
Pentadecyl	**(4-27m)**

Figure 4-6. Synthesis of 21-alkylhentetraconta-1,40-dienes (**4-27 a-m**).

Alkylation of various primary nitriles with 11-bromo-undec-1-ene (structure **4-6** in Figure 4-2) proceeded efficiently to give the corresponding monomers with different branches in high overall yields. The efficiency of alkylation with a longer alkenyl bromide (in this case 20-bromoicos-1-ene, **4-23**) was first examined with hexanenitrile **4-25e** using the previously reported procedure[156] but, mostly mono-alkylated nitrile was recovered in every trial. The melting point of alkenyl bromide **4-23** (T_m=32^{o}C) limits the use of cannula wires and syringes to maintain the anhydrous conditions necessary for the correct stoichiometric ratio of lithium diisopropyl amine (LDA) to alkyl bromide during

the addition of alkylating agent. The di-alkylated nitrile, 2-butyl-2-(icos-19-enyl)docos-21-enenitrile, **4-26e** was purified from the mono-alkylated adduct via consecutive column chromatographic separations. The formation of mono-alkylated nitrile and the multi-step purification resulted in yields as low as 19%. In order to increase the yield, the alkylation procedure was modified by use of a reaction tube to fulfill the anhydrous conditions. This modification enabled nearly quantitative di-alkylation of the nitrile without formation of the mono-alkylated adduct (yield = 98%). Only one column separation was then adequate to purify compound **4-26e**. Decyanation of nitrile **4-26e** was achieved with potassium metal via radical chemistry. The resulting tertiary radical after decyanation was quenched by abstraction of hydrogen from *t*-BuOH to give α,ω-diene monomer **4-27e** in high yield. This two-step alkylation/decyanation route was employed to generate monomers having branches from methyl to pentadecyl **4-27 (a-m)** in moderate to high yields.

4.2 Polymer Synthesis and Primary Structure Characterization

Monomers **4-27a-m** were condensed to form the corresponding unsaturated ADMET polymers (Figure 4-7). Because of the relatively high melt viscosity of the resulting polymers (**4-28a-m**), the polymerization temperature was set to 85^{o}C. At that elevated temperature Ru-based catalysts are prone to have low turnover numbers and to generate Ru-H species[159-161], which would cause isomerization problems and disrupt the symmetrical nature of the monomer[162,163]. Therefore, monomers **4-27a-m** were condensed to form unsaturated ADMET polymers using Schrocks` [Mo] catalyst for clean metathesis chemistry. Due to the oxophilic nature of [Mo] catalysts, all the manipulations prior to polymerization and catalyst addition (catalyst to monomer ratio 1:500) were performed in a glove box. Polymerization was initiated by melting the

monomer at 50 ^{o}C and the temperature was set to 85^{o}C to be able to stir the viscous polymer melt.

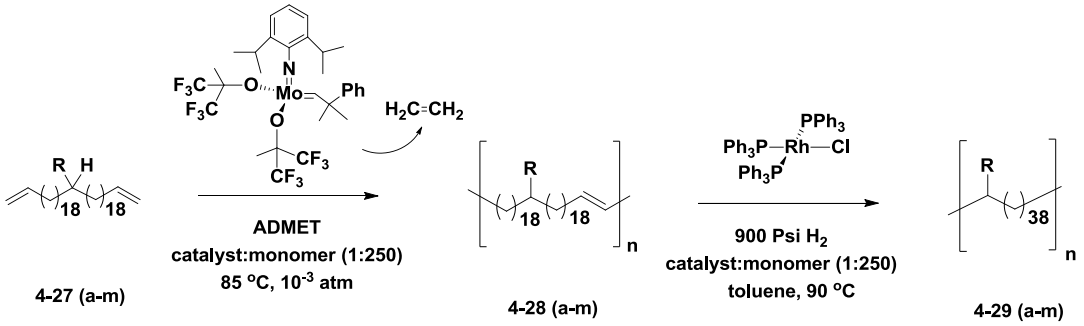

Unsaturated polymer	Branch (R)	Saturated polymer
4-28a	Methyl	4-29a
4-28b	Ethyl	4-29b
4-28c	Propyl	4-29c
4-28d	*iso*-propyl	4-29d
4-28e	Butyl	4-29e
4-28f	*iso*-butyl	4-29f
4-28g	Pentyl	4-29g
4-28h	Hexyl	4-29h
4-28i	Heptyl	4-29i
4-28j	Octyl	4-29j
4-28k	Nonyl	4-29k
4-28l	Decyl	4-29l
4-28m	Pentadecyl	4-29m

Figure 4-7. Synthesis of precision polymers possessing a branch on every 39th carbon.

After 24 hours of reaction, the polymer was cooled to RT, another portion of [Mo] catalyst (catalyst to monomer ratio 1:500) was added in the glove box, and the temperature was set back to 85^{o}C. ADMET polymerization proceeded smoothly to give the desired unsaturated linear polymers **4-28a-m** with no detectable side reactions. Disappearance of terminal olefin signals in ^{1}H NMR spectra (Figure 4-8) proved the complete conversion, which is necessary for any step-growth polymerization. Unsaturated polymers (**4-28a-m**) were hydrogenated using Wilkinson`s catalyst

(catalyst to monomer ratio 1:250) to yield the precision polyethylenes (polymers **4-29a-m**) possessing branches from methyl to pentadecyl on every 39th carbon.

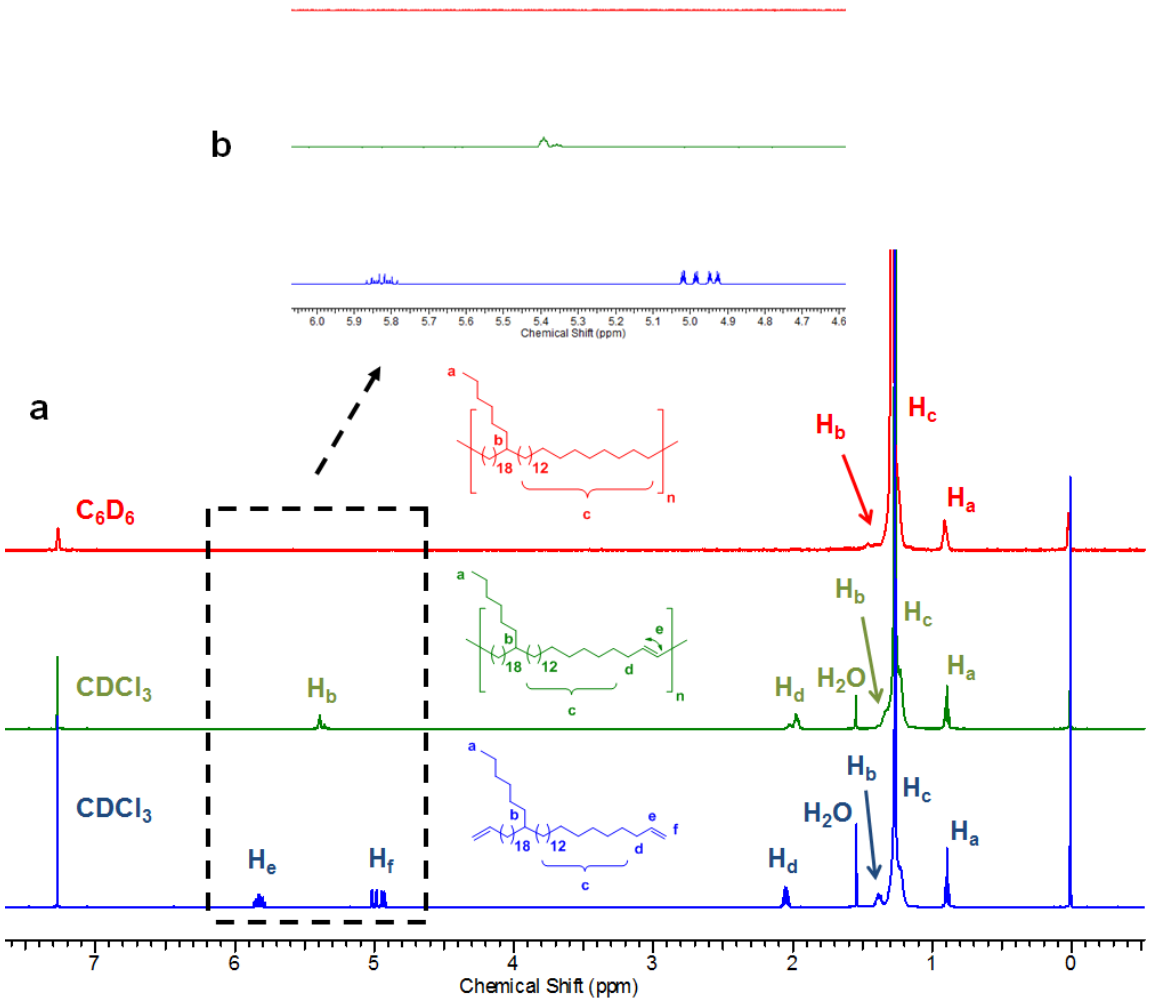

Figure 4-8. A) ^{1}H 500 MHz NMR spectra of monomer (**4-27h**), unsaturated (**4-28h**) and saturated (**4-29h**) polymers. B) olefinic region shown in higher magnification.

The polymerization and hydrogenation steps were followed with ^{1}H NMR spectroscopy. As an example, Figure 4-8 illustrates the ^{1}H NMR spectra of hexyl branched polymer, **4-29h**, and its precursors. ADMET polymerization of monomer **4-27h** yielded the unsaturated polymer, **4-28h**. Formation of the ADMET polymer resulted in loss of the terminal olefin signals (5.0 and 5.8 ppm) and the appearance of the internal olefin at 5.4 ppm (Figure 4-8). Exhaustive hydrogenation of the internal olefins with

Wilkinson`s catalyst generated **4-29h**, corresponding to polyethylene with hexyl branches on every 39th carbon, with complete loss of the olefinic signals on ^{1}H NMR.

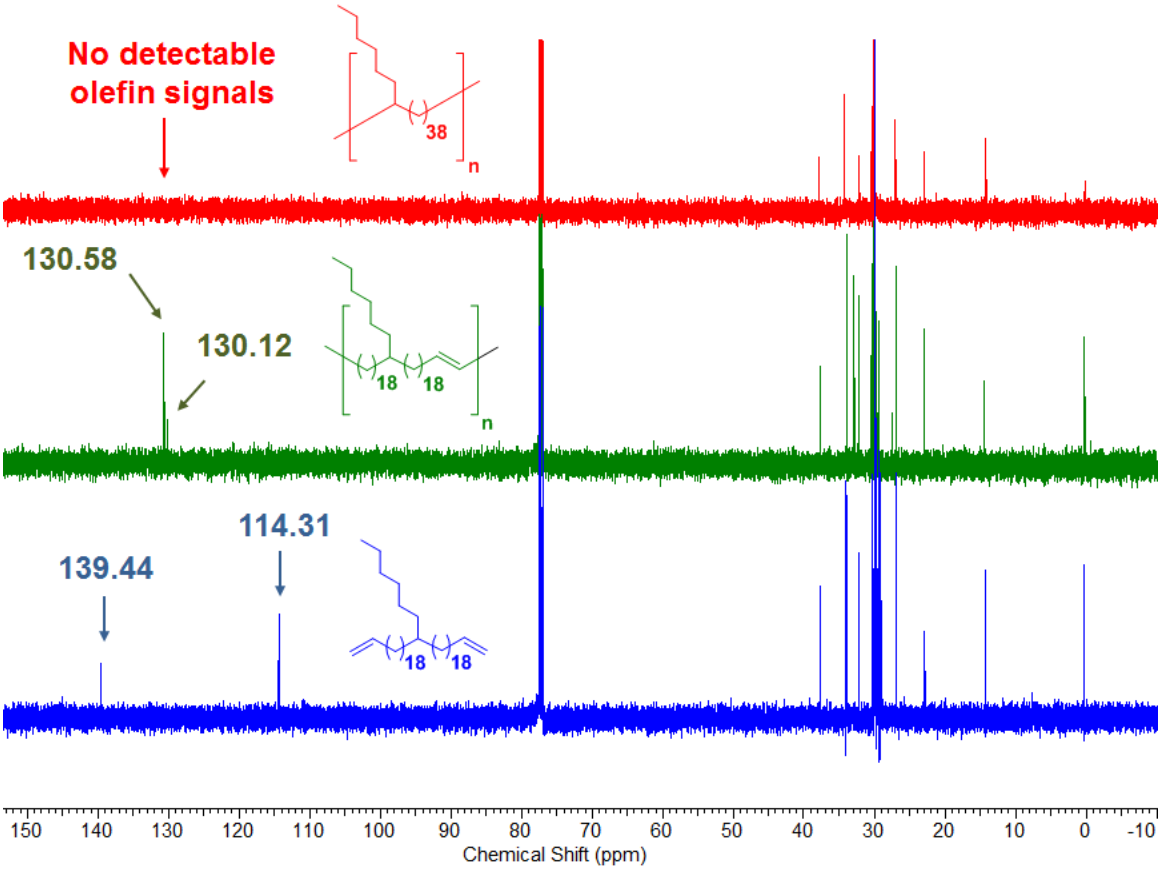

Figure 4-9. ^{13}C 126 MHz NMR spectra of monomer (**4-27h**), unsaturated (**4-28h**) and saturated (**4-29h**) polymers.

Polymerization and hydrogenation of monomer **4-27h** was also monitored with ^{13}C NMR spectroscopy (Figure 4-9). Comparison of the ^{13}C NMR spectra for the monomer **4-27h** and unsaturated polymer **4-28h** indicates the disappearance of the signals belonging to the terminal olefin at 114.31 and 139.44 ppm and formation of the new internal olefin (*cis* olefin at 130.12 ppm, minor product, and *trans* olefin at 130.58 ppm, major product) generated by the metathesis chemistry. Hydrogenation of the internal olefin with Wilkinson`s catalyst yielded the saturated polymer **4-29h** with no detectable trace of olefins. Infrared (IR) spectroscopy was also used to monitor this

transformation (Figure 4-10). Disappearance of the out-of-plane C-H bend absorption at 969 cm^{-1} indicates the complete absence of C=C in the polymer backbone and proves the full conversion for the hydrogenation step.

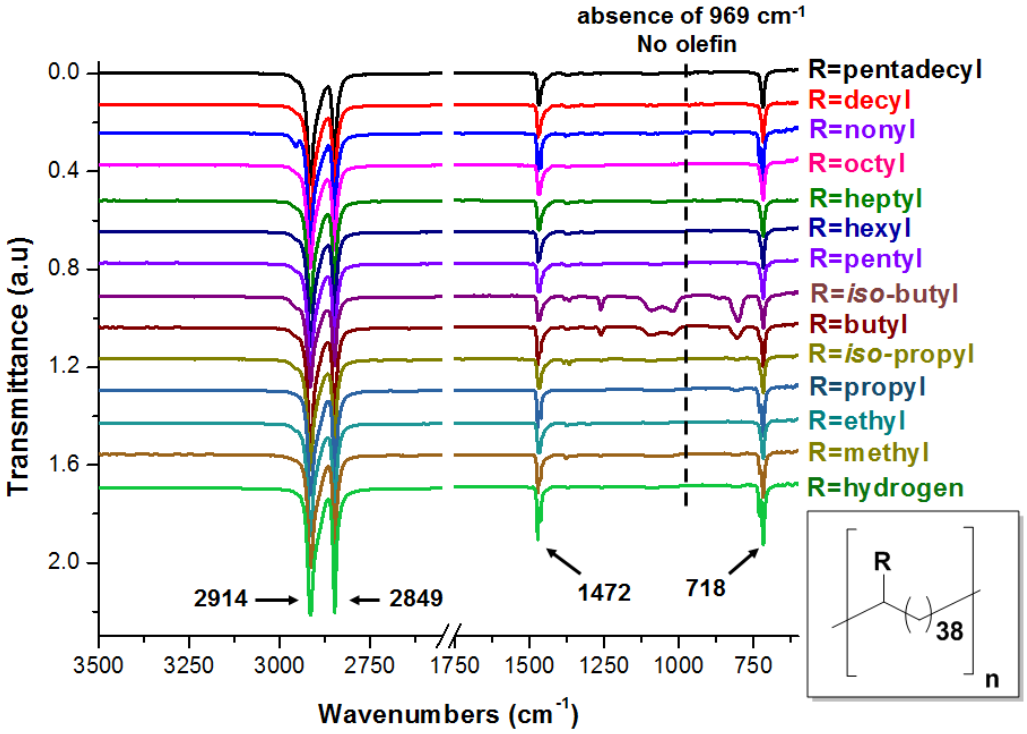

Figure 4-10. Infrared spectra for the precisely branched polymers **4-29a-(methyl)**, **4-29b-(ethyl)**, **4-29c-(propyl)**, **4-29d-(*iso*-propyl)**, **4-29e-(butyl)**, **4-29f-(*iso*-butyl)**, **4-29g-(pentyl)**, **4-29h-(hexyl)**, **4-29i-(heptyl)**, **4-29j-(octyl)**, **4-29k-(nonyl)**, **4-29l-(decyl)**, **4-29m-(pentadecyl)** and **ADMET PE**.

After hydrogenation, solutions of saturated polymers were concentrated and precipitated into methanol. It is important to note that the solubility characteristics of polymers **4-29a-m** (soluble in toluene, dichlorobenzene, trichlorobenzene, etc. at high temperatures) are similar to those of polyethylenes prepared by chain polymerization. Molecular weight data were obtained using high temperature gel permeation chromatography (GPC) in 1,2,4-trichlorobenzene at 135 ^{o}C relative to polystyrene standards. Table 4-1 illustrates the weight average molecular weights for the precisely branched unsaturated and saturated polymers.

Table 4-1. Molecular weights and thermal data for precisely branched polymers

Branch identity on every 39th carbon	T_m (°C) (peak)	ΔH_m (J/g)	$\overline{M}w$[a] (kg/mol) (PDI[b]) Unsaturated	Saturated
No branch	134	204	70.2 (2.7)	70.2 (2.7)
Methyl	92	137	33.7 (2.2)	92.7 (2.0)
Ethyl	76	93	56.7 (2.2)	53.1 (2.4)
Propyl	78	71	217 (3.1)	225 (3.0)
iso-propyl	77	74	107 (2.0)	144 (3.5)
Butyl	75	66	60.2 (2.3)	66.5 (2.5)
iso-butyl	73	51	22.6 (2.5)	54.8 (2.4)
Pentyl	74	88	29.3 (2.2)	30.2 (2.0)
Hexyl	73	85	30.5 (2.3)	30.5 (1.9)
Heptyl	74	85	76.6 (3.0)	74.2 (2.9)
Octyl	74	73	200 (3.6)	181 (3.3)
Nonyl	73	84	35.9 (2.4)	34.3 (2.2)
Decyl	71	76	28.0 (2.4)	27.7 (1.8)
Pentadecyl	70	83	58.0 (2.4)	55.9 (2.4)

[a]Molecular weight data were collected by GPC in 1,2,4-trichlorobenzene at 135 °C relative to polystyrene standards. [b]PDI, polydispersity index $\overline{M}w/\overline{M}_n$.

4.3 Primary Structure Characterization of Precisely Branched Polymers

Control over the primary structure of the final precision polymer is governed by the precision established on the molecular level. The purity of the monomers and the absence of any side reactions during the polymerization ensure the successful polycondensation chemistry and level of control. Upon close inspection of the ^{13}C NMR data for the polymers, it can be concluded that the branches are precisely placed along the polyethylene main backbone with none of the undesired branches due to chain transfer typically observed during chain-growth chemistry. Figures 4-11, 4-13 & 4-14 show a portion (10-55 ppm) of the ^{13}C NMR spectra for precise polymers having branches from methyl to octyl. All spectra are dominated by a singlet at 29.99 ppm corresponding to methylenes on the main polyethylene chain. Note that the presence of

alkyl branches precisely placed along the main chain affects the chemical shifts of carbons located within three CH_2 units from an individual branch[114].

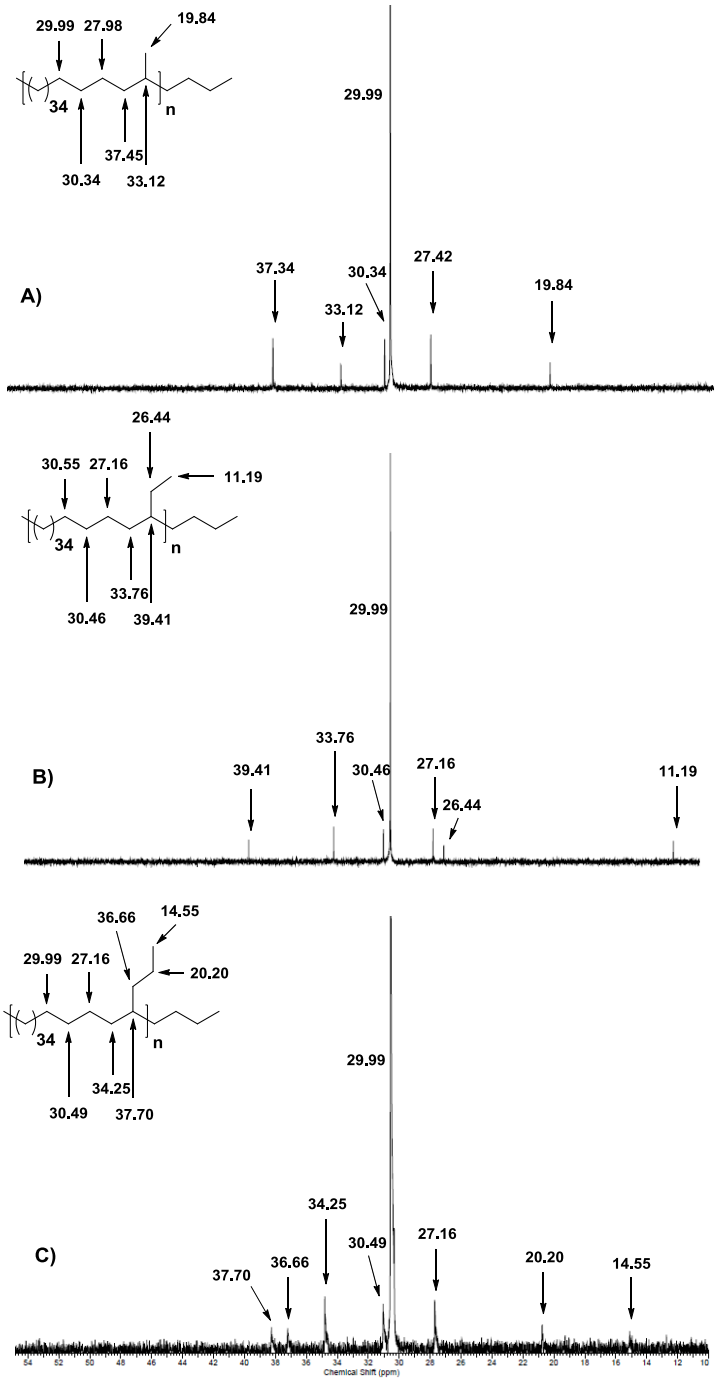

Figure 4-11. Comparison of ^{13}C NMR spectra for precision polymers A) **4-29a-(methyl)**, B) **4-29b-(ethyl)** and C) **4-29c-(propyl)**.

To demonstrate the effect of branch identity on ^{13}C NMR chemical shifts in a consistent manner, nomenclature defined by Randall[164] is used (Figure 4-12). Methylene carbons along the backbone of a polymer chain are identified by a pair of Greek letters to indicate the distance to branches. Carbons on the branch are identified by iB_n where "i" indicates the position in the branch starting with the terminal methyl carbon, and the subscript "n" indicates the length of the branch.

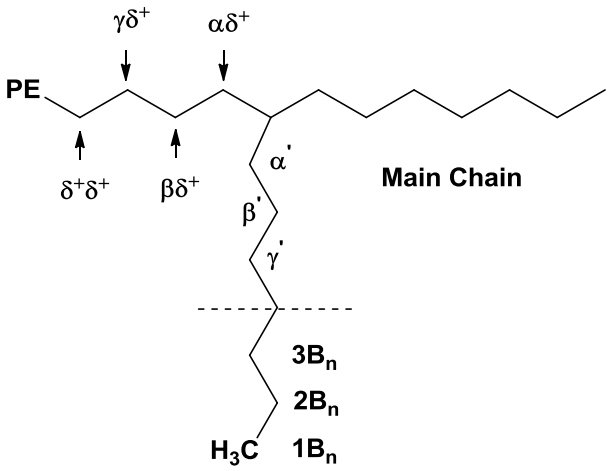

Figure 4-12. Commonly accepted nomenclature used to identify the positions of different carbons.

In the spectrum for **4-29a-(methyl)** which is polyethylene containing methyl branches on every 39th backbone carbon (Figure 4-11A), the resonances belonging to the methyl branch, α` (19.84 ppm), as well as main chain carbons $\alpha\delta^+$ (37.45 ppm), $\beta\delta^+$ (27.98 ppm), $\gamma\delta^+$ (30.34 ppm), $\delta^+\delta^+$ (29.99 ppm) and the carbon at the branch point (33.12 ppm) indicates that only methyl branches are present, in good agreement with previously reported[114] experimental data and predicted values[165]. Introduction of ethyl branches changes the chemical shifts of both backbone and side chain carbons (Figure 4-11B). The terminal methyl carbon ($1B_2$) is now more shielded by the presence of a methylene unit, which results in a predictable shift to upfield (11.19 ppm). On the other

hand, the methine carbon is deshielded with more electron delocalization and shifts downfield (39.41 ppm) compared to the methyl branched polymer. All the chemical shifts shown in Figure 4-11B for the polymer **4-29b-(ethyl)** are in good agreement with previously reported ethylene/1-butene and hydrogenated polybutadiene systems[86,166-168].

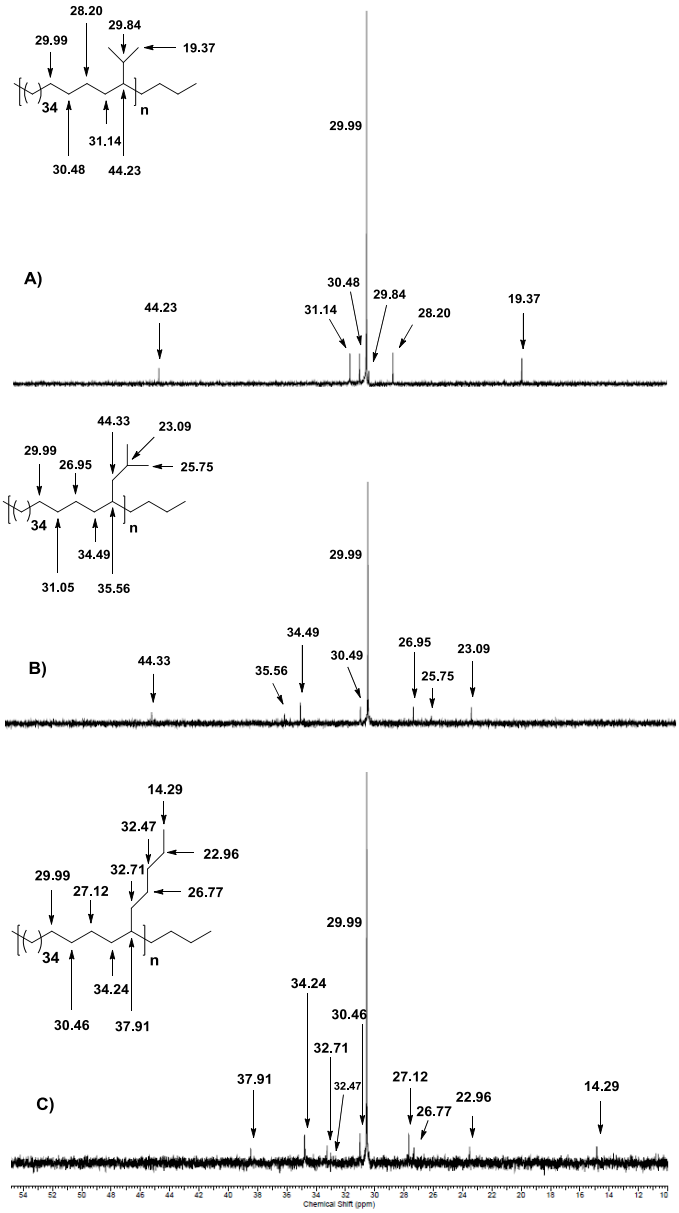

Figure 4-13. Comparison of ^{13}C NMR spectra for precision polymers A) **4-29d-(*iso*-propyl)**, B) **4-29f-(*iso*-butyl)** and C) **4-29g-(pentyl)**.

In the spectrum for **4-29d-(propyl)** (Figure 4-11C), the resonances belonging to the propyl branch, α` (14.55 ppm), β` (20.20 ppm), γ` (36.66 ppm), $\alpha\delta^+$ (34.25 ppm), $\beta\delta^+$ (27.16 ppm), $\gamma\delta^+$ (30.49 ppm), $\delta^+\delta^+$ (29.99 ppm) and the methine carbon (37.70 ppm) indicate that only propyl branches are present, in good agreement with previously reported data on chain-growth polymers obtained by copolymerization of ethylene with 1-pentene[169-171].

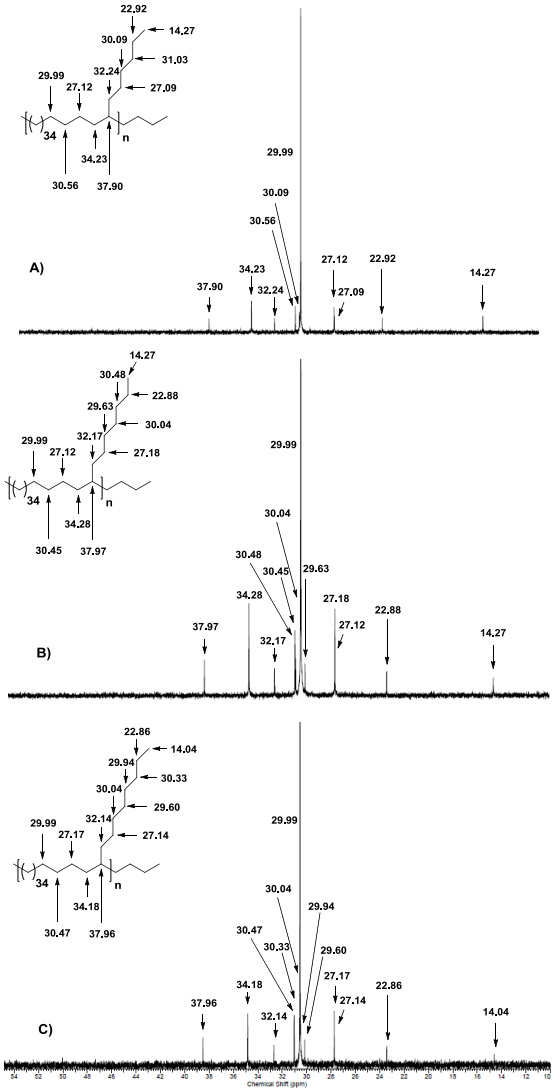

Figure 4-14. Comparison of ^{13}C NMR spectra for precision polymers A) **4-29h-(hexyl)**, B) **4-29i-(heptyl)** and C) **4-29j-(octyl)**.

It is also interesting to compare the propyl branched polymer with the *iso*-propyl branched isomer. The ^{13}C NMR spectrum of polymer **4-29d-(*iso*-propyl)** is presented in Figure 4-13A. Both terminal methyl carbons on the *iso*-propyl branch and the methine carbon are deshielded compared to the propyl branch to give 19.37 and 44.23 ppm, respectively. Starting from the pentyl branched polymer **4-29g-(pentyl)**, all the longer linear branched precision polymers display very similar spectral patterns with slight differences as shown in Figures 4-13C and 4-14.

4.4 Experimental Section

4.4.1 Instrumentation

All ^{1}H NMR (300 MHz) and ^{13}C NMR (75 MHz) spectra of starting materials, intermediates and monomers were recorded in $CDCl_3$. For polymer characterization, ^{1}H NMR (500 MHz) and ^{13}C NMR (126 MHz) instrumentation were used and spectra were recorded in either $CDCl_3$ or C_6D_6. Chemical shifts were referenced to signals from $CDCl_3$ (7.24 ppm for ^{1}H, 77.23 ppm for ^{13}C) with 0.03% v/v TMS and from C_6D_6 (7.16 ppm for ^{1}H, 128.39 ppm for ^{13}C) as an internal reference, and the temperature was maintained at either 25 or 65^{o}C. High Resolution Mass Spectrometry (HRMS) was carried out using an Agilent 6210 TOF-MS mass spectrometer in the Direct Analysis in Real-Time (DART) mode with an IonSense DART Source. Thin layer chromatography (TLC) was used to monitor all reactions and was performed on glass plates coated with silica gel (250 μm thickness). Column chromatography was performed using ultrapure silica gel (40-63 μm, 60 Å pore size).

Gel Permeation Chromatography (GPC) was performed using an Alliance GPC 2000 with an internal differential Refractive Index Detector (RID), internal differential viscosity detector (DP), and a precision angle light scattering detector (LS) at the Max

Planck Institute for Polymer Research, Mainz, Germany. The light scattering signal was collected at a 15° angle, and the three in-line detectors were operated in series in the order LS-DRI-DP. The chromatography was performed at 135°C using a PLgel MIXED-B column (10 μm PD, 8.0 mm ID, 300 mm total length) with HPLC grade 1,2,4-trichlorobenzene as the mobile phase at a flow rate of 1.0 mL/min. Injections were made at 0.05-0.07% w/v sample concentration using a 322.5 μL injection volume. In the case of universal calibration, retention times were calibrated versus narrow-range molecular weight polystyrene standards (purchased from Polymer Standard Service PSS in Mainz, Germany). IR data were obtained using a Perkin-Elmer Spectrum One FTIR equipped with a $LiTaO_3$ detector. The unsaturated polymer sample was prepared by solution-casting a thin film from toluene onto a KBr salt plate and the hydrogenated polymer sample was prepared by solution-casting a thin film from boiling toluene onto a KBr salt plate.

4.4.2 Materials

Chemicals were purchased from the Aldrich Chemical Co. and used as received unless otherwise noted. Grubb`s first generation catalyst, bis(tricyclohexylphosphine)benzylidineruthenium(IV) dichloride, was kindly provided by Materia, Inc. Schrock`s molybdenum metathesis catalyst, $[(CF_3)_2CH_3CO]_2$(N-2,6-C_6H_3-*i*-Pr_2)Mo=CHC$(CH_3)_2$Ph, and Wilkinson's rhodium hydrogenation catalyst, $RhCl(PPh_3)_3$, were purchased from Strem Chemical. Ruthenium and Molybdenum catalysts were stored in an argon-filled glovebox prior to use. Tetrahydrofuran (THF) and toluene were freshly obtained from Butler Polymer Research Laboratories anhydrous solvent preparation unit. HPLC grade 1,2,4-trichlorobenzene was purchased from the Applichem GmbH. All the nitriles and alkenyl bromide starting materials, as well as

hexamethylphosphoramide and diisopropyl amine were distilled over CaH_2. All reactions were carried out in flame-dried glassware under argon unless otherwise stated.

4.4.3 Procedures

Synthesis of 11- Bromo-undec-1-ene (4-6). A solution of 11-undecen-1-ol, **4-20**, (34.11g, 0.20 mol) and CBr_4 (73.45 g, 0.22 mol) in CH_2Cl_2 (120 mL) was prepared in a 500-mL round bottomed flask and cooled to 0^oC. Triphenyl phosphine (58g, 0.22 mol) was added in small portions over a period of 20 minutes. An exothermic reaction occurred, which was left stirring at 0^oC for 1hr and 40 min, then at RT for 2 hours. The crude product was filtered over a silica column, and the solution was concentrated by evaporation, until a white precipitate formed. The liquid was poured into 400 mL of hexane with stirring and more solid (triphenylphosphine oxide, $O=PPh_3$) precipitated. The solution was decanted leaving the solid in the flask, and the hexane solution was concentrated to obtain more precipitate. The solid was filtrated, and the hexane solution was evaporated to obtain 81.65 g of yellow liquid, which was fractionally distilled under reduced pressure (6 torr) to remove the bromoform, the by-product. Compound **2** (41.9 g) was collected as a colorless liquid. (Yield= 90%) The ^1H NMR spectrum was consistent with the published spectrum[172].

Synthesis of 1,20- dibromo-eicos-10-ene (4-21). In a 50-mL round bottomed flask, 11-bromo-undec-1-ene, **4-6**, (50g, 0.215mol) was mixed with 0.310g, 3.76×10^{-4} mmol, of Grubbs 1^{st} generation catalyst at RT (22^oC) and warmed to 45^oC for reaction under argon. It was left at 45^oC under Ar for 28 hr and finally under vacuum (7 torr) for 24 hr. The reaction was quenched with 5 mL ethyl vinyl ether and dissolved in 100 mL toluene. The toluene solution was concentrated and then poured into 1.0 L cold methanol. The methanol mixture was left in the refrigerator overnight, and white crystals were obtained.

After vacuum filtration 15 g of a crystalline material was obtained (Yield = 80%). The ^{1}H NMR spectrum was consistent with the published spectrum[172].

Synthesis of 1,20-Dibromoeicosane (4-22). Compound **4-21,** 1,20-dibromo-eicos-10-ene (10. 691g, 24.44 mmol) was dissolved in 90 mL degassed toluene, placed in a Parr bomb with 1.1 mg, 1.89×10^{-3} mmol, Wilkinson`s catalyst, and left to react at 55^{o}C under 900 psi of hydrogen for 4 days. Purification of the product by column chromatography with toluene afforded 10.30 g of a white solid. (Yield = 96%) The ^{1}H NMR spectrum was consistent with the published spectrum[172].

Synthesis of 20-Bromo-eicos-1-ene (4-23). In a 250 mL round bottomed flask, compound **4-22** (10.30 g, 23.4 mmol) was dissolved in 2:1 THF/toluene mixture producing a 1 M solution. The mixture was cooled using an ice water bath, and potassium *tert*-butoxide (3.92g, 35.1 mmol) was added in small portions over 30 min. After addition, the reaction turned cloudy and was allowed to stir at 0^{o}C for 1 h. The reaction was quenched using water (25 mL), followed by 1 M HCl (25 mL). The organic layer was extracted and washed with 1M HCl (15 mL), saturated Na_2CO_3 (15 mL), and 15 mL of water, followed by drying with magnesium sulfate. The solvents were evaporated and the crude product was further purified by column chromatograhy using hexane as the eluent. Compound **4-23** (4.85 g) was collected as a white solid. (Yield= 42%) The ^{1}H NMR spectrum was consistent with the published spectrum[172].

Synthesis of 2-methyl-2-(eicos-19-en-1-yl)docos-21-enenitrile (4-26a). Into a 100 mL 3-neck round bottomed flask equipped with a stir bar, THF (5 ml) was added and cooled to -78^{o}C under nitrogen. Diisopropyl amine (0.6 mL) and 2.0 mL of 2.0 M n-BuLi (freshly titrated) were added and warmed to 0^{o}C to prepare lithium diisopropyl amine

(LDA) solution in situ. The LDA solution was cooled to -78^{o}C and propionitrile **4-25a** (0.090 mL, 1.29 mmol) was added. The mixture was allowed to return to RT and was stirred for 30 minutes at RT. Separately, 20-bromo-eicos-1-ene, **4-23**, (1.171 g, 3.26 mmol) was added to a 50 mL flame-dried schlenk flask and kept under high vacuum prior to use at 50^{o}C, the LDA solution was transferred to the Schlenk flask at -78^{o}C, and the resulting mixture was slowly warmed to 0^{o}C and stirred for 12 hours at that temperature. The reaction was quenched with addition of diethyl ether (40 mL) and water (10 mL). The organic phase was extracted three times with ether (3x 30 mL), washed with brine, and dried over $MgSO_4$(s). The solvents were evaporated and the crude product was further purified by column chromatograhy using toluene/hexane as the eluent. Because of the very similar retardation factors between mono and di-alkylated nitriles, the toluene/hexane concentration was varied during the separation (toluene concentration was increased from 5% to 30% in 5% increments for each 250 mL portion of eluent.) After purification, 0.861 g of compound **4-26a** was collected as white crystals (Yield = 86%) The following spectral properties were observed; ^{1}H NMR ($CDCl_3$) δ ppm 0.92 (s, 3H), 1.14 - 1.52 (br, 68 H), 2.05 (td, J_1=7.64 Hz, J_2=6.51 Hz, 4 H), 4.85 - 5.09 (m, 4 H), 5.66 - 5.95 (m, 2 H); ^{13}C NMR ($CDCl_3$): δ (ppm) 18.10, 24.22, 24.98, 29.18, 29.44, 29.69, 29.82, 29.93, 30.07, 34.02, 36.82, 36.95, 39.62, 114.25 (vinyl CH_2), 126.34 (-CN), 139.46 (vinyl CH); EI/HRMS: $[M]^+$ calculated for $C_{43}H_{81}N$: 611.6364, found: 611.6314. Elemental analysis calculated for $C_{43}H_{81}N$: 84.37 C, 13.37 H, 2.29 N; found: 84.24 C, 13.65 H, 2.38 N.

Synthesis of 2-ethyl-2-(icos-19-en-1-yl)docos-21-enenitrile (4-26b). The same procedure described above for the synthesis of compound **4-26a** was followed. After

purification, 0.439 g of compound **4-26b** was collected as white crystals (Yield=86%). The following spectral properties were observed; ^{1}H NMR ($CDCl_3$) δ ppm 1.00 (t, J=7.36 Hz, 3H), 1.18 - 1.44 (br, 70 H), 2.04 (td, J_1=7.65 Hz, J_2=6.51 Hz, 4 H), 4.87 - 5.08 (m, 4 H), 5.69 – 6.11 (m, 2 H); ^{13}C NMR ($CDCl_3$): δ (ppm) 24.53, 24.93, 29.14, 29.40, 29.69, 29.82, 29.95, 33.96, 34.09, 35.77, 41.33, 114.29 (vinyl CH_2), 124.51 (-CN), 139.52 (vinyl CH); EI/HRMS: $[M]^+$ calculated for $C_{44}H_{83}N$: 626.6598, found: 626.6611. Elemental analysis calculated for $C_{44}H_{83}N$: 84.40 C, 13.36 H, 2.22 N; found: 83.53 C, 13.23 H, 2.22 N.

Synthesis of 2-propyl-2-(icos-19-en-1-yl)docos-21-enenitrile (4-26c). The same procedure described above for the synthesis of compound **4-26a** was followed. After purification, 0.543 g of compound **4-26c** was collected as white crystals (Yield = 73%). The following spectral properties were observed; ^{1}H NMR ($CDCl_3$) δ ppm 0.96 (t, *J*=6.79 Hz, 3 H), 1.19-1.45 (br, 72 H), 2.05 (td, J_1=7.63 Hz, J_2=6.50 Hz, 4 H), 4.88 - 5.07 (m, 4 H), 5.72 - 5.94 (m, 2 H); ^{13}C NMR ($CDCl_3$): δ (ppm) 14.42, 15.80, 16.63, 24.50, 29.19, 29.33, 29.88, 30.02, 34.02, 34.16, 36.37, 40.79, 114.24 (vinyl CH_2), 124.74 (-CN), 139.51 (vinyl CH); EI/HRMS: $[M]^+$ calculated for $C_{45}H_{85}N$: 640.9755, found: 640.6762. Elemental analysis calculated for $C_{45}H_{85}N$: 84.43 C, 13.38 H, 2.19 N; found: 84.58 C, 13.19 H, 2.20 N.

Synthesis of 2-*iso*-propyl-2-(icos-19-en-1-yl)docos-21-enenitrile (4-26d). The same procedure described above for the synthesis of compound **4-26a** was followed. After purification, 0.569 g of compound **4-26d** was collected as white crystals (Yield = 83%). The following spectral properties were observed; ^{1}H NMR ($CDCl_3$) δ ppm 1.02 (d, *J*=6.80 Hz, 6 H), 1.16-1.44 (br, 72 H), 2.06 (td, J_1=7.64 Hz, J_2=6.52 Hz, 4 H), 4.88 - 5.07

(m, 4 H), 5.73 - 5.92 (m, 2 H); ^{13}C NMR ($CDCl_3$): δ (ppm) 14.45, 15.66, 16.64, 24.50, 29.21, 29.35, 29.90, 30.02, 34.04, 34.13, 35.63, 41.10, 114.29 (vinyl CH_2), 124.48 (-CN), 139.52 (vinyl CH); EI/HRMS: $[M]^+$ calculated for $C_{45}H_{85}N$: 640.6755, found: 640.6777. Elemental analysis calculated for $C_{45}H_{85}N$: 84.43 C, 13.38 H, 2.19 N; found: 84.21 C, 13.24 H, 2.16 N.

Synthesis of 2-*iso*-butyl-2-(icos-19-en-1-yl)docos-21-enenitrile (4-26f). The same procedure described above for the synthesis of compound **4-26a** was followed. After purification, 0.435 g of compound **4.26f** was collected as white crystals (Yield = 56%). The following spectral properties were observed; ^{1}H NMR ($CDCl_3$) δ ppm 1.07 (d, *J*=6.79 Hz, 6 H), 1.13-1.48 (s, 74 H), 2.04 (td, J_1=7.65 Hz, J_2=6.50 Hz, 4 H), 4.88 - 5.09 (m, 4 H), 5.73 - 5.92 (m, 2 H); ^{13}C NMR ($CDCl_3$): δ (ppm) 23.27, 23.31, 25.51, 25.62, 26.71, 29.13, 29.35, 29.68, 29.79, 30.01, 30.34, 30.45, 34.07, 35.06, 35.17, 44.07, 44.18, 114.24 (vinyl CH_2), 124.73 (-CN), 139.50 (vinyl CH); EI/HRMS: $[M]^+$ calculated for $C_{46}H_{87}N$: 654.6911, found: 654.6911. Elemental analysis calculated for $C_{46}H_{87}N$: 84.45 C, 13.40 H, 2.14 N; found: 84.47 C, 13.32 H, 2.17 N.

Synthesis of 2-butyl-2-(icos-19-en-1-yl)docos-21-enenitrile (4-26e). The same procedure described above for the synthesis of compound **4-26a** was followed. After purification, 0.435 g of compound **4-26e** was collected as white crystals (Yield = 85%). The following spectral properties were observed; ^{1}H NMR ($CDCl_3$) δ (ppm) 0.94 (t, J=6.79, 3H), 1.20-1.35 (m, 74H), 2.05 (td, J_1=7.63 Hz, J_2=6.51 Hz, 4 H), 4.91-5.04 (m, 4H), 5.78-5.87 (m, 2H) ; ^{13}C NMR ($CDCl_3$) : δ (ppm) 14.14, 23.11, 24.49, 26.66, 29.18, 29.39, 29.58, 29.66, 29.74, 29.85, 29.92, 34.05, 36.33, 40.83, 114.29 (vinyl CH_2), 129.92 (-CN), 139.50 (vinyl CH); EI/HRMS: $[M]^+$ calculated for $C_{46}H_{87}N$: 653.6839,

found: 653.6917. Elemental analysis calculated for $C_{46}H_{87}N$: 84.45 C, 13.40 H, 2.14 N; found: 84.47 C, 13.38 H, 2.17 N.

Synthesis of 2-pentyl-2-(icos-19-en-1-yl)docos-21-enenitrile (4-26g). The same procedure described above for the synthesis of compound **4-26a** was followed. After purification, 0.435 g of compound **4-26g** was collected as white crystals (Yield = 42%). The following spectral properties were observed; ^{1}H NMR ($CDCl_3$) δ ppm 0.91 (t, *J*=6.80 Hz, 3 H), 1.14 - 1.47 (m, 76 H), 2.05 (td, J_1=7.64 Hz, J_2=6.51 Hz, 4 H), 4.86 - 5.08 (m, 4 H), 5.72 - 5.92 (m, 2 H); ^{13}C NMR ($CDCl_3$): δ (ppm) 14.23, 22.64, 24.11, 24.25, 24.51, 26.52, 29.05, 29.19, 29.32, 29.59, 29.72, 29.99, 32.12, 33.99, 36.26, 40.80, 114.25 (vinyl CH_2), 124.80 (-CN), 139.49 (vinyl CH); EI/HRMS: $[M]^+$ calculated for $C_{47}H_{89}N$: 668.7068, found: 668.7098. Elemental analysis calculated for $C_{47}H_{89}N$: 84.48 C, 13.42 H, 2.10 N; found: 84.66 C, 13.32 H, 2.23 N.

Synthesis of 2-hexyl-2-(icos-19-en-1-yl)docos-21-enenitrile (4-26h). The same procedure described above for the synthesis of compound **4-26a** was followed. After purification, 0.581 g of compound **4-26h** was collected as white crystals (Yield = 70%). The following spectral properties were observed; ^{1}H NMR ($CDCl_3$) δ ppm 0.88 (t, J=6.79, 3 H), 1.10 - 1.45 (br, 78 H), 2.04 (td, J_1=7.63 Hz, J_2=6.51 Hz, 4 H), 4.85 - 5.08 (m, 4 H), 5.68 - 5.95 (m, 2 H); ^{13}C NMR ($CDCl_3$): δ (ppm) 14.40, 22.87, 22.99, 26.57, 26.69, 26.93, 29.08, 29.20, 29.44, 29.68, 29.79, 29.91, 30.39, 32.66, 33.85, 33.97, 34.09, 37.55, 37.67, 114.30 (vinyl CH_2), 124.80 (-CN), 139.48 (vinyl CH); EI/HRMS: $[M]^+$ calculated for $C_{48}H_{91}N$: 682.7224, found: 682.7241. Elemental analysis calculated for $C_{48}H_{91}N$: 84.50 C, 13.44 H, 2.05 N; found: 84.53 C, 13.45 H, 2.19 N.

Synthesis of 2-heptyl-2-(icos-19-en-1-yl)docos-21-enenitrile (4-26i). The same procedure described above for the synthesis of compound **4-26a** was followed. After purification, 0.581 g of compound **4-26i** was collected as white crystals (Yield = 38%). The following spectral properties were observed; ^{1}H NMR δ ppm 0.87 (t, *J*=6.80 Hz, 3 H), 1.06 - 1.43 (m, 80 H), 2.05 (td, J_1=7.60 Hz, J_2=6.54 Hz, 4 H), 4.86 - 5.08 (m, 4 H), 5.72 - 5.93 (m, 2 H); ^{13}C NMR ($CDCl_3$): δ (ppm) 14.83, 20.06, 20.46, 20.60, 26.89, 29.17, 29.31, 29.44, 29.71, 29.84, 29.98, 30.38, 32.79, 33.86, 34.00, 37.35, 37.48, 49.41, 114.26 (vinyl CH_2), 124.31 (-CN), 139.45 (vinyl CH); EI/HRMS: $[M]^+$ calculated for $C_{49}H_{93}N$: 696.7381, found: 696.7402. Elemental analysis calculated for $C_{49}H_{93}N$: 84.53 C, 13.46 H, 2.01 N; found: 83.65 C, 13.40 H, 1.98 N.

Synthesis of 2-octyl-2-(icos-19-en-1-yl)docos-21-enenitrile (4-26j). The same procedure described above for the synthesis of compound **4-26a** was followed. After purification, 0.581 g of compound **4-26j** was collected as white crystals (Yield = 95%). The following spectral properties were observed; ^{1}H NMR δ ppm 0.88 (t, *J*=6.79 Hz, 3 H), 1.11 - 1.41 (m, 82 H), 2.06 (td, J_1=7.64 Hz, J_2=6.49 Hz, 4 H), 4.88 - 5.11 (m, 4 H), 5.74 - 5.98 (m, 2 H); ^{13}C NMR ($CDCl_3$): δ (ppm) 14.97, 20.09, 20.38, 20.55, 26.89, 29.15, 29.44, 29.48, 29.71, 29.94, 29.92, 30.33, 32.88, 33.97, 37.40, 48.44, 114.30 (vinyl CH_2), 124.34 (-CN), 139.50 (vinyl CH); EI/HRMS: $[M]^+$ calculated for $C_{50}H_{95}N$: 710.7537, found: 710.7554. Elemental analysis calculated for $C_{50}H_{95}N$: 84.55 C, 13.48 H, 1.97 N; found: 84.54 C, 13.42 H, 2.06 N.

Synthesis of dodecanenitrile (4-25k). In a flame-dried 250 ml three neck round bottomed flask equipped with reflux condenser and stir bar, 1-bromodecane (10.89 g, 49.25 mmol) was added and dissolved in 35 mL of anhydrous DMF. Sodium cyanide

(3.088 g, 63.00 mmol) was dissolved in 50 mL anhydrous DMF and added to the 1-bromodecane solution in one portion under Ar flow. The reaction mixture was stirred for 24 hours at 65^{o}C and then quenched with 100 mL DI water. The organic phase was extracted with Et_2O (3x50 mL) and dried over $MgSO_4$. The crude product was filtered, concentrated, and further purified via column chromatography with hexane/EtOAc 9/1 as eluent to give dodecanenitrile (5.29 g, 31.64 mmol) as a colorless oil (Yield = 64%). The following spectral properties were observed; ^{1}H NMR ($CDCl_3$) δ ppm 0.87 (t, *J*=6.80 Hz, 3 H), 1.26 (br. s., 12 H), 1.37 - 1.51 (m, 2 H), 1.56 - 1.72 (m, 2 H), 2.32 (t, *J*=7.08 Hz, 2 H); ^{13}C NMR ($CDCl_3$) δ ppm 14.04, 17.05, 22.64, 25.37, 28.63, 28.75, 29.25, 29.30, 29.45, 31.84, 119.76 (-CN); EI/HRMS: $[M+NH_4]^+$ calculated for $C_{12}H_{23}N$: 185.2012, found: 185.2018. Elemental analysis calculated for $C_{12}H_{23}N$: 78.97 C, 12.65 H, 8.37 N; found: 79.03 C, 12.74 H, 8.30 N.

Synthesis of 2-nonyl-2-(icos-19-en-1-yl)docos-21-enenitrile (4-26k). The same procedure described above for the synthesis of compound **4-26a** was followed using the dodecanenitrile synthesized from 1-bromodecane. After purification, 0.659 g of compound **4-26k** was collected as white crystals (Yield = 78%). The following spectral properties were observed; ^{1}H NMR δ ppm 0.89 (t, *J*=6.80 Hz, 3 H), 1.14 - 1.47 (m, 84 H), 2.04 (td, J_1=7.62 Hz, J_2=6.56 Hz, 4 H), 4.86 - 5.08 (m, 4 H), 5.71 - 5.94 (m, 2 H); ^{13}C NMR ($CDCl_3$): δ (ppm) 14.23, 22.65, 24.18, 24.24, 24.56, 26.50, 29.02, 29.24, 29.33, 29.61, 29.80, 29.97, 32.16, 33.92, 36.28, 40.84, 114.24 (vinyl CH_2), 124.81 (-CN), 139.50 (vinyl CH); EI/HRMS: $[M]^+$ calculated for $C_{51}H_{97}N$: 724.7694, found: 724.7710. Elemental analysis calculated for $C_{51}H_{97}N$: 84.57 C, 13.50 H, 1.93 N; found: 84.75 C, 13.61 H, 1.98 N.

Synthesis of 2-decyl-2-(icos-19-en-1-yl)docos-21-enenitrile (4-26l). The same procedure described above for the synthesis of compound **4-26a** was followed. After purification, 0.553 g of compound **4-26l** was collected as white crystals (Yield = 56%). The following spectral properties were observed; ^{1}H NMR ($CDCl_3$) δ ppm 0.91 (t, *J*=6.79 Hz, 3 H), 1.12 - 1.45 (m, 86 H), 2.06 (td, J_1=7.63 Hz, J_2=6.58 Hz, 4 H), 4.84 - 5.06 (m, 4 H), 5.72 - 5.95 (m, 2 H); ^{13}C NMR ($CDCl_3$): δ (ppm) 14.21, 22.67, 24.19, 24.22, 24.58, 26.52, 29.04, 29.20, 29.35, 29.63, 29.84, 29.94, 32.18, 33.94, 36.28, 40.85, 114.25 (vinyl CH_2), 124.80 (-CN), 139.49 (vinyl CH); EI/HRMS: $[M]^+$ calculated for $C_{52}H_{99}N$: 738.7850, found: 738.7881. Elemental analysis calculated for $C_{52}H_{99}N$: 84.59 C, 13.51 H, 1.90 N; found: 84.82 C, 13.60 H, 2.00 N.

Synthesis of 2-pentadecyl-2-(icos-19-en-1-yl)docos-21-enenitrile (4-26m). The same procedure described above for the synthesis of compound **7a** was followed. After purification, 0.737 g of compound **7m** was collected as white crystals (Yield = 65%). The following spectral properties were observed; ^{1}H NMR ($CDCl_3$) δ ppm 0.90 (d, *J*=6.79 Hz, 3 H), 1.10 - 1.46 (m, 96 H), 2.05 (td, J_1=7.61 Hz, J_2=6.51 Hz, 4 H), 4.85 - 5.09 (m, 4 H), 5.75 - 5.90 (m, 2 H); ^{13}C NMR ($CDCl_3$): δ ppm 14.34, 22.92, 26.93, 29.18, 29.39, 29.59, 29.74, 29.85, 29.90, 29.94, 30.38, 32.16, 33.92, 34.05, 37.61, 114.28 (vinyl CH_2), 124.79 (-CN), 139.49 (vinyl CH); EI/HRMS: $[M]^+$ calculated for $C_{57}H_{109}N$: 808.8639, found: 808.8655. Elemental analysis calculated for $C_{57}H_{109}N$: 84.68 C, 13.59 H, 1.73 N; found: 84.81 C, 13.33 H, 1.82 N.

Synthesis of 21-methylhentetraconta-1,40-diene (4-27a). Potassium metal (0.45 g, 11.5 mmol), HMPA (0.9 mL, 6.76 mmol), and diethyl ether (20 mL) were transferred to a 100 mL 3 necked round bottomed flask equipped with a stir bar, addition funnel,

and argon inlet adaptor. A solution of the alkylcyano α,ω-diolefin **4-26a** (0.861 g, 1.34 mmol) and t-BuOH (0.6 mL, 10.38 mmol) in diethyl ether (20 mL) was added dropwise to the reactor at 0^{o}C. The reaction mixture was warmed to RT and stirred for 25 hours. The reaction was quenched with isopropanol (20 mL), extracted three times with diethyl ether (3x50 mL), washed with brine (50 mL) and dried over $MgSO_4$. The solution was filtered, concentrated by rotary evaporation and purified by column chromatograhy using hexane as the eluent. Compound **4-27a** was collected as white crystals (0.659 g, 1.12 mmol). (Yield= 84%) The following spectral properties were observed; ^{1}H NMR ($CDCl_3$) δ ppm 0.84 (d, *J*=6.20 Hz, 3 H), 1.27 (br, 68 H), 2.05 (td, J_1=7.64 Hz, J_2=6.51 Hz, 4 H), 4.83 - 5.10 (m, 4 H), 5.71 - 5.94 (m, 2 H) ^{13}C NMR ($CDCl_3$): δ ppm 19.95, 27.31, 29.18, 29.39, 29.74, 29.85, 29.93, 30.26, 34.05, 37.32, 114.28 (vinyl CH_2), 139.51 (vinyl CH). Elemental analysis calculated for $C_{42}H_{82}$: 85.92 C, 14.08 H; found: 85.78 C, 14.24 H.

Synthesis of 21-ethylhentetraconta-1,40-diene (4-27b). The same procedure described above for the synthesis of compound **4-27a** was followed. After purification, 0.519 g of compound **4-27b** was collected as white crystals (Yield = 95%) The following spectral properties were observed; ^{1}H NMR ($CDCl_3$); δ ppm 0.90 (t, *J*=6.80 Hz, 3 H), 1.05 - 1.45 (m, 70 H), 2.04 (td, J_1=7.65 Hz, J_2=6.51 Hz, 4 H), 4.84 - 5.09 (m, 4 H), 5.74 - 5.90 (m, 2 H) ^{13}C NMR ($CDCl_3$): δ ppm 14.36, 22.96, 26.61, 26.93, 29.19, 29.39, 29.75, 29.86, 29.90, 29.94, 30.39, 32.63, 33.89, 33.92, 34.05, 37.63, 114.28 (vinyl CH_2), 139.49 (vinyl CH). Elemental analysis calculated for $C_{43}H_{84}$: 85.92 C, 14.08 H; found: 86.08 C, 14.09 H.

Synthesis of 21-propylhentetraconta-1,40-diene (4-27c). The same procedure described above for the synthesis of compound **4-27a** was followed. After purification,

0.349 g of compound **4-27c** was collected as white crystals (Yield = 76%) The following spectral properties were observed; ^{1}H NMR ($CDCl_3$) δ ppm 0.96 (t, *J*=6.80 Hz, 3 H), 1.27 (s, 34 H), 2.05 (td, J_1=7.63 Hz, J_2=6.50 Hz, 4 H), 4.83 - 5.10 (m, 4 H), 5.70 - 5.94 (m, 2 H) ^{13}C NMR ($CDCl_3$) δ ppm 14.47, 17.90, 24.50, 29.18, 29.38, 29.66, 29.74, 29.85, 29.92, 34.05, 36.36, 40.86, 114.28 (vinyl CH_2), 139.49 (vinyl CH). Elemental analysis calculated for $C_{44}H_{86}$: 85.91 C, 14.09 H; found: 86.04 C, 14.10 H.

Synthesis of 21-iso-propylhentetraconta-1,40-diene (4-27d). The same procedure described above for the synthesis of compound **4-27a** was followed. After purification, 0.473 g of compound **4-27d** was collected as white crystals (Yield = 82%) The following spectral properties were observed; ^{1}H NMR ($CDCl_3$) δ ppm 0.82 (d, *J*=6.50 Hz, 6 H), 1.27 (s, 72 H), 2.06 (td, J_1=7.64 Hz, J_2=6.52 Hz, 4 H), 4.80 - 5.13 (m, 4 H), 5.71 - 5.95 (m, 2 H) ^{13}C NMR ($CDCl_3$) δ ppm 19.43, 27.99, 29.18, 29.39, 29.74, 29.94, 30.41, 30.75, 34.05, 43.91, 114.28 (vinyl CH_2), 139.51 (vinyl CH). Elemental analysis calculated for $C_{44}H_{86}$: 85.91 C, 14.09 H; found: 86.11 C, 14.18 H.

Synthesis of 21-butylhentetraconta-1,40-diene (4-27e). The same procedure described above for the synthesis of compound **4-27a** was followed. After purification, 0.229 g of compound **4-27e** was collected as white crystals (Yield = 98%) The following spectral properties were observed; ^{1}H NMR ($CDCl_3$): δ (ppm) 0.91 (t, J=6.79, 3H), 1.24-1.41 (br, 74H), 2.05 (td, J_1=7.63 Hz, J_2=6.51 Hz, 4 H), 4.91-5.04 (m, 4H), 5.78-5.87 (m, 2H) ; ^{13}C NMR ($CDCl_3$) : δ (ppm) 14.42, 23.43, 26.97, 29.22, 29.43, 29.42, 29.79, 29.90, 29.98, 30.43, 33.65, 33.96, 37.64, 114.31 (vinyl CH_2), 139.45 (vinyl CH); Elemental analysis calculated for $C_{45}H_{88}$: 85.90 C, 14.10 H; found: 85.93 C, 14.06 H.

Synthesis of 21-*iso*-butylhentetraconta-1,40-diene (4-27f). The same procedure described above for the synthesis of compound **4-27a** was followed. After purification, 0.329 g of compound **4-27f** was collected as white crystals (Yield = 71%) The following spectral properties were observed; ^{1}H NMR ($CDCl_3$) δ ppm 0.86 (d, *J*=6.51 Hz, 6 H), 1.27 (s, 74 H), 2.04 (td, J_1=7.65 Hz, J_2=6.50 Hz, 4 H), 4.85 - 5.11 (m, 4 H), 5.70 - 5.94 (m, 2 H); ^{13}C NMR ($CDCl_3$) δ ppm 23.23, 25.53, 26.70, 29.18, 29.40, 29.75, 29.86, 29.94, 30.41, 34.05, 34.10, 35.13, 44.11, 114.29 (vinyl CH_2), 139.49 (vinyl CH). Elemental analysis calculated for $C_{45}H_{88}$: 85.90 C, 14.10 H; found: 86.17 C, 14.02 H.

Synthesis of 21-pentylhentetraconta-1,40-diene (4-27g). The same procedure described above for the synthesis of compound **4-27a** was followed. After purification, 0.265 g of compound **4-27g** was collected as white crystals (Yield = 85%) The following spectral properties were observed; ^{1}H NMR ($CDCl_3$) δ ppm 0.91 (t, *J*=6.79 Hz, 3 H), 1.14 - 1.47 (m, 76 H), 2.05 (td, J_1=7.64 Hz, J_2=6.51 Hz, 4 H), 4.86 - 5.08 (m, 4 H), 5.72 - 5.92 (m, 2 H); ^{13}C NMR ($CDCl_3$) δ ppm 14.36, 22.95, 26.60, 26.92, 29.18, 29.39, 29.74, 29.85, 29.94, 30.38, 32.62, 33.91, 34.05, 37.62, 114.28 (vinyl CH_2), 139.49 (vinyl CH). Elemental analysis calculated for $C_{45}H_{88}$: 85.90 C, 14.10 H; found: 86.00 C, 14.04 H.

Synthesis of 21-hexylhentetraconta-1,40-diene (4-27h). The same procedure described above for the synthesis of compound **4-27a** was followed. After purification, 0.416 g of compound **4-27h** was collected as white crystals (Yield = 88%) The following spectral properties were observed; ^{1}H NMR ($CDCl_3$) δ ppm 0.89 (t, *J*=6.80 Hz, 3 H), 1.27 (br, 78 H), 2.04 (td, J_1=7.63 Hz, J_2=6.51 Hz, 4 H), 4.87 - 5.07 (m, 4 H), 5.74 - 5.91 (m, 2 H); ^{13}C NMR ($CDCl_3$) δ ppm 14.35, 22.94, 26.92, 29.18, 29.39, 29.74, 29.85, 29.90, 29.93, 30.06, 30.38, 32.19, 33.92, 33.94, 34.05, 37.62, 114.28 (vinyl CH_2),

139.49 (vinyl CH). Elemental analysis calculated for $C_{46}H_{90}$: 85.89 C, 14.11 H; found: 86.00 C, 14.17 H.

Synthesis of 21-heptylhentetraconta-1,40-diene (4-27i). The same procedure described above for the synthesis of compound **4-27a** was followed. After purification, 0.262 g of compound **4-27i** was collected as white crystals (Yield = 93%) The following spectral properties were observed; ^{1}H NMR ($CDCl_3$) δ ppm 0.88 (t, *J*=6.80 Hz, 3 H), 1.26 (br, 80 H), 2.05 (td, J_1=7.60 Hz, J_2=6.54 Hz, 4 H), 4.85 - 5.09 (m, 4 H), 5.70 - 5.91 (m, 2 H); ^{13}C NMR ($CDCl_3$) δ ppm 14.35, 22.93, 26.93, 29.18, 29.39, 29.62, 29.74, 29.85, 29.94, 30.38, 32.17, 33.92, 34.05, 37.62, 114.28 (vinyl CH_2), 139.50 (vinyl CH). Elemental analysis calculated for $C_{48}H_{94}$: 85.89 C, 14.11 H; found: 85.63 C, 14.25 H.

Synthesis of 21-octylhentetraconta-1,40-diene (4-27j). The same procedure described above for the synthesis of compound **4-27a** was followed. After purification, 0.452 g of compound **4-27j** was collected as white crystals (Yield = 85%) The following spectral properties were observed; ^{1}H NMR ($CDCl_3$) δ ppm 0.89 (t, *J*=6.80 Hz, 3 H), 1.27 (br, 82 H), 2.06 (td, J_1=7.64 Hz, J_2=6.49 Hz, 4 H), 4.82 - 5.12 (m, 4 H), 5.69 - 6.00 (m, 2 H); ^{13}C NMR ($CDCl_3$) δ ppm 14.35, 22.92, 26.92, 29.18, 29.38, 29.60, 29.74, 29.85, 29.94, 30.38, 32.16, 33.92, 34.05, 37.61, 114.29 (vinyl CH_2), 139.51 (vinyl CH). Elemental analysis calculated for $C_{49}H_{96}$: 85.88 C, 14.12 H; found: 85.84 C, 13.98 H.

Synthesis of 21-nonylhentetraconta-1,40-diene (4-27k). The same procedure described above for the synthesis of compound **4-27a** was followed. After purification, 0.452 g of compound **4-27k** was collected as white crystals (Yield = 85%). The following spectral properties were observed; ^{1}H NMR ($CDCl_3$) δ ppm 0.89 (t, *J*=6.80 Hz, 3 H), 1.04 - 1.45 (br, 84 H), 2.04 (td, J_1=7.62 Hz, J_2=6.56 Hz, 4 H), 4.86 - 5.07 (m, 3 H), 5.73 -

5.91 (m, 1 H); ^{13}C NMR ($CDCl_3$) δ ppm 14.35, 22.92, 26.93, 29.19, 29.39, 29.60, 29.74, 29.85, 29.90, 29.94, 30.38, 32.16, 33.92, 34.05, 37.62, 114.28 (vinyl CH_2), 139.50 (vinyl CH). Elemental analysis calculated for $C_{50}H_{98}$: 85.87 C, 14.13 H; found: 85.79 C, 14.20 H.

Synthesis of 21-decylhentetraconta-1,40-diene (4-27l). The same procedure described above for the synthesis of compound **4-27a** was followed. After purification, 0.425 g of compound **4-27l** was collected as white crystals (Yield = 84%) The following spectral properties were observed; ^{1}H NMR ($CDCl_3$) δ ppm 0.88 (t, *J*=6.80 Hz, 3 H), 1.27 (br, 86 H), 2.06 (td, J_1=7.63 Hz, J_2=6.58 Hz, 4 H), 4.83 - 5.10 (m, 4 H), 5.70 - 5.95 (m, 2 H); ^{13}C NMR ($CDCl_3$) δ ppm 14.36, 22.93, 26.93, 29.19, 29.40, 29.60, 29.75, 29.86, 29.94, 30.39, 32.16, 33.92, 34.06, 37.61, 114.29 (vinyl CH_2), 139.50 (vinyl CH). Elemental analysis calculated for $C_{51}H_{100}$: 85.87 C, 14.13 H; found: 85.64 C, 14.27 H.

Synthesis of 21-pentadecylhentetraconta-1,40-diene (4-27m). The same procedure described above for the synthesis of compound **4-27a** was followed. After purification, 0.437 g of compound **4-27m** was collected as white crystals (Yield = 90%) The following spectral properties were observed; ^{1}H NMR ($CDCl_3$) δ ppm 0.87 (t, *J*=6.80 Hz, 3 H), 1.27 (br, 96 H), 2.05 (td, J_1=7.61 Hz, J_2=6.51 Hz, 4 H), 4.86 - 5.07 (m, 4 H), 5.73 - 5.91 (m, 2 H); ^{13}C NMR ($CDCl_3$) δ ppm 14.34, 22.92, 26.93, 29.18, 29.39, 29.59, 29.74, 29.85, 29.90, 29.94, 30.38, 32.16, 33.92, 34.05, 37.61, 114.28 (vinyl CH_2), 139.49 (vinyl CH). Elemental analysis calculated for $C_{56}H_{110}$: 85.85 C, 14.15 H; found: 85.72 C, 14.22 H.

Polymerization of 21-methylhentetraconta-1,40-diene (4-28a). Monomer **4-27a** (0.335 g, 0.57 mmol) was placed in a 25 ml flame dried Schlenk tube under Ar and

heated to 75^{o}C using an oil bath and high vacuum (10^{-5} torr). After 2 hours of stirring at these conditions, the monomer was cooled to room temperature and the Schlenk tube was placed into the glove box. Schrock catalyst, (0.9 mg, 1.17 x 10^{-3} mmol; catalyst to monomer ratio = 1:500) was added, the Schlenk tube was removed from the glove box and connected to high vacuum. Polymerization was initiated by melting the monomer at 50^{o}C and the temperature was set to 85^{o}C to enable stirring of the viscous polymer melt. After 24 hours, the polymer was cooled to RT and another 0.9 mg portion of Schrock catalyst was added in the glove box. After 24 hours, the Schlenk tube was opened to air and the polymer was dissolved in 5 mL of toluene. The polymer solution was poured into acidic methanol to precipitate the polymer. The polymer was filtered, re-dissolved and re-precipitated two more times to remove the traces of catalyst. Compound **4-28a** (0.295 g) was recovered as a white solid (yield=92%). The following spectral properties were observed; ^{1}H NMR (300 MHz, C_6D_6) δ ppm 0.97 (d, *J*=6.20 Hz, 3 H), 1.38 (br, 68 H), 1.96 - 2.24 (m, 4 H), 5.38 - 5.64 (m, 2 H); ^{13}C NMR (75 MHz, C_6D_6) δ ppm 26.06, 27.97, 29.99, 30.54, 30.90, 33.43, 33.67, 37.18, 38.00, 131.16.

Polymerization of 21-ethylhentetraconta-1,40-diene (4-28b). The same procedure described above for the synthesis of polymer **4-28a** was followed. After purification, 0.320 g of compound **4-28b** was collected (Yield = 87%) The following spectral properties were observed; ^{1}H NMR (500 MHz, $CDCl_3$) δ ppm 0.89 (t, *J*=6.80 Hz, 3 H), 1.06 - 1.44 (br, 70 H), 1.88 - 2.09 (m, 4 H), 5.28 - 5.46 (m, 2 H); ^{13}C NMR (126 MHz, $CDCl_3$) δ ppm 14.36, 22.96, 26.61, 26.94, 27.44, 29.42, 29.56, 29.77, 29.8, 29.90, 29.95, 30.01, 30.40, 32.63, 32.84, 33.88, 33.93, 37.63, 130.11, 130.57.

Polymerization of 21-propylhentetraconta-1,40-diene (4-28c). The same procedure described above for the synthesis of polymer **4-28a** was followed. After purification, 0.320 g of compound **4-28c** was collected (Yield = 92%) The following spectral properties were observed; ^{1}H NMR (299 MHz, $CDCl_3$) δ ppm 0.89 (t, *J*=6.20 Hz, 3 H), 1.27 (br, 72 H), 1.85 - 2.14 (m, 4 H), 5.28 - 5.51 (m, 2 H); ^{13}C NMR (75 MHz, $CDCl_3$) δ ppm 14.79, 20.05, 26.93, 29.42, 29.78, 29.95, 30.41, 32.84, 33.93, 36.35, 37.41, 130.57.

Polymerization of 21-*iso*-propylhentetraconta-1,40-diene (4-28d). The same procedure described above for the synthesis of polymer **4-28a** was followed. After purification, 0.320 g of compound **4-28d** was collected (Yield = 90%) The following spectral properties were observed; ^{1}H NMR (299 MHz, $CDCl_3$) δ ppm 0.81 (d, *J*=6.50 Hz, 6 H), 1.26 (br, 70 H), 1.85 - 2.11 (m, 4 H), 5.28 - 5.48 (m, 2 H); ^{13}C NMR (75 MHz, $CDCl_3$) δ ppm 19.43, 28.00, 29.42, 29.78, 29.95, 30.42, 30.75, 32.84, 43.92, 130.58.

Polymerization of 21-butylhentetraconta-1,40-diene (4-28e). The same procedure described above for the synthesis of polymer **4-28a** was followed. After purification, 0.270 g of compound **4-28e** was collected (Yield = 90%) The following spectral properties were observed; ^{1}H NMR (299 MHz, $CDCl_3$) δ ppm 0.90 (t, *J*=6.80 Hz, 3 H), 1.01 - 1.49 (br, 74 H), 1.86 - 2.13 (m, 4 H), 5.25 - 5.47 (m, 2 H); ^{13}C NMR (75 MHz, $CDCl_3$) δ ppm 14.40, 23.40, 26.94, 29.41, 29.77, 29.95, 30.40, 32.84, 33.93, 37.60, 130.57.

Polymerization of 21-*iso*-butylhentetraconta-1,40-diene (4-28f). The same procedure described above for the synthesis of polymer **4-28a** was followed. After purification, 0.270 g of compound **4-28f** was collected (Yield = 83%) The following

spectral properties were observed; ^{1}H NMR (299 MHz, $CDCl_3$) δ ppm 0.86 (d, *J*=6.50 Hz, 6 H), 1.27 (br, 74 H), 1.85 - 2.13 (m, 4 H), 5.25 - 5.50 (m, 2 H); ^{13}C NMR (75 MHz, $CDCl_3$) δ ppm 23.23, 25.53, 26.71, 29.41, 29.56, 29.78, 29.95, 30.41, 32.84, 34.11, 35.13, 44.10, 130.11, 130.57.

Polymerization of 21-pentylhentetraconta-1,40-diene (4-28g). The same procedure described above for the synthesis of polymer **4-28a** was followed. After purification, 0.298 g of compound **4-28g** was collected (Yield = 89%) The following spectral properties were observed; ^{1}H NMR (500 MHz, $CDCl_3$) ppm 0.83 (t, *J*=6.80 Hz, 3 H), 1.27 (br, 76 H), 1.86 - 2.10 (m, 4 H), 5.27 - 5.48 (m, 2 H); ^{13}C NMR (126 MHz, $CDCl_3$) ppm 11.11, 26.13, 26.98, 27.44, 29.42, 29.56, 29.77, 29.81, 29.90, 29.95, 30.40, 32.84, 33.45, 39.09, 130.12, 130.58.

Polymerization of 21-hexylhentetraconta-1,40-diene (4-28h). The same procedure described above for the synthesis of polymer **4-28a** was followed. After purification, 0.233 g of compound **4-28h** was collected (Yield = 84%) The following spectral properties were observed; ^{1}H NMR (500 MHz, $CDCl_3$) δ ppm 0.89 (t, *J*=6.80 Hz, 3 H), 1.03 - 1.46 (br, 78 H), 1.85 - 2.10 (m, 4 H), 5.29 - 5.48 (m, 2 H); ^{13}C NMR (126 MHz, $CDCl_3$) δ ppm 14.38, 22.97, 26.94, 26.97, 27.47, 29.44, 29.59, 29.81, 29.84, 29.93, 29.98, 30.10, 30.43, 32.19, 32.22, 32.87, 33.96, 37.66, 130.14, 130.60.

Polymerization of 21-heptylhentetraconta-1,40-diene (4-28i). The same procedure described above for the synthesis of polymer **4-28a** was followed. After purification, 0.165 g of compound **4-28i** was collected (Yield = 88%) The following spectral properties were observed; ^{1}H NMR (500 MHz, $CDCl_3$) δ ppm 0.88 (t, *J*=6.80 Hz, 3 H), 1.26 (br, 80 H), 1.87 - 2.10 (m, 4 H), 5.26 - 5.47 (m, 2 H); ^{13}C NMR (126 MHz,

$CDCl_3$) δ ppm 14.35, 22.93, 26.94, 27.45, 29.42, 29.56, 29.63, 29.78, 29.90, 29.96, 30.36, 30.40, 32.18, 32.84, 33.94, 37.63, 130.11, 130.57.

Polymerization of 21-octylhentetraconta-1,40-diene (4-28j). The same procedure described above for the synthesis of polymer **4-28a** was followed. After purification, 0.232 g of compound **4-28j** was collected (Yield = 90%) The following spectral properties were observed; ^{1}H NMR (500 MHz, $CDCl_3$) δ ppm 0.91 (t, *J*=6.80 Hz, 3 H), 1.29 (br, 82 H), 1.88 - 2.13 (m, 4 H), 5.28 - 5.50 (m, 2 H); ^{13}C NMR (126 MHz, $CDCl_3$) δ ppm 14.24, 22.92, 27.10, 27.53, 29.46, 29.60, 29.80, 29.92, 29.98, 30.43, 32.20, 32.84, 34.21, 37.87, 130.16, 130.64.

Polymerization of 21-nonylhentetraconta-1,40-diene (4-28k). The same procedure described above for the synthesis of polymer **4-28a** was followed. After purification, 0.330 g of compound **4-28k** was collected (Yield = 90%) The following spectral properties were observed; ^{1}H NMR (500 MHz, $CDCl_3$) δ ppm 0.89 (t, *J*=6.80 Hz, 3 H), 1.27 (br, 84 H), 1.88 - 2.15 (m, 4 H), 5.29 - 5.52 (m, 2 H); ^{13}C NMR (75 MHz, $CDCl_3$) δ ppm 14.37, 22.96, 26.61, 26.94, 29.42, 29.78, 29.95, 30.40, 32.63, 32.84, 33.93, 37.63, 130.11, 130.58.

Polymerization of 21-decylhentetraconta-1,40-diene (4-28l). The same procedure described above for the synthesis of polymer **4-28a** was followed. After purification, 0.272 g of compound **4-28l** was collected (Yield = 71%) The following spectral properties were observed; ^{1}H NMR (500 MHz, $CDCl_3$) δ ppm 0.90 (t, *J*=6.80 Hz, 3 H), 1.02 - 1.46 (br, 86 H), 1.87 - 2.11 (m, 4 H), 5.25 - 5.49 (m, 2 H); ^{13}C NMR (126 MHz, $CDCl_3$) δ ppm 14.35, 22.93, 26.94, 27.44, 29.42, 29.56, 29.60, 29.78, 29.90, 29.96, 30.39, 32.16, 32.84, 33.94, 37.62, 130.11, 130.57.

Polymerization of 21-pentadecylhentetraconta-1,40-diene (4-28m). The same procedure described above for the synthesis of polymer **4-28a** was followed. After purification, 0.296 g of compound **4-28m** was collected (Yield = 86%) The following spectral properties were observed; ^{1}H NMR (500 MHz, $CDCl_3$) δ ppm 0.88 (t, *J*=6.80 Hz, 3 H), 1.27 (br, 96 H), 1.87 - 2.10 (m, 4 H), 5.29 - 5.49 (m, 2 H); ^{13}C NMR (126 MHz, $CDCl_3$) δ ppm 14.35, 22.92, 26.94, 29.42, 29.60, 29.78, 29.90, 29.96, 30.40, 32.16, 32.85, 33.94, 37.62, 130.10, 130.57.

Hydrogenation of methyl branched polymer (4-29a). In a 125 mL Parr bomb glass sleeve, unsaturated polymer **4-28a** (0.252 g) was dissolved in 40 mL degassed toluene. Wilkinson`s hydrogenation catalyst (0.7 mg, 7.6×10^{-4} mmol; catalyst to monomer ratio 1:250) was added and the bomb was charged with 900 psi of hydrogen. The reaction was allowed to proceed for three days at 90^{o}C. The polymer solution was concentrated and poured into acidic methanol and the resulting precipitate was then filtered and dissolved in 5 mL toluene. The polymer was re-dissolved and re-precipitated two more times to remove the traces of catalyst. Polymer **4-29a** (0.177 g) was collected as a white solid (yield=70%). The following spectral properties were observed; ^{1}H NMR (500 MHz, C_6D_6) δ ppm 0.96 (d, *J*=6.20 Hz, 3 H), 1.17 - 1.56 (br, 74 H); ^{13}C NMR (126 MHz, C_6D_6) δ ppm 19.84, 27.42, 29.99, 30.34, 33.12, 37.34.

Hydrogenation of ethyl branched polymer (4-29b). The same procedure described above for the synthesis of saturated polymer **4-29a** was followed. After purification, 0.273 g of polymer **4-29b** was collected (Yield = 96%) The following spectral properties were observed; ^{1}H NMR (500 MHz, C_6D_6) δ ppm 0.90 (t, *J*=6.80 Hz, 3 H), 1.28 (br, 76 H); ^{13}C NMR (126 MHz, C_6D_6) δ ppm 11.19, 26.44, 27.16, 29.99, 30.46, 33.76, 39.41.

Hydrogenation of propyl branched polymer (4-29c). The same procedure described above for the synthesis of saturated polymer **4-29a** was followed. After purification, 0.200 g of polymer **4-29c** was collected (Yield = 96%) The following spectral properties were observed; ^{1}H NMR (500 MHz, C_6D_6) δ ppm 0.95 (t, *J*=6.80 Hz, 3 H), 1.38 (s, 78 H); ^{13}C NMR (126 MHz, C_6D_6) δ ppm 14.55, 20.20, 27.16, 29.99, 30.49, 34.25, 36.66, 37.70.

Hydrogenation of *iso*-propyl branched polymer (4-29d). The same procedure described above for the synthesis of saturated polymer **4-29a** was followed. After purification, 0.302 g of polymer **4-29d** was collected (Yield = 93%) The following spectral properties were observed; ^{1}H NMR (500 MHz, C_6D_6) δ ppm 0.93 (d, *J*=6.50 Hz, 6 H), 1.38 (br, 78 H); ^{13}C NMR (126 MHz, C_6D_6) δ ppm 19.37, 28.20, 29.84, 29.99, 30.48, 31.14, 44.23.

Hydrogenation of butyl branched polymer (4-29e). The same procedure from the synthesis of saturated polymer **4-29a** was followed. After the purification, 0.302 g of polymer **4-29e** were collected (Yield = 93%). The following spectral properties were observed; ^{1}H NMR (500 MHz, C_6D_6) δ ppm 0.92 (t, *J*=6.80 Hz, 3 H), 1.29 (br, 80 H)**;** ^{13}C NMR (126 MHz, C_6D_6) δ ppm 14.28, 22.68, 26.80, 29.99, 30.45, 32.75, 34.27, 37.88.

Hydrogenation of *iso*-butyl branched polymer (4-29f). The same procedure described above for the synthesis of saturated polymer **4-29a** was followed. After purification, 0.037 g of polymer **4-29f** was collected (Yield = 28%) The following spectral properties were observed; ^{1}H NMR (500 MHz, C_6D_6) δ ppm 1.07 (d, *J*=6.59 Hz, 6 H), 1.37 - 1.61 (br, 80 H); ^{13}C NMR (126 MHz, C_6D_6) δ ppm 23.09, 25.75, 26.95, 29.99, 30.49, 34.49, 35.56, 44.43.

Hydrogenation of pentyl branched polymer (4-29g). The same procedure described above for the synthesis of saturated polymer **4-29a** was followed. After purification, 0.141 g of polymer **4-29g** was collected (Yield = 85%) The following spectral properties were observed; ^{1}H NMR (500 MHz, C_6D_6) δ ppm 0.91 (t, *J*=6.80 Hz, 3 H), 1.29 (s, 82 H); ^{13}C NMR (126 MHz, C_6D_6) δ ppm 14.29, 22.96, 26.77, 27.12, 29.99, 30.46, 32.47, 32.71, 34.24, 37.91.

Hydrogenation of hexyl branched polymer (4-29h). The same procedure described above for the synthesis of saturated polymer **4-29a** was followed. After purification, 0.205 g of polymer **4-29h** was collected (Yield = 85%) The following spectral properties were observed; ^{1}H NMR (500 MHz, C_6D_6) δ ppm 0.91 (t, *J*=6.80 Hz, 3 H), 1.29 (br, 84 H)**;** ^{13}C NMR (126 MHz, C_6D_6) δ ppm 14.27, 22.92, 27.09, 27.12, 29.99, 30.09, 30.56, 32.24, 34.23, 37.90.

Hydrogenation of heptyl branched polymer (4-29i). The same procedure described above for the synthesis of saturated polymer **4-29a** was followed. After purification, 0.205 g of polymer **4-29i** was collected (Yield = 85%) The following spectral properties were observed; ^{1}H NMR (500 MHz, C_6D_6) δ ppm 1.05 (t, *J*=6.80 Hz, 3 H), 1.49 (br. s., 86 H); ^{13}C NMR (126 MHz, C_6D_6) δ ppm 14.27, 22.88, 27.12, 27.18, 29.63, 29.99, 30.04, 30.45, 30.48, 32.17, 34.28, 37.97.

Hydrogenation of octyl branched polymer (4-29j). The same procedure described above for the synthesis of saturated polymer **4-29a** was followed. After purification, 0.186 g of polymer **4-29i** was collected (Yield = 89%) The following spectral properties were observed; ^{1}H NMR (500 MHz, C_6D_6) δ ppm 0.91 (t, *J*=6.80 Hz, 3 H), 1.36 (br. s.,

75 H); ^{13}C NMR (126 MHz, C_6D_6) δ ppm 14.04, 22.86, 27.14, 27.17, 29.60, 29.94, 29.99, 30.04, 30.33, 30.47, 32.14, 34.18, 37.96.

Hydrogenation of nonyl branched polymer (4-29k). The same procedure described above for the synthesis of saturated polymer **4-29a** was followed. After purification, 0.263 g of polymer **4-29k** was collected (Yield = 88%) The following spectral properties were observed; ^{1}H NMR (500 MHz, C_6D_6) δ ppm 0.90 (t, *J*=6.80 Hz, 3 H), 1.28 (br, 89 H)**;** ^{13}C NMR (126 MHz, C_6D_6) δ ppm 14.26, 22.94, 27.03, 27.07, 29.99, 30.09, 30.48, 30.51, 32.23, 34.11, 37.97.

Hydrogenation of decyl branched polymer (4-29l). The same procedure described above for the synthesis of saturated polymer **4-29a** was followed. After purification, 0.263 g of polymer **4-29l** was collected (Yield = 88%) The following spectral properties were observed; ^{1}H NMR (500 MHz, C_6D_6) δ ppm 0.91 (t, *J*=6.80 Hz, 3 H), 1.28 (br, 92 H)**;** ^{13}C NMR (126 MHz, C_6D_6) δ ppm 14.24, 22.85, 27.08, 27.15, 29.59, 29.99, 30.07, 30.48, 30.51, 32.12, 34.31, 37.89

Hydrogenation of pentadecyl branched polymer (4-29m). The same procedure described above for the synthesis of saturated polymer **4-29a** was followed. After the purification, 0.215 g of polymer **4-29k** was collected (Yield = 86%) The following spectral properties were observed; ^{1}H NMR (500 MHz, C_6D_6) δ ppm 0.88 (t, *J*=6.80 Hz, 3 H), 1.28 (s, 83 H); ^{13}C NMR (126 MHz, C_6D_6) δ ppm 14.35, 22.84, 27.15, 27.21, 29.59, 29.99, 30.01, 30.42, 30.45, 32.23, 34.31, 37.93.

CHAPTER 5
CHARACTERIZATION OF PRECISION POLYETHYLENE WITH BRANCHES ON EVERY 39TH CARBON[3]

5.1 Thermal Behavior of Precisely Branched Polymers

Thermal behavior of chain polymerized ethylene/α-olefin copolymers is mainly influenced by short chain branching (SCB) and SCB distribution[108,152]. Various studies have been verified the effect of SCB and SCB distribution on the ultimate thermal properties of copolymers[98,173-177].

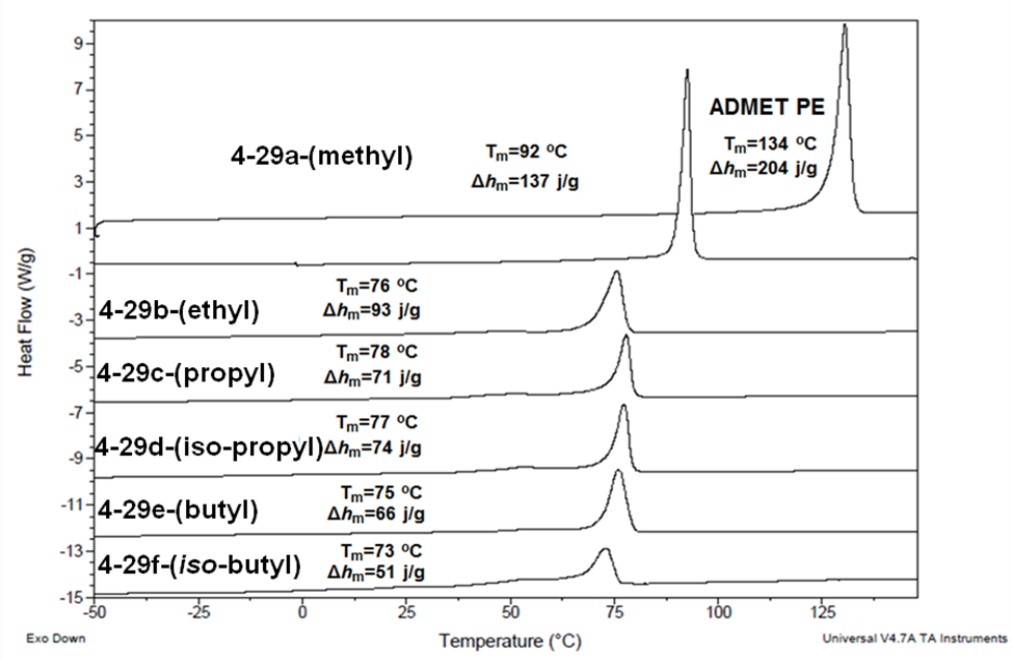

Figure 5-1. Differential scanning calorimetry thermograms for 2nd heating cycles of (top to bottom) **ADMET PE**, **4-29a-(methyl)**, **4-29b-(ethyl)**, **4-29c-(propyl)**, **4-29d-(iso-propyl)**, **4-29e-(butyl)** and **4-29f-(iso-butyl)** with groups precisely placed on every 39th carbon. Heating rate=10°C/min.

The limited control over the primary structure of such chain-growth copolymers results in heterogeneous SCB distribution and hampers the interpretation of the thermal data. The precision polymers described here present a quite different picture. Because

[3] Part of this chapter is adapted with permission from (Zuluaga, F.; Inci, B.; Nozue, Y.; Hosoda, S.; Wagener, K. B. *Macromolecules*, **2009**, 42, 4953). Copyright (2009) American Chemical Society.

the distance between the branches is set at the monomer level, the branch identity can be systematically changed to examine the effect of individual branches on properties. Figures 5-1 and 5-2 present the DSC thermograms of linear **ADMET PE** and precise polymers having branches from methyl to pentadecyl increasing both length and bulkiness.

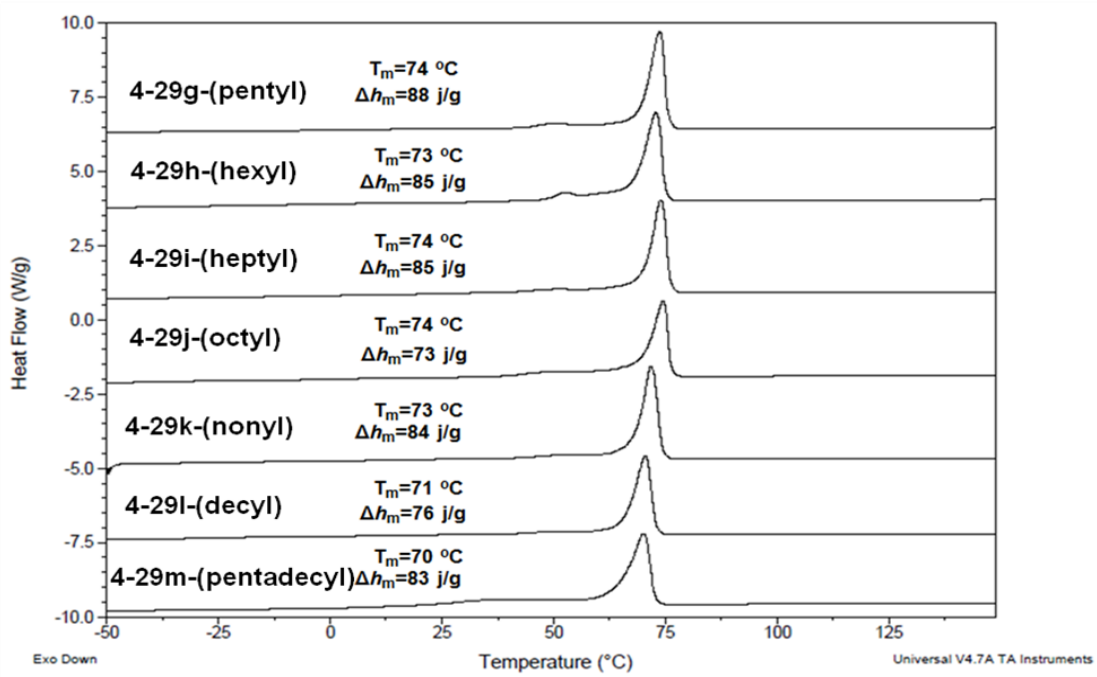

Figure 5-2. Differential scanning calorimetry thermograms for 2nd heating cycles of precision polymers **4-29g-(pentyl)**, **4-29h-(hexyl)**, **4-29i-(heptyl)**, **4-29j-(octyl)**, **4-29k-(nonyl)** and **4-29l-(decyl)** and **4-29m-(pentadecyl)** with groups precisely placed on every 39th carbon. Heating rate=10°C/min.

It is immediately obvious that methyl branching significantly reduces the melting point of ADMET polyethylene: On the other hand, all further branches, from ethyl to pentadecyl, produce polymers that have very similar (in some cases identical) melting points. As discussed further below, this behavior may be attributed to a change in morphology from a situation where the methyl branch is included in the polymer's unit cell, to one where branches of greater mass are excluded from the unit cell. It is

important to note that the ethyl branch is included in the unit cell when the branch is placed on every 21st carbon[158]. Increasing the distance between two consecutive branches from 20 carbons (10.0 mole% branch) to 38 carbons (5.26 mole% branch) expels the ethyl branches from the crystal lattice into the amorphous phase. Similar observations were also reported for commercial ethylene/1-butene and hydrogenated polybutadiene systems, where the ethyl branch is mostly found in the amorphous region[84,178,179].

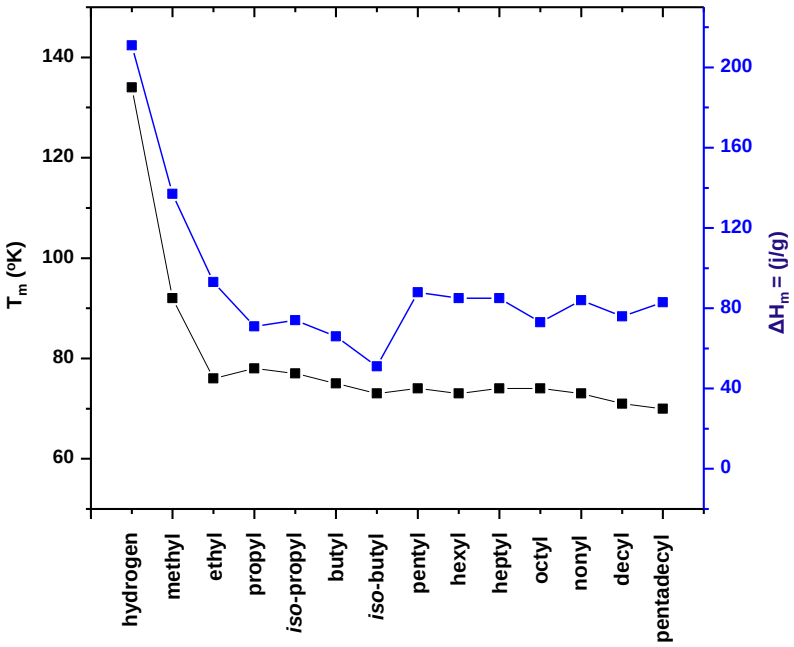

Figure 5-3. Dependence of branch identity on melting point and heat of fusion.

As shown in Figure 5-3, unbranched ADMET polyethylene displays thermal behavior virtually the same as that of high density polyethylene (T_m=134°C, ΔH_m=204 J/g). Incorporation of methyl branches precisely placed on every 39th carbon, polymer **4-29a-(methyl)**, disrupts the crystal structure and decreases the melting temperature to 92°C and the enthalpy of fusion to 137 J/g. A similar trend is observed when the branch

is an ethyl group, **4-29b-(ethyl)**: The melting point decreases below that of **4-29a-(methyl)** (T_m = 76°C with a heat of fusion ΔH_m=93 J/g). Depression of both the melting temperature and the heat of fusion shows that the disruption of the crystal structure is even greater with the presence of the larger ethyl defects. However, extension of the branch size from ethyl to propyl, **4-29c-(propyl)**, does not lead to further decreases (T_m=78°C and ΔH_m=71 J/g). Similar behavior is observed for precision polyethylene possessing longer branches. These homologous polymers with long branches also display sharp well-defined endothermic transitions. Overall, the thermal behavior of precision polymers is consistent with their chain polymerized ethylene/α-olefin analogs, in which the methyl branch is included in the unit cell, and the branches equal to and larger than an ethyl group are excluded.

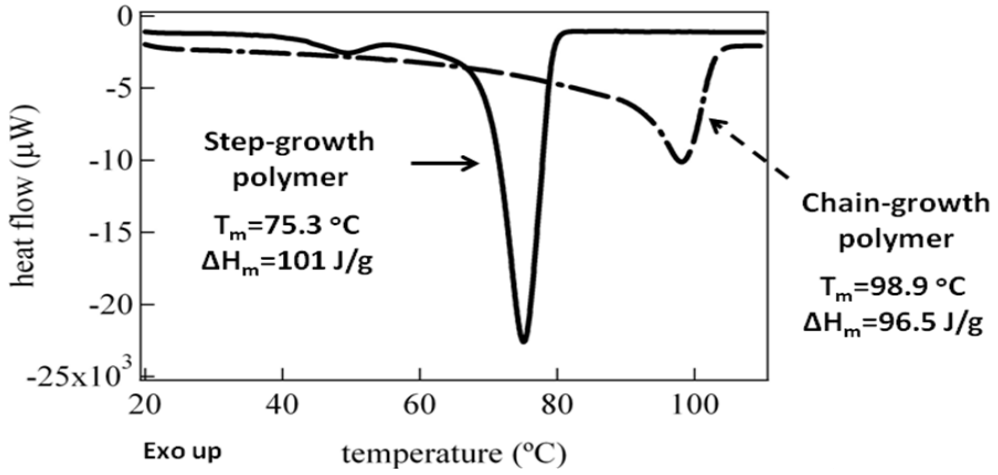

Figure 5-4. Comparison of the thermal behavior of the precision polymer **4-29e-(butyl)** and ethylene/1-hexene copolymer prepared via chain polymerization with a metallocene catalyst. Both profiles are the 2nd heating curves with a heating rate of 10°C/min.

Similar to previously reported[114,116,158] alkyl branched precision polymers, ADMET PE and polymers **4-29a-m** show narrow and well defined melting endotherms,

with none of the broadening observed for analogous copolymers obtained via chain polymerization[152,180,181].

Figure 5-4 compares the thermal behavior of precision polymer **4-29e-(butyl)**[182] to that of a copolymer of ethylene and 1-hexene having the same net concentration of butyl branches along the polymer backbone (although not regularly spaced) prepared via chain polymerization with a metallocene catalyst. The metallocene copolymer displays a higher melting point (98.9^{o}C) than the precision ADMET polymer (75.3^{o}C) and shows a broader melting transition (Figure 5-4).

5.2 Determination of Morphology and Crystal Structure of Precision Polymers

5.2.1 IR Spectroscopy

In addition to primary structure determination, IR spectroscopy can also be used to delineate the morphological picture of polyolefins[183]. IR absorption band regions at 710-740 cm^{-1}and 1450-1480 cm^{-1}, corresponding to the CH_2 rocking and scissor modes, respectively, are known to be very sensitive to the crystal packing behavior of polyethylene[183]. The presence of the orthorhombic unit cell structure is demonstrated by the characteristic Davydov splitting of these absorption bands due to strong intermolecular interactions within the individual polymer chains, whereas no splitting occurs for the metastable triclinic, monoclinic or hexagonal crystal structures[183].

Figure 5-5 illustrates CH_2 rocking and scissor band regions of the precisely branched thirteen polymers **4-29a-m** and **ADMET PE**. The orthorhombic crystal structure of **ADMET PE** is evidenced by two distinct signals at 1462 cm^{-1} and 1472 cm^{-1} for the CH_2 rocking band, 718 cm^{-1} and 730 cm^{-1} for CH_2 scissor band. The same splitting pattern is observed for precision polymers **4-29a-(methyl)**, **4-29c-(propyl)**, **4-29e-(butyl)** and **4-29k-(nonyl)**. The other precisely branched polymers display single

absorption bands for the rocking and scissor regions, indicating the absence of the orthorhombic crystal behavior, as previously reported for precision polymers with shorter branch spacing[114,116,158].

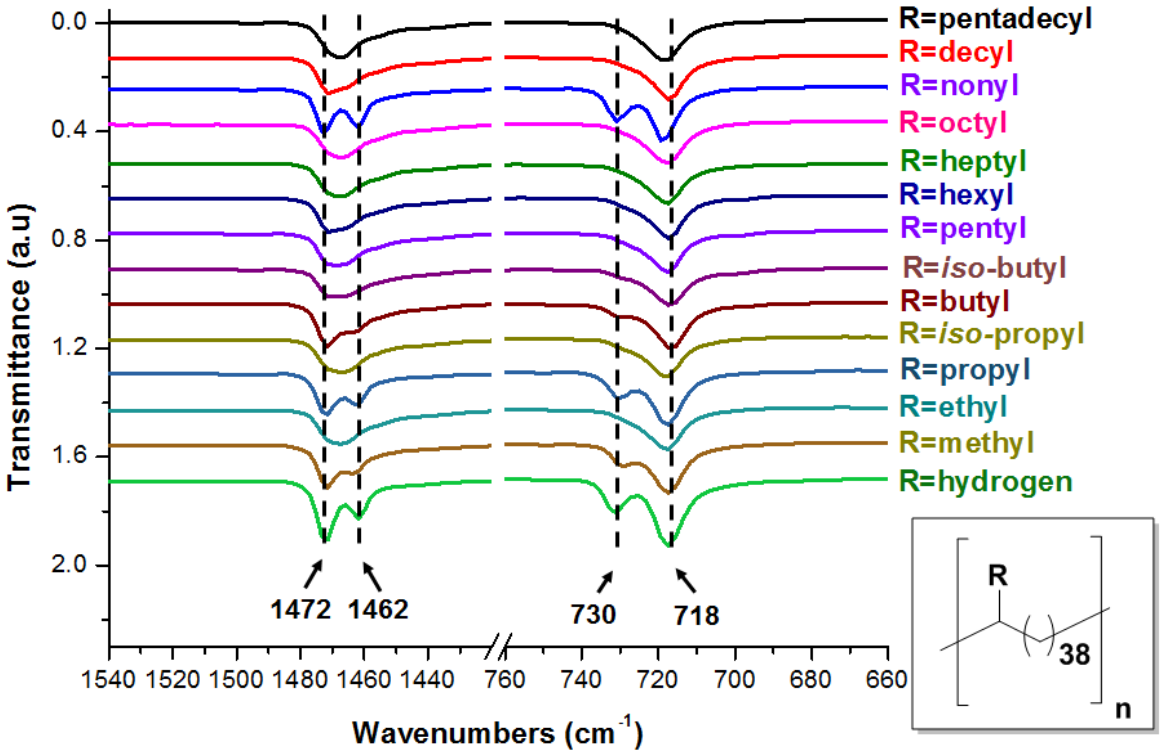

Figure 5-5. The CH_2 rocking and scissors band regions for the precisely branched polymers **4-29a-(methyl)**, **4-29b-(ethyl)**, **4-29c-(propyl)**, **4-29d-(*iso*-propyl)**, **4-29e-(butyl)**, **4-29f-(*iso*-butyl)**, **4-29g-(pentyl)**, **4-29h-(hexyl)**, **4-29i-(heptyl)**, **4-29j-(octyl)**, **4-29k-(nonyl)**, **4-29l-(decyl)**, **4-29m-(pentadecyl)** and **ADMET PE**. All the polymers were analyzed as prepared without any thermal treatment.

Tashiro *et al.* carried out a temperature dependent study to investigate the orthorhombic to hexagonal phase transition in crystals of ultradrawn high modulus polyethylene samples subjected to high tensile stress[183] and demonstrated the change in the rocking band region as a function of the temperature. As the temperature reaches close to the melting point of polyethylene, the intensity of the orthorhombic absorption peaks (1471 cm^{-1} and 1462 cm^{-1}) gradually decreases and a new peak appears at 1466

cm^{-1} corresponding to the hexagonal crystal structure[183]. The single peaks at 1466 cm^{-1} for precision polymers **4-29b-(ethyl)**, **4-29d-(*iso*-propyl)**, **4-29f-(*iso*-butyl)**, **4-29g-(pentyl)**, **4-29h-(hexyl)**, **4-29i-(heptyl)**, **4-29j-(octyl)**, **4-29l-(decyl)** and **4-29m-(pentadecyl)** suggests the formation of a metastable crystalline phase (usually observed at high temperature and pressure conditions for high density polyethylene) at room temperature. Room temperature stabilization of this highly disordered phase is a direct result of the branch being present.

5.2.2 Solid State ^{13}C NMR

Solid State ^{13}C NMR spectroscopy is a powerful technique to demonstrate the detailed structure and molecular motions for various solid polymers[184-186]. The phase structure of the amorphous, the amorphous-crystalline interfacial, and the crystalline phases for semi-crystalline polymers can be verified by examining ^{13}C spin-lattice relaxation and spin-spin relaxation behavior[84,187-191]. Figure 5-6 shows the 10-45 ppm region (methylene carbons) of the cross polarization (CP)/ magic angle spinning (MAS) high resolution solid state ^{13}C NMR spectra of precision polymers **4-29a-(methyl)**, **4-29b-(ethyl)**, **4-29c-(propyl)**, **4-29e-(butyl)**, **4-29k-(nonyl)** and **4-29m-(pentadecyl)**. These spectra indicate that the introduction of branches leads to lattice distortion and local conformational disorder, where the type of crystal structure and polymer morphology is strongly dependent on the branch identity.

The first feature observed in Figure 5-6 is that the all six slowly cooled samples have the isotropic chemical shift at 32.9 ppm, corresponding to crystalline methylene carbons. A singlet at 32.9 ppm is equivalent to the all-trans crystalline methylene in **ADMET PE**[123] (32.8 ppm), given that the solution grown single crystal of **4-29a-(methyl)**

polymer is found to have distorted orthorhombic unit cell structure with an extended “a” unit cell parameter (Table 5-2).

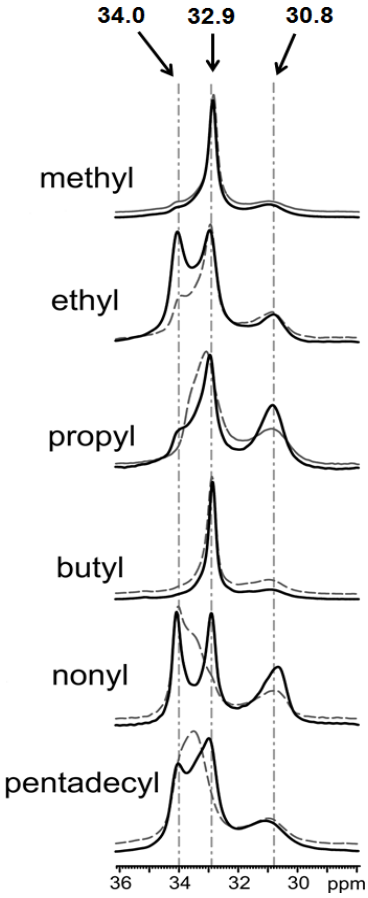

Figure 5-6. CP/MAS spectra of precision polymers **4-29a-(methyl)**, **4-29b-(ethyl)**, **4-29c-(propyl)**, **4-29e-(butyl)**, **4-29k-(nonyl)** and **4-29m-(pentadecyl)**. ^{13}C NMR spectra are recorded at RT. Short CP contact time (1ms) was chosen to increase the intensity of the crystalline region prominently. Dashed lines represent polymers rapidly cooled from melt at 50^{o}C/min while solid lines represent polymers slowly cooled from melt at 0.5^{o}C/min.

Introduction of ethyl branches on every 39th carbon disrupts the crystal structure of unbranched **ADMET PE** even more. The small hump at 34.0 ppm in the spectrum of **4-29a-(methyl)** becomes a shoulder in rapidly cooled **4-29b-(ethyl)**. For the slowly cooled **4-29b-(ethyl)** sample, the peak at 34.0 ppm becomes more obvious, suggesting the coexistence of two crystalline morphologies. Similar peaks in the downfield region (34.1

ppm) were previously reported for precision polymers having chlorine and bromine substituents at every 19th carbon and these were attributed to the existence of triclinic unit cell structure[123].

In the case of the propyl branched polymer **4-29c-(propyl)**, the rapidly cooled sample exhibits a broad unsymmetrical singlet at 32.9 ppm but slow cooling results in a shoulder at 34.0 ppm with much lower intensity than the 34.0 ppm resonance for polymer **4-29b-(ethyl)**. This suggests that **4-29c-(propyl)** exists in the *all*-trans conformation. A similar trend is observed as we incorporate the butyl branches (polymer **4-29e-(butyl)**), where the peak at 34.0 ppm diminishes and the *all*-trans conformation of methylene units forms exclusively. With this in mind, it can be concluded that methyl branches are included in the crystalline lattice, and that branches equal to or larger than ethyl are expelled from the lattice. However, ethyl and propyl branches are not large enough to be fully excluded from the unit cell, and these branches are positioned in both the amorphous and crystalline phases. Slow cooling of polymers **4-29b-(ethyl)** and **4-29c-(propyl)** from melt provides sufficient time for the branches to be partially incorporated (especially for the ethyl branch) into the crystalline lattice.

For the polymers possessing longer branches (nonyl and pentadecyl), the solid state ^{13}C NMR spectra of slowly cooled samples (the bottom two graphs in Figure 5-6) show two distinct chemical shifts in the crystalline region, indicating the coexistence of two crystalline phases. Because of their branch sizes, polymers **4-29k-(nonyl)** and **4-29m-(pentadecyl)** are expected to display spectra similar to that polymer **4-29e-(butyl)**, with fully excluded side chains. This unexpected observation of two crystalline phases

for both **4-29k-(nonyl)** and **4-29m-(pentadecyl)** is presumably due to co-crystallization of the long branches with the main polymer chain.

The spectra in Figure 5-6 also provide information about the amorphous phase. Amorphous carbons of polymers **4-29a-(methyl)**, **4-29b-(ethyl)**, **4-29c-(propyl)** and **4-29e-(butyl)** exhibit broad peaks centered at 30.8 ppm, whereas polymers **4-29k-(nonyl)** and **4-29m-(pentadecyl)** display peaks at 30.6 and 31.0 ppm, respectively. The reason for the observed differences in peak positions remains unclear, but it is possible that long branches have different effect on the organization of the amorphous region.

5.2.3 Wide Angle X-ray Diffraction (WAXD)

Wide angle X-ray diffraction (WAXD) measurements further support the observation of a change in polymer morphology as a function of branch size. WAXD diffractograms of precision polymers having branches from methyl to pentadecyl are shown in Figures 5-7 & 5-8. These patterns indicate that the introduction of branches leads to lattice distortion and local conformational disorder, where the type of crystal structure and polymer morphology is strongly dependent on the branch identity.

For the sake of comparison, **ADMET PE** is displayed at the bottom of Figure 5-7. It exhibits the typical orthorhombic crystal form with two characteristic crystalline peaks superimposed on the amorphous halo, exactly the same as for high density polyethylene made by chain propagation chemistry. The more intense peak at scattering angle 21.5^{o} and the less intense one at 24.0^{o} correspond to reflection planes (110) and (200), respectively. Introduction of precisely placed methyl branches on every 39^{th} carbon (polymer **4-29a-(methyl)** in Figure 5-7) disturbs the unit cell of **ADMET PE** and shifts the scattering angles to 21.1^{o} and 23.0^{o}. Electron diffraction measurements

for the solution grown single crystals of polymer **4-29a-(methyl)** indicate the formation of the disturbed orthorhombic unit cell with an extended “a” value (Table 5-2).

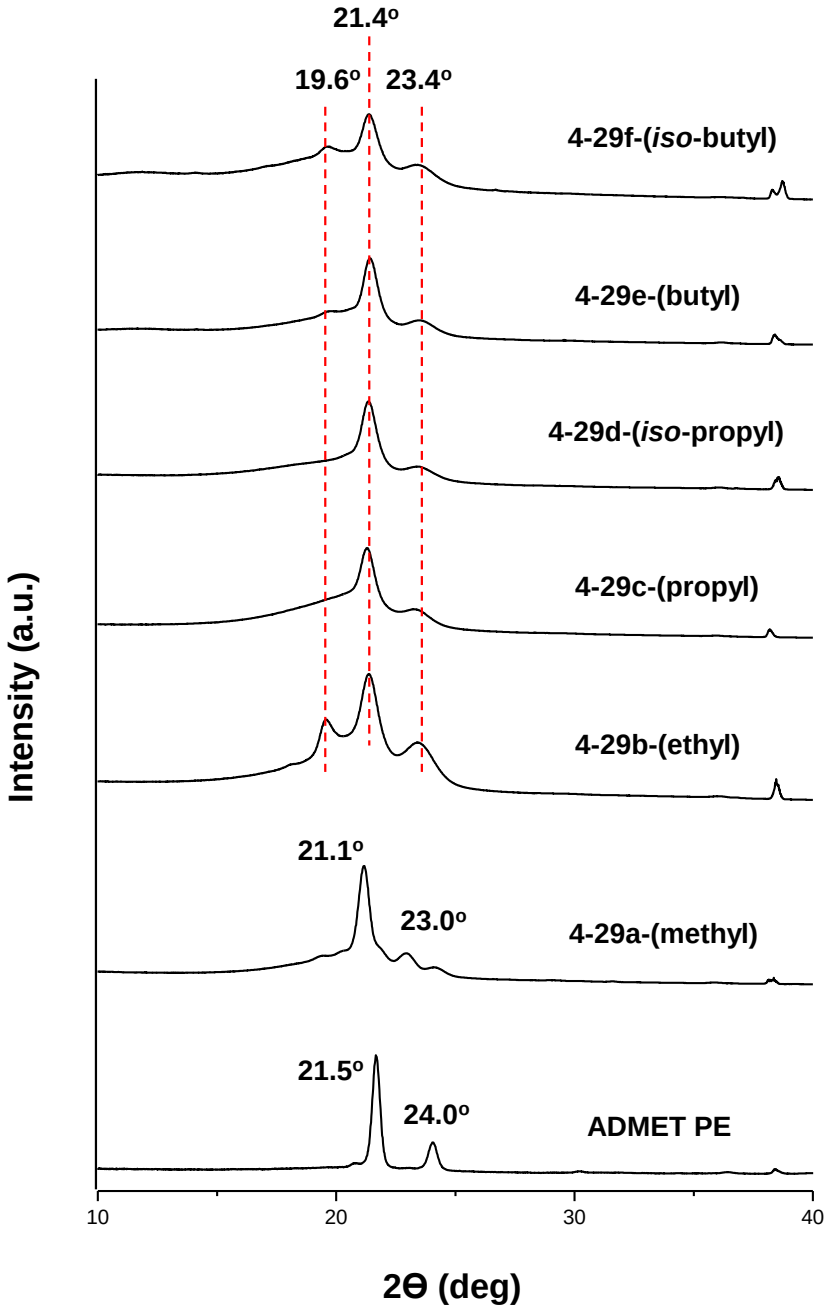

Figure 5-7. Wide angle X-ray diffraction patterns for precision polymers **4-29a-(methyl)**, **4-29b-(ethyl)**, **4-29c-(propyl)**, **4-29d-(*iso*-propyl), 4-29e-(butyl)**, **4-29f-(*iso*-butyl)** and **ADMET PE** obtained at RT. Prior to data acquisition, all samples were heated to 20^{o}C above the melting temperature of each polymer to remove the thermal history, and then cooled to room temperature at a rate of 50^{o}C/min.

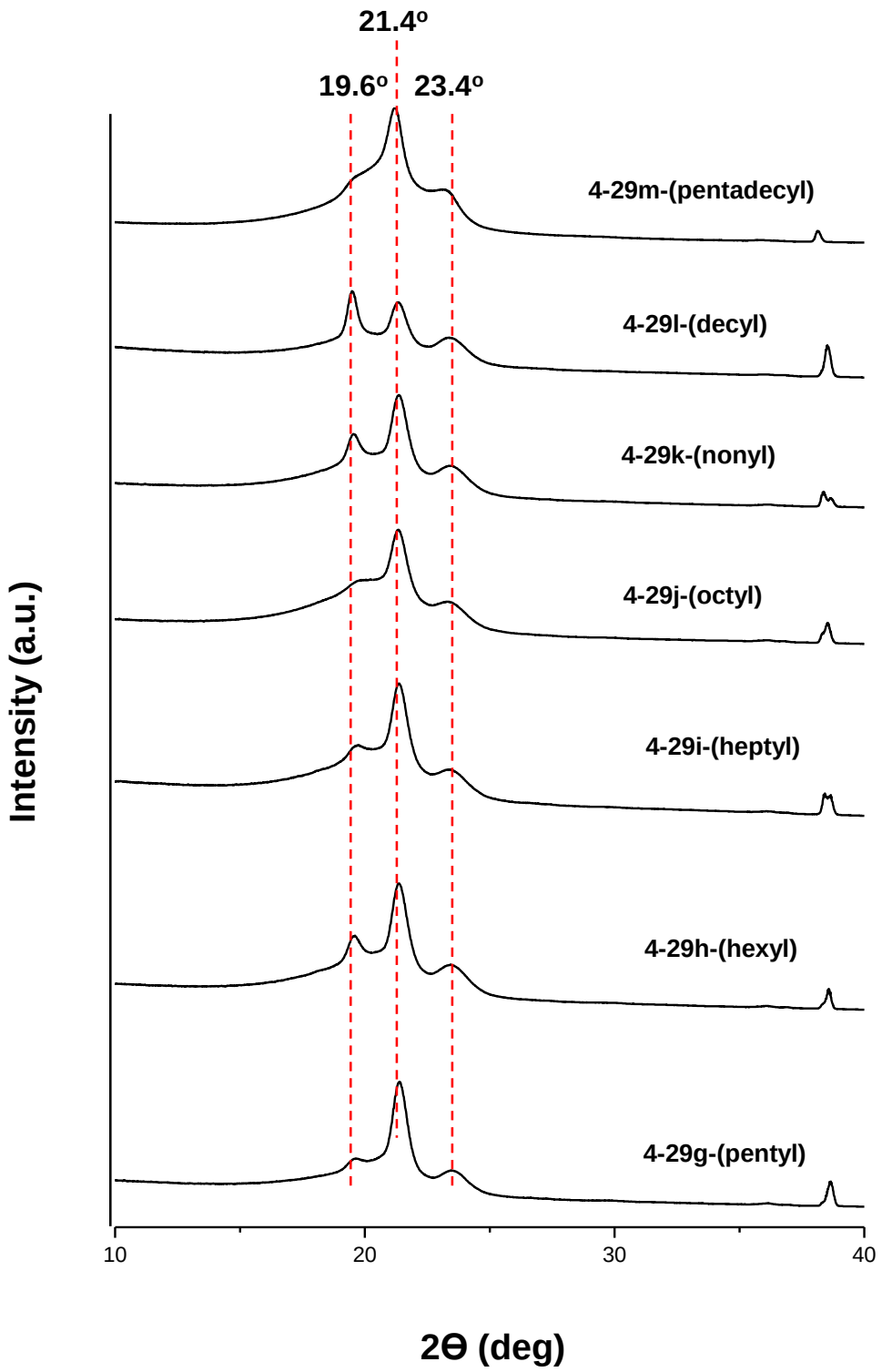

Figure 5-8. Wide angle X-ray diffraction patterns for precision polymers **4-29g-(pentyl)**, **4-29h-(hexyl)**, **4-29i-(heptyl)**, **4-29j-(octyl), 4-29k-(nonyl)**, **4-29l-(decyl)** and **4-29m-(pentadecyl)** obtained at RT. Prior to data acquisition, all samples were heated to 20^{o}C above the melting temperature of each polymer, and then cooled to room temperature at a rate of 50^{o}C/min.

For the polymers possessing larger branches (from ethyl to decyl), the WAXD diffractograms show nearly identical scattering patterns, in which the crystalline peaks shift to 21.4^{o} and 23.4^{o} (Figures 5-7 and 5-8), indicating the existence of similar morphologies. Interestingly, polymer **4-29m-(pentadecyl)** displays different scattering peak values (21.2^{o} and 23.2^{o}) than polymers having branches from ethyl to decyl.

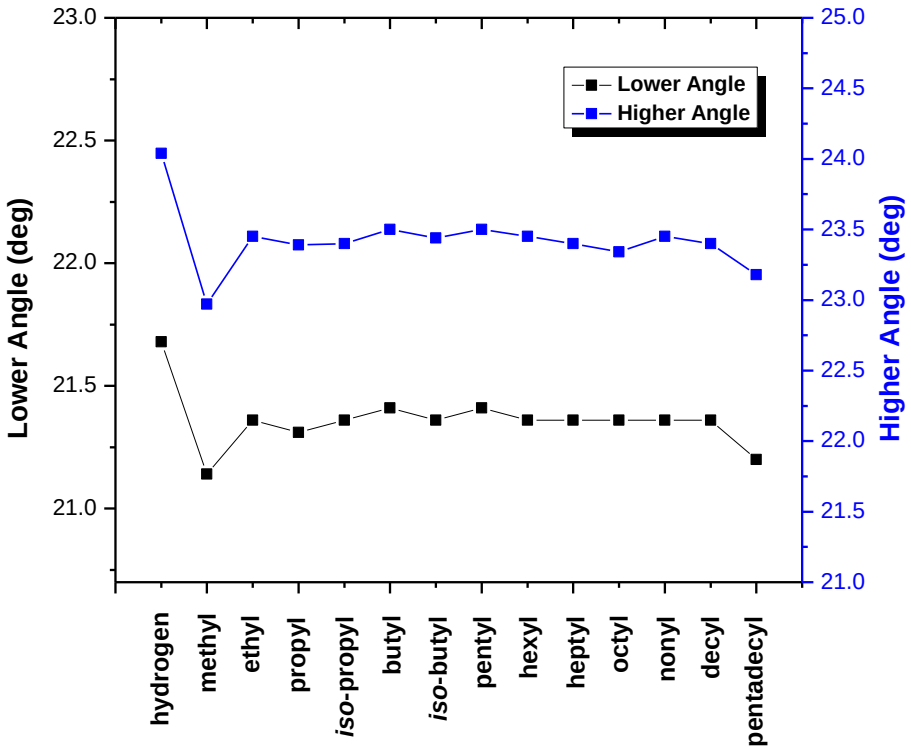

Figure 5-9. Scattering angles of two strong reflections for alkyl branched precision polymers. The blue graph is for the reflection at higher angle while the black one is for the reflection at lower angle.

To better understand these observations, the scattering angles of two strong diffraction peaks are plotted as a function of branch identity in Figure 5-9. The decrease of scattering angles for methyl branched polymer **4-29a-(methyl)** indicates the larger d-spacing between the diffraction planes, suggesting the inclusion of the methyl branches into the unit cell. A clear morphology change for polymers ranging from **4-29b-(ethyl)** to

4-29l-(decyl) is evidenced by the increase of scattering angles, confirming the exclusion of branches from the unit cell. It is important to note that precision polymer **4-29m-(pentadecyl)** exhibits a distinct morphological behavior, in which the relatively long pentadecyl branch presumably co-crystallizes with the main polymer chain, thereby increasing the d-spacing between the diffraction planes.

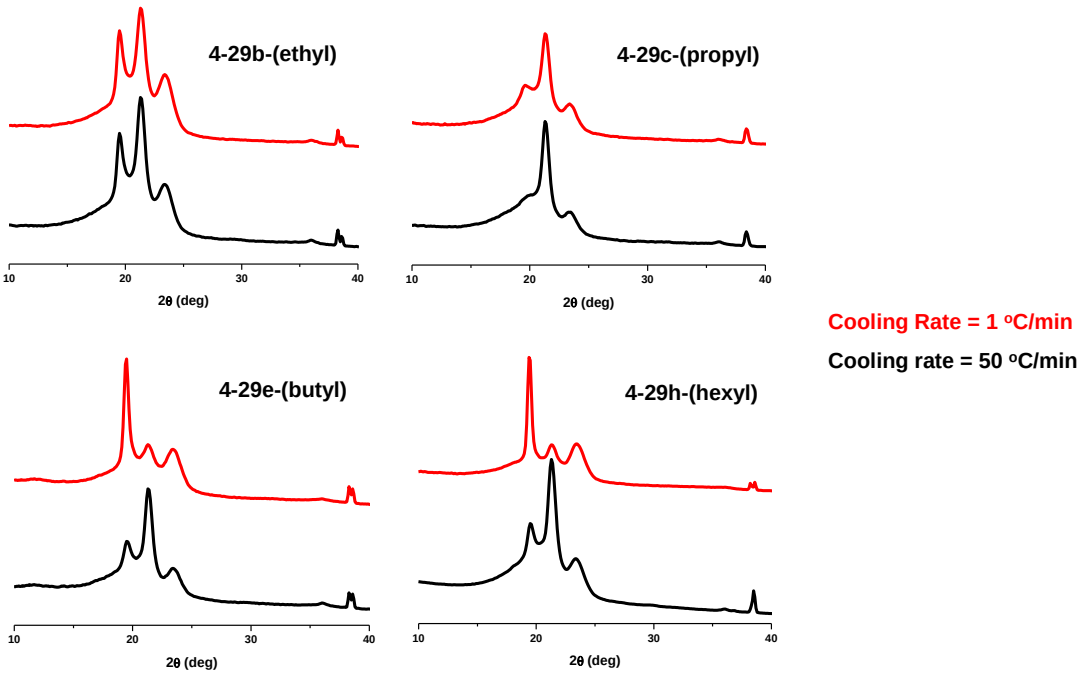

Figure 5-10. Wide angle X-ray diffraction patterns for precision polymers **4-29b-(ethyl)**, **4-29c-(propyl)**, **4-29e-(butyl)** and **4-29h-(hexyl)** obtained at RT. Prior to data acquisition, all samples were heated to 20°C above the melting temperature of each polymer, and then cooled to room temperature at a rate of either 1°C/min or 50°C/min.

An interesting aspect of the WAXS profiles for most precision polymers is the appearance of the crystalline peak in the amorphous halo region (peak at 19.6°), suggesting the possible co-existence of metastable crystal packing. The extent of the metastable phase formation was further investigated with temperature-controlled WAXD measurements. In doing so, the polymer in question was heated to 20°C above its

melting temperature and then cooled at a rate of either 1°C/min or 50°C/min, as shown in Figures 5-10 and 5-11.

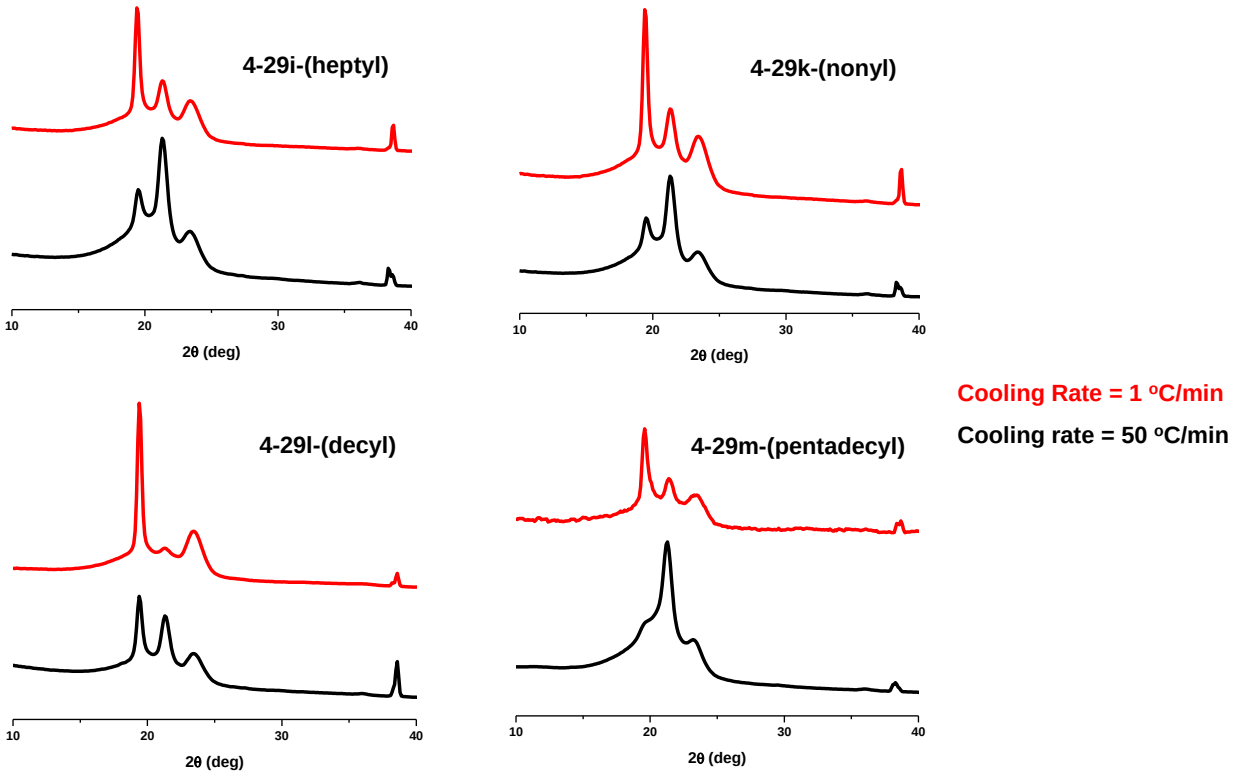

Figure 5-11. Wide angle X-ray diffraction patterns for precision polymers **4-29i-(heptyl)**, **4-29k-(nonyl)**, **4-29l-(decyl)** and **4-29m-(pentadecyl)** obtained at RT. Prior to data acquisition, all samples were heated to 20°C above the melting temperature of each polymer, and then cooled to room temperature at a rate of 1°C/min or 50°C/min.

Precision polymers having branches equal to or greater in mass than butyl exhibit strong thermal history dependence. For samples cooled at 1°C/min, these polymers show an increase in the intensity of the peak at 19.6° and a decrease in the intensity of the peak at 21.4°, compared to the corresponding peaks for sample cooled at 50°C/min. The WAXD profiles of polymers **4-29b-(ethyl)** and **4-29c-(propyl)** display subtle thermal history dependence, but **ADMET PE** and **4-29a-(methyl)** generate virtually the same

diffraction patterns for both cooling rates (not shown in Figures 5-10 & 5-11). Slow cooling extends the stabilization of the metastable crystal formation, especially for longer branched precision polymers.

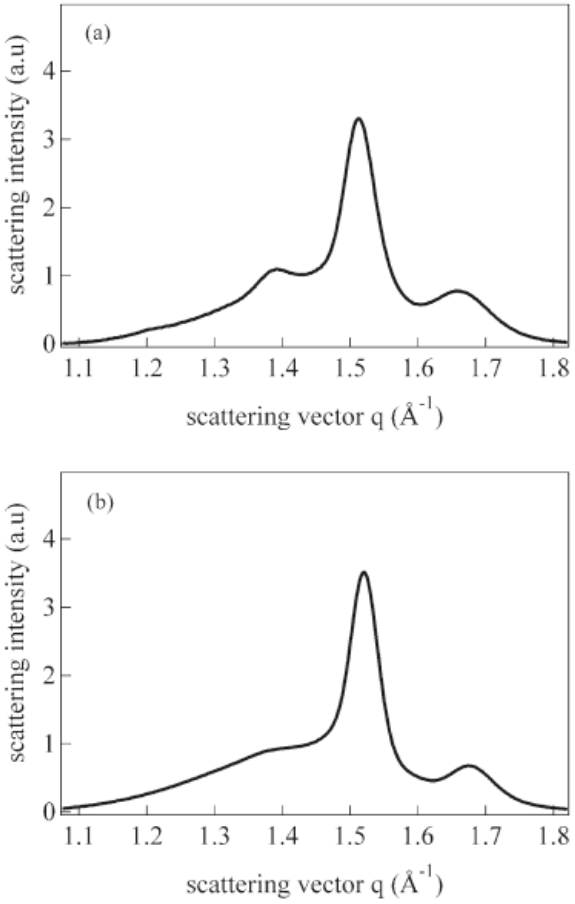

Figure 5-12. WAXD pattern of a) Precision polymer **4-29e-(butyl)** and b) Ethylene/1-hexene copolymer prepared via chain polymerization with a metallocene catalyst. Both samples were cooled to RT from melt at 60^{o}C/min.

In Figure 5-12, the WAXD behavior of precision polymer **4-29e-(butyl)** is compared to that of a copolymer of ethylene and 1-hexene having the same net concentration of butyl branches along the polymer backbone, but prepared via chain polymerization with a metallocene catalyst[182]. Unlike the precision polymer **4-29e-(butyl)**, metallocene ethylene/1-hexene copolymer does not exhibit a crystalline peak at

the amorphous halo region. Formation of a metastable crystal phase is a direct result of the precise branch placement along the polymer backbone.

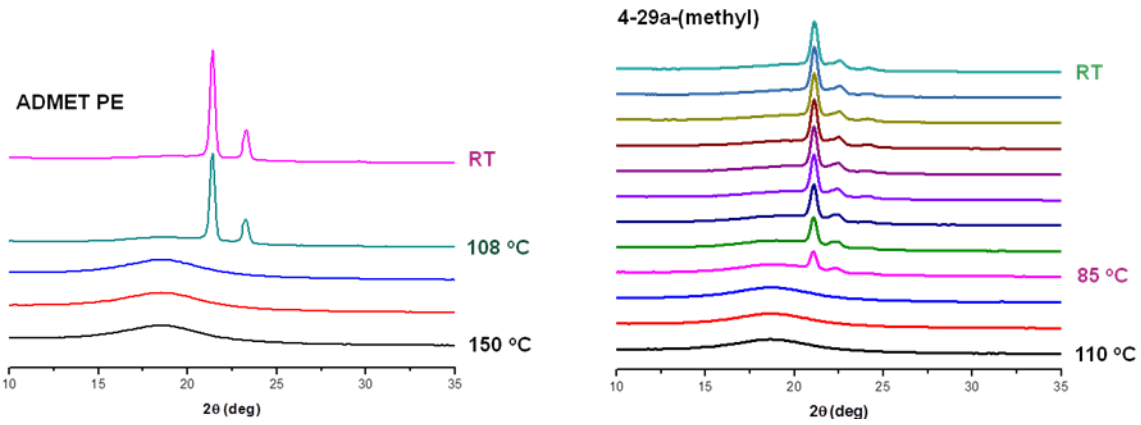

Figure 5-13. Temperature dependent Wide angle X-ray diffraction patterns for **ADMET PE** and methyl branched precision polymer **4-29a-(methyl)**. Both samples were heated to 20^{o}C above the melting temperature of each polymer, and then cooled to room temperature at a rate of 1^{o}C/min. X-ray data were collected in situ during cooling.

In situ WAXD measurements for some of the precision polymers were employed to delineate the morphology development as the polymers were cooled from the melt (cooling rate=1^{o}C/min), as shown in Figures 5-13 and 5-14. **ADMET PE** is also displayed in Figure 5-12 exhibiting the typical orthorhombic crystal structure with two characteristic peaks at the crystallization temperature (T_c=108^{o}C). The **ADMET PE** sample is cooled with a rate of 1^{o}C/min from the molten state and the amorphous halo readily transformed to a well defined orthorhombic crystalline scattering peak pattern when the system reached the crystallization temperature. Similar to **ADMET PE**, the precision polymer **4-29a-(methyl)** quickly forms the orthorhombic unit cell at its crystallization temperature (T_c=85^{o}C).

In the case of polymers with longer branches (**4-29b-(ethyl)**, **4-29c-(propyl)** and **4-29e-(butyl)**), in situ WAXD measurements exhibit a significantly different morphology development motif compared to **ADMET PE** and **4-29a-(methyl)**. For example, X-ray diffraction peak positions of the precision polymer **4-29b-(ethyl)** experience an unusual shift during the cooling experiment (Figure 5-14).

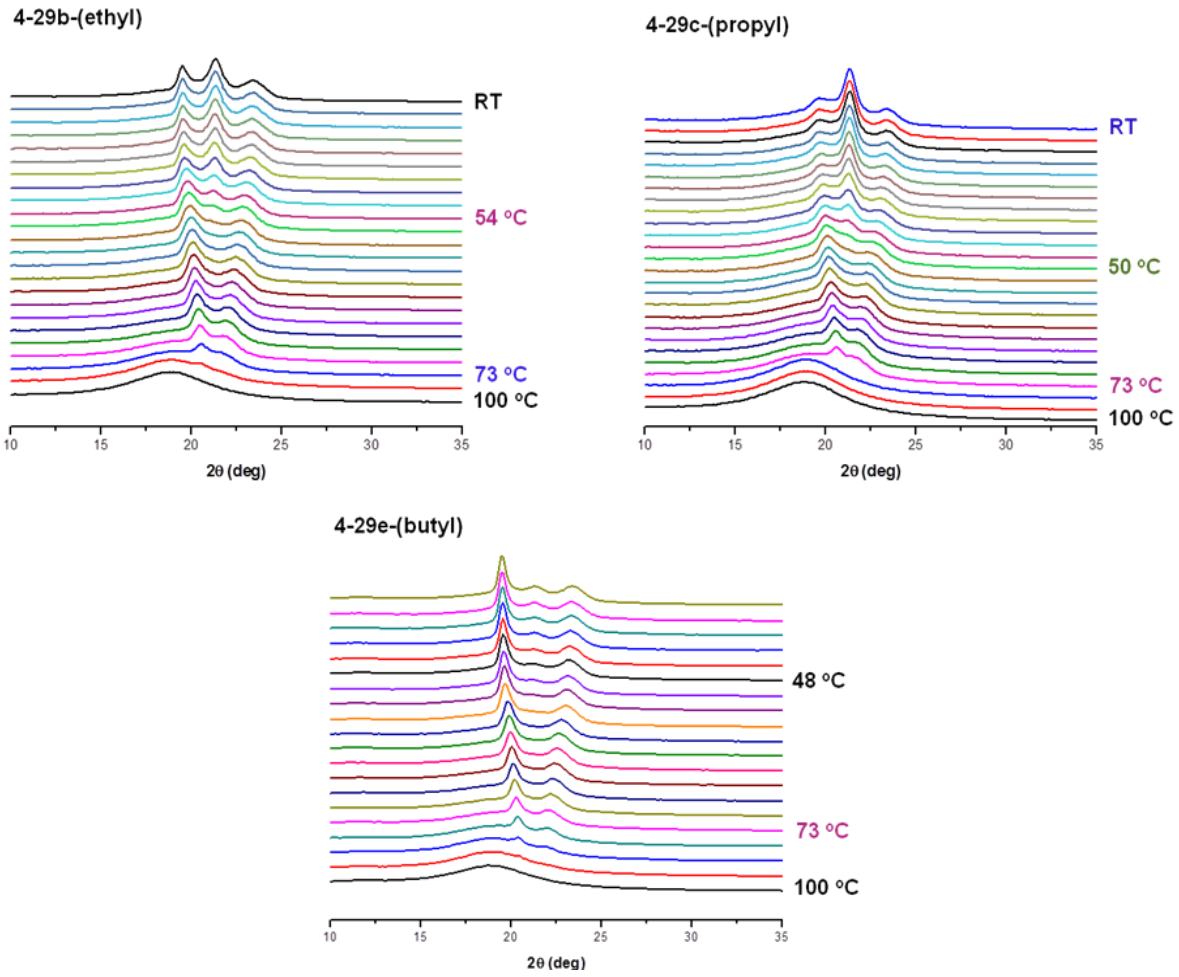

Figure 5-14. Temperature dependent Wide angle X-ray diffraction patterns for precision polymers **4-29b-(ethyl)**, **4-29c-(propyl)** and **4-29e-(butyl)**. All polymer samples were heated to 20^{o}C above the melting temperature of each polymer, and then cooled to room temperature at a rate of 1^{o}C/min. X-ray data were collected in situ during cooling.

The two diffraction peaks at 20.5^{o} and 21.8^{o} appear at the crystallization temperature of polymer **4-29b-(ethyl)** (73^{o}C) and shift to 19.6^{o} and 23.4^{o}, respectively, as the system is cooled to RT. Appearance of the 21.4^{o} peak at 54^{o}C suggests the existence of the two different crystalline morphologies. It is interesting to note that the crystalline phase appearing at 73^{o}C is metastable in nature, and its unit cell dimensions continue changing even well below the crystallization temperature. This is a direct result of precise branch placement. As the crystallization temperature is reached, polymer backbone crystallization starts and the system attempts to expel the ethyl branch outside to the crystalline phase. However, the precisely placed adjacent ethyl branch temporarily enters the unit cell, but it subsequently expelled back to the amorphous phase. This “frustrated crystallization” behavior is also seen for the precision polymers **4-29c-(propyl)** and **4-29e-(butyl)**.

5.2.4 Transmission Electron Microscopy (TEM)

The CP/MAS NMR and WAXD measurements were used to investigate melt crystallized samples to delineate the morphology and the crystal structure of the precision polymers. Transmission Electron Microscopy (TEM) was used to analyze the lamellar nature of solution-grown polyethylene single crystals[192-197]. The TEM images of the solution grown single crystals of **ADMET PE** and precision polymers are illustrated in Figure 5-15.

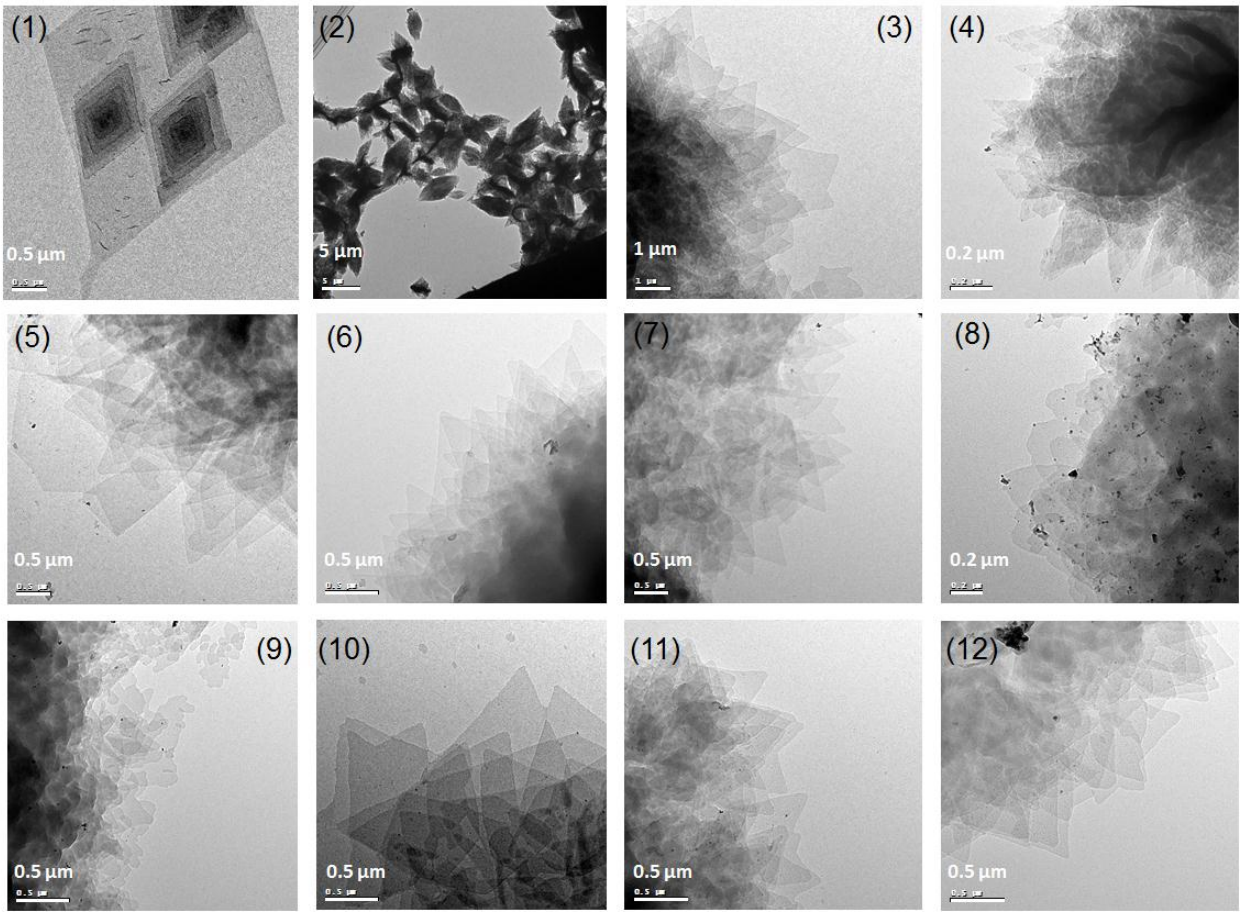

Figure 5-15. TEM images of 1) **ADMET PE**, 2) **4-29a-(methyl)**, 3) **4-29c-(propyl)**, 4) **4-29d-(*iso*-propyl)**, 5) **4-29e-(butyl)**, 6) **4-29g-(pentyl)**, 7) **4-29h-(hexyl)**, 8) **4-29i-(heptyl)**, 9) **4-29j-(octyl)**, 10) **4-29k-(nonyl)**, 11) **4-29l-(decyl)** and 12) **4-29m-(pentadecyl)**. **ADMET PE** and **4-29a-(methyl)** crystals were grown from 0.03 wt% C_2Cl_4 solution, and all the other polymer single crystals were grown from 0.03% o-xylene solution.

Lozenge-shaped rhombohedral single crystals were observed for **ADMET PE** and precisely branched polyethylene samples, consistent with the previous reports on solution-grown HDPE single crystals[195,196]. The lamellae thickness of each polymer single crystal was determined using the previously published protocol[198]. As shown in Table 5-1, methyl branching reduces the lamellae thickness of **ADMET PE**, but all further branches, from ethyl to pentadecyl, produce polymers that have very similar lamellae thicknesses.

Table 5-1. Lamellae thicknesses of **ADMET PE** and precision polymers determined by TEM.

Polymer	Thickness (nm)
ADMET PE	9.75
4-29a-(methyl)	7.09
4-29b-(ethyl)	4.79
4-29e-(butyl)	4.25
4-29g-(pentyl)	5.03
4-29h-(hexyl)	4.17
4-29i-(heptyl)	4.39
4-29j-(octyl)	4.06
4-29k-(nonyl)	4.67
4-29l-(decyl)	4.16
4-29m-(pentadecyl)	5.33

These results provide additional evidence of a clear change in morphology of these polymers from a situation where the methyl branch is included in the polymer's unit cell, to one where branches of greater mass are excluded from the unit cell.

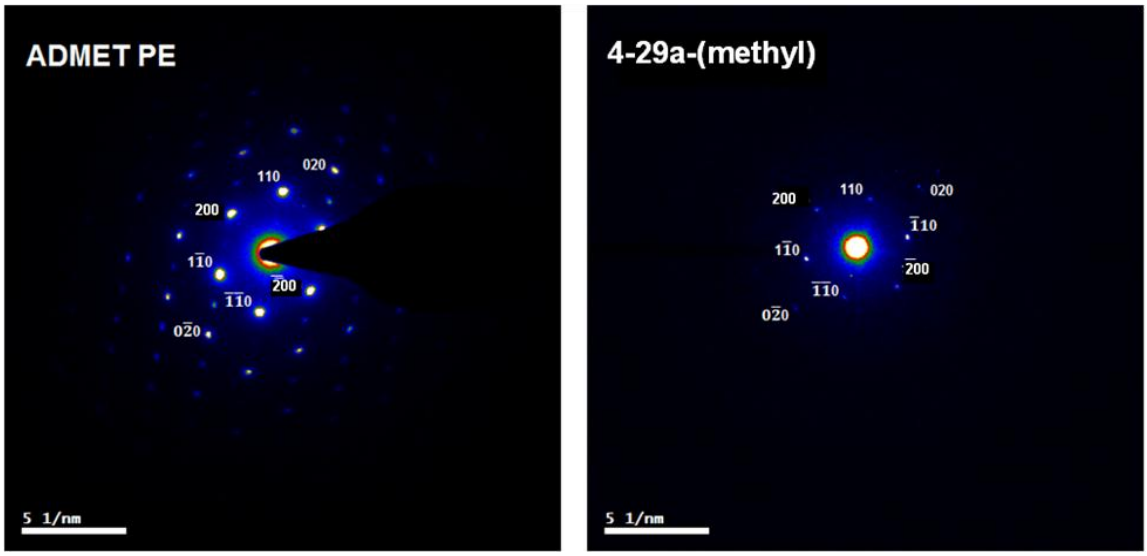

Figure 5-16. Selected area single crystal electron diffraction patterns of **ADMET PE** and polymer **4-29a-(methyl)**.

Selected area single crystal electron diffraction patterns of **ADMET PE** and polymer **4-29a-(methyl)** are illustrated in Figure 5-16. Unlike the WAXD diffractograms of melt crystallized polymers, single crystal electron diffraction patterns provide

information from higher order diffractions and give a better picture of the unit cell configuration. Calculated unit cell parameters of **ADMET PE** and polymer **4-29a-(methyl)** are presented in Table 5-2 together with previously reported data for HDPE[2].

Table 5-2. Unit cell dimensions of **HDPE**, **ADMET PE** and **4-29a-(methyl)**

Polymer	Unit Cell	a, Å	b, Å	c, Å
HDPE	Orthorhombic	7.42	4.95	2.55
ADMET PE	Orthorhombic	7.48	4.98	2.55
4-29a-(methyl)	Orthorhombic	7.75	4.93	2.55

Introduction of precisely placed methyl branches on every 39th carbon extends the "a" parameter of the orthorhombic unit cell, confirming the incorporation of the methyl branches.

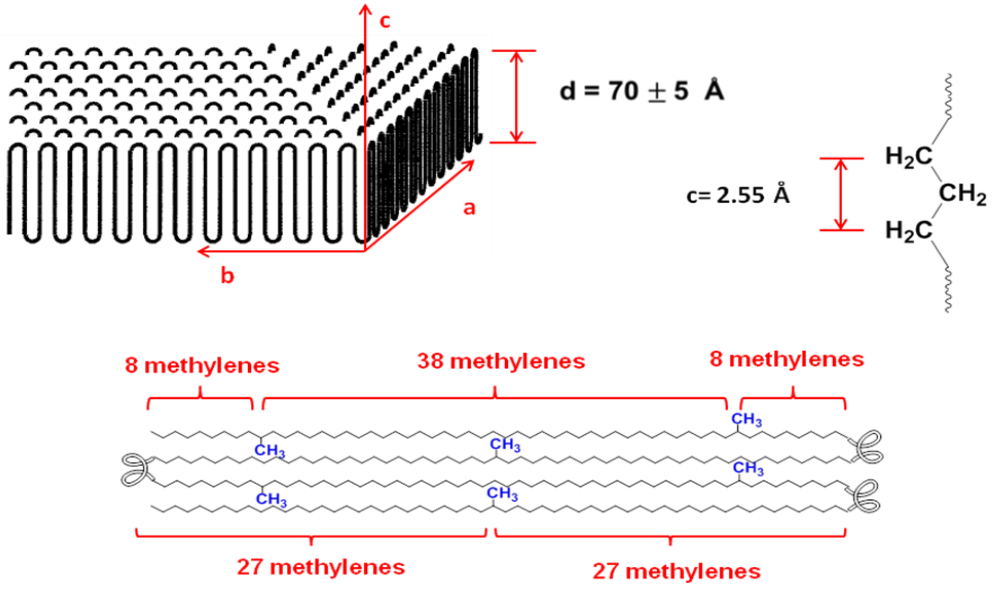

Figure 5-17. Structural model for precision polymer **4-29a-(methyl)**. Methyl branches are incorporated into the unit cell and lamellae stem length is estimated to be 54 methylene units.

Figure 5-17 demonstrates the structural model for precision polymer **4-29a-(methyl)**, in which the lamellae stem length is estimated to be 54 methylene units and three methylene units are used at the folding point.

5.3 Instrumentation and Sample Preparation

Differential scanning calorimetry (DSC) was performed using a TA Instruments DSC Q1000 equipped with a controlled cooling accessory at a heating and cooling rate of 10°C/min unless otherwise specified. Calibrations were made using indium and freshly distilled *n*-octane as the standards for peak temperature transitions and indium for the enthalpy standard.

IR data were obtained using a Perkin-Elmer Spectrum One FTIR outfitted with a $LiTaO_3$ detector. Polymer samples were prepared by solution-casting thin films from boiling toluene onto KBr salt plates.

Wide-angle X-ray (WAXS) powder diffraction data were collected on a Mar345 Image Plate Detector with plate diameter of 345 mm and outside dimensions (515 mm * 398 mm * 350 mm), using the Cu Kα radiation (λ = 0.15417 nm) induced by a generator operating at 40 kV and 150 mA. Diffraction patterns were recorded for 2θ-values ranging from 10° to 40°. Each diffractogram for the in situ WAXD measurements was collected using an accumulation time of 300 seconds. The temperature control unit was attached to the sample holder, and all the cooling experiments were performed at either 1^oC/min or 50^oC/min.

Solid state NMR was carried out utilizing a Bruker spectrometer equipped with a Bruker Avance II+ console working at ^1H Larmor frequency of 850 MHz. Polymer samples were tightly and evenly packed in 2.5 mm rotors, and CP-MAS spectra were acquired using 1 ms contact time and 10 kHz MAS conditions.

For TEM sample preparation, carbon black was evaporated under 10^{-3} atm onto the mica slides to form uniform carbon layers of 5-10 nm thickness. The carbon layer

was removed with DI water and regular mesh TEM copper grids were coated by dipping them in water. One drop of polymer stock solution (0.03 wt%) was deposited onto the carbon coated copper grid and solvent was evaporated at RT under the hood. TEM images obtained on a Tecnai F20 (FEI) transmission electron microscope operated at an acceleration voltage of 200 kV. In order to reduce beam damage to the polymer specimen, a low dose exposure protocol was applied for image acquisition.

Thickness images were obtained using a FEI Tecnai F20 electron microscope equipped with a Gatan imaging filter (GIF) and a slow scan CCD (charged-coupled device) camera. The GIF system allows both parallel-detection EELS and energy-filtered imaging/diffraction. A CCD camera can digitally collect electron images and diffraction patterns. By coupling the CCD camera to a computer, energy-filtered images could be acquired and processed in a quantitative manner. An energy window was used to select an energy range of low electrons. Taking two consecutive images from the same sample, one with the slit positioned at the zero-loss peak and one without the slit, yields two images, the elastical filtered image I_0 and the inelastic image I_t. After aligning both images for possible sample drift, the relative thickness at each point of the images was given by: $t/\lambda = \ln(I_0/I_t)$, in which lambda is the mean free path of the respective material for the respective electron energy (200 kV). Calculation of the mean free path scales the image to an absolute thickness mapping.

CHAPTER 6
SYNTHESIS AND CHARACTERIZATION OF PRECISION POLYETHYLENE WITH BRANCHES ON EVERY 75TH CARBON[4]

6.1 Monomer Synthesis

As illustrated in Table 2-1, commercial LLDPEs predominantly have α-olefin incorporation ratios of 2-5 mole% with melting points in the range from 100 to 125^{o}C. While the precision polymers described in Chapters 4 and 5 provide model systems for fundamental research, they still suffer from their relatively low melting points. This chapter describes efforts to prepare precision polyethylene with longer ethylene run length and increased melting point.

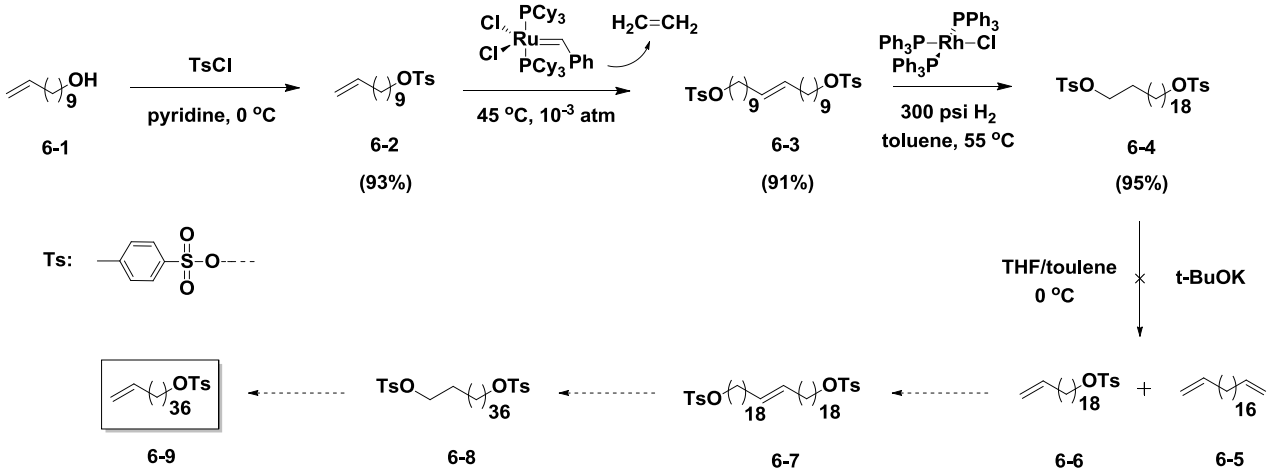

Figure 6-1. Synthetic strategy to generate alkylating agent with 36 methylene run length.

Increasing the run length at the monomer level requires reproducible synthesis of alkylating agent, requiring several tedious column chromatography passes for purification of long alkenyl bromides. Figure 6-1 outlines the first-try synthetic strategy which targeted octatriacont-37-en-1-yl 4-methylbenzenesulfonate (compound **6-9**) to generate monomers with 36 methylene run length.

[4] Part of this chapter is adapted with permission from (Inci, B.; Wagener, K. B. *Journal of the American Chemical Society*, **2011**, 133, 11872). Copyright (2011) American Chemical Society.

In this synthetic scheme, the tosylated alcohol is preferred over the bromide as a leaving group to increase the polarity difference between compounds **6-5** and **6-6** and facilitate the column chromatographic separation. Commercially available undec-10-en-1-ol (**6-1**) was tosylated with *p*-toluenesulfonyl chloride in the presence of pyridine to yield compound **6-2**. Self-metathesis and hydrogenation of alkenyl tosylate gave icosane-1,20-diyl bis(4-methylbenzenesulfonate) **6-4** in high yield. However, the elimination step with *t*-BuOK to give compounds **6-5** and **6-6** was not successful. While the conversion of a tosylate to the corresponding alkene is a common strategy, the elimination is usually done in two steps[199-201]. Thus, the tosylates are generally converted first to the iodide and then subjected to elimination[202]. From the purification viewpoint, formation of alkenyl iodide will not enhance the polarity difference between the mono and di-elimination products.

Another synthetic strategy (Figure 6-2) was followed to increase the ethylene run length utilizing compound **6-4**. In this synthetic scheme, 1.5 equivalents of alkenyl bromide **6-10** is coupled with icosane-1,20-diyl bis(4-methylbenzenesulfonate) **6-4** to generate hentriacont-30-en-1-yl 4-methylbenzenesulfonate (**6-11**).

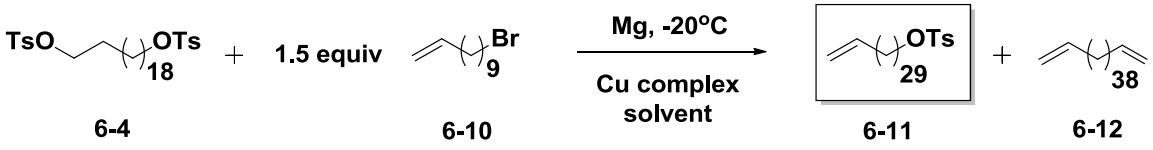

Figure 6-2. Synthetic strategy to generate alkylating agent with 29 methylene run length.

Typical Grignard conditions were employed with Mg at -20^{o}C, but the desired tosylate substitution was not observed. Copper based complexes[203-206] and salts[207] are widely used in carbon-carbon bond forming reactions and exhibit highly selective

substitutions with alkyl and alkenyl groups with aryl halides or tosylates. The effects of the copper species on the Grignard coupling reaction were examined and the results are presented in Table 6-1. Catalyst loadings of 10 mole% were employed, but in addition to desired alkenyl tosylate **6-11**, double substitution product **6-12** was also observed. After purification, compound **6-11** was recovered in very low yields.

Table 6-1. Effect of copper species on Grignard coupling.

Type of Cu species	Mole%	Solvent	Yield(%)
no addition	--	THF	no substitution
CuI	10.0	THF	0.5
CuI	10.0	THF/toluene (2:1)	1.6
Li_2CuCl_4	10.0	THF/toluene (2:1)	5.2
Bu_2CuLi	10.0	THF/toluene (2:1)	1.8

Increasing the yield of the Grignard reaction shown in Figure 6-2 requires the use of a more efficient catalyst system. Burns et.al. reported a highly effective copper catalyst for the coupling of Grignard reagents with tosylates and mesylates[208]. Synthesis includes the preparation of $CuBrSMe_2$, LiBr and LiSPh in THF solution to form thiophenol and a LiBr ligated copper species to increase the nucleophilicity of the Grignard reagent. The procedure was previously utilized[118] for the preparation of the hexyl branched symmetrical diene monomers with shorter ethylene run lengths, and moderate yields (55-60%) were obtained for the coupling reaction.

This synthetic methodology was employed for the preparation of monomer **6-17**, as shown in Figure 6-3. The symmetrical α,ω-diene **6-13** starting material with a 9 methylene run length was generated according to a previously published two-step alkylation/decyanation procedure[156,157]. Hydroboration/oxidation and subsequent mesylation gave compound **6-15** in a moderate overall yield (41%). Mesylated di-functional alcohol was intended to couple with the Grignard reagent **6-16** in the

presence of an equimolar mixture of copper bromide dimethyl sulfate, lithium bromide and lithium thiophenolate in THF. It is important to note that, unlike the alkenyl tosylate route (Figure 6-2), Grignard coupling is performed after the branch incorporation to ensure double substitution with 2 equivalents of alkenyl magnesium bromide **6-16**.

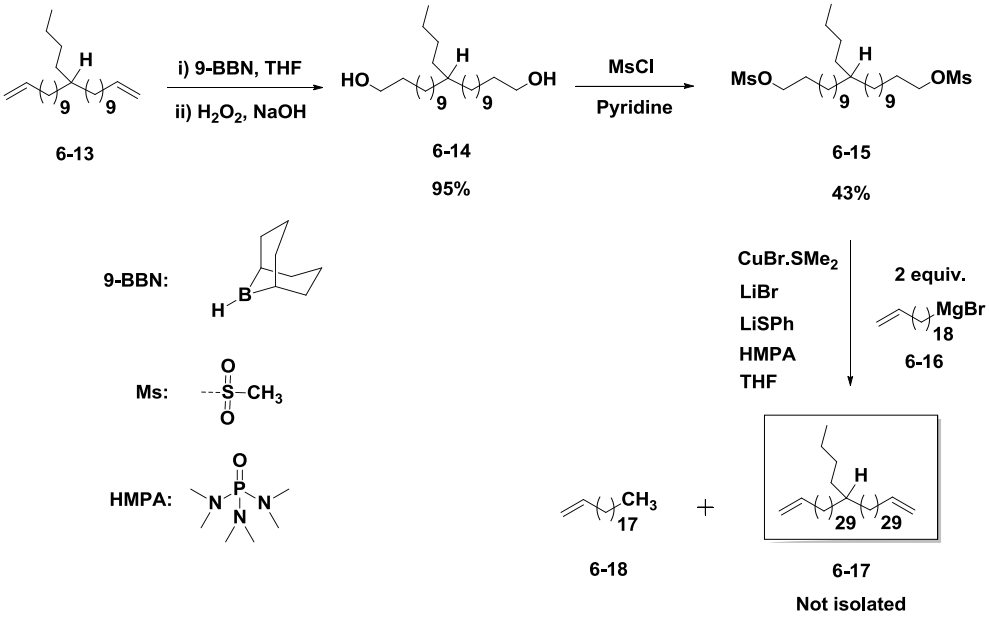

Figure 6-3. Synthetic strategy to generate monomer **6-17** with 29 methylene run length.

Purification of the crude product yielded a mixture of monomer **6-17** and undesired compound **6-18**. During the work-up step, unreacted Grignard reagent abstracts a proton from water and forms icos-1-ene (**6-18**). Monomer **6-17** could not be isolated, because of the insufficient polarity difference between compound **6-17** and **6-18**.

The successful synthesis of alkenyl bromide with a 36 methylene run length is shown in Figure 6-4. The scheme includes self-metathesis of 20-bromo-eicos-1-ene **6-19** (preparation of compound **6-19** is described in Chapter 4) in the presence of first generation Grubbs` metathesis catalyst and hydrogenation of unsaturated dibromide **6-20** with Wilkinson`s catalyst to give 1,38-dibromooctatriacontane (**6-21**). Because of the

low solubility of compound **6-21** in THF, the reaction temperature was set to 40^{o}C, and 1.5 equivalents of *t*-BuOK was used for dehydrohalogenation of alkyl dibromide **6-21** to suppress (but not eliminate entirely) the formation of the di-elimination product **6-23**.

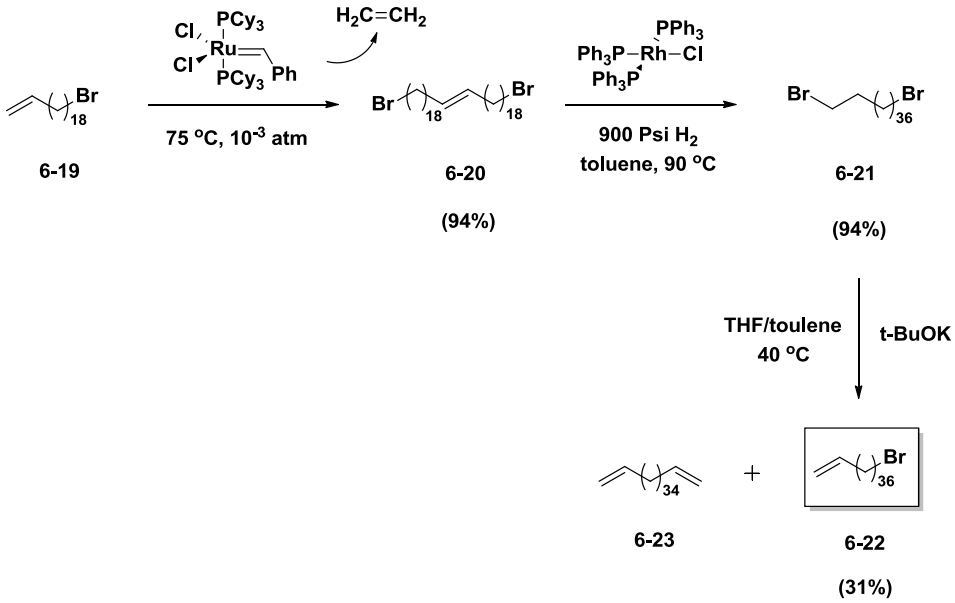

Figure 6-4. Synthesis of alkenyl bromide **6-22** with 36 methylene run length.

The crude mixture contained the desired alkenyl bromide **6-22**, the di-elimination product **6-23**, and unreacted starting material, all with close retardation factors by thin layer chromatography. Due to the similar polarities of these three species and the relatively low room temperature solubility of the crude mixture in hexane, the special purification procedure was followed. The crude mixture was first dissolved in toluene and mixed with a small amount of silica gel to form a slurry. Toluene was slowly evaporated and the crude mixture adsorbed on silica particles were added on freshly packed (technical grade hexane is used for column packing) column to form a uniform layer. Then, another uniform layer of pristine silica gel was added on top of the crude layer. Hexane was slowly added to the column without disturbing both layers. Flow rate of the column was also adjusted to obtain the most efficient separation. Ultrapure silica

gel with small particle size (5-20 µm, 60 Å pore size) is used for column packing. After four column chromatography passes, the desired alkenyl bromide **6-22** was recovered in moderate yield (31%).

As described in Chapter 4, alkylation of various primary nitriles with 20-bromoicos-1-ene **6-19** works efficiently and gives the corresponding monomers with different branches in moderate to high overall yields. The efficiency of alkylation with a longer alkenyl bromide (in this case 38-bromooctatriacont-1-ene, **6-22**) was reacted with hexanenitrile **6-24** (Figure 6-5) in the presence of lithium diisopropyl amide (LDA).

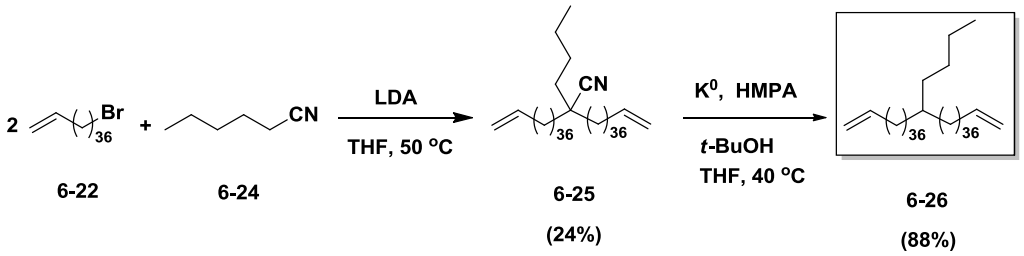

Figure 6-5. Synthesis of symmetrical α,ω-diene monomer with a butyl branch on every 39th carbon.

Because of the low solubility of **6-22** in THF at low temperatures, toluene was used as a co-solvent. However, the low solubility of LDA in toluene dramatically decreased the efficiency of the alkylation. Thus, the traditional procedure (ie, addition of base at -78^{o}C and alkylation at 0^{o}C) for nitrile alkylation was not followed, and 50^{o}C was selected as the reaction temperature in THF. The elevated temperature increased the likelihood of undesired side reactions, such as alkenyl bromide elimination. After purification,2-butyl-2-(octatriacont-37-en-1-yl)tetracont-39-enenitrile (**6-25**) was recovered in moderate yield (24%). The decyanation step was also performed at

elevated temperature (40^{o}C) and 39-butylheptaheptaconta-1,76-diene (**6-26**) was recovered in a reasonably high yield (88%).

6.2 Polymer Synthesis and Characterization

Because of the relatively high melting point of monomer **6-22** (T_m=77^{o}C), the polymerization temperature was set to 100^{o}C, where Ru-based catalysts are prone to have low turnover numbers and to generate Ru-H species[159-161], which would cause isomerization problems and disrupt the symmetrical nature of the monomer[162,163]. Therefore, monomer **6-26** was condensed to form the unsaturated ADMET polymer using Schrocks` [Mo] catalyst for clean metathesis chemistry as shown in Figure 6-6.

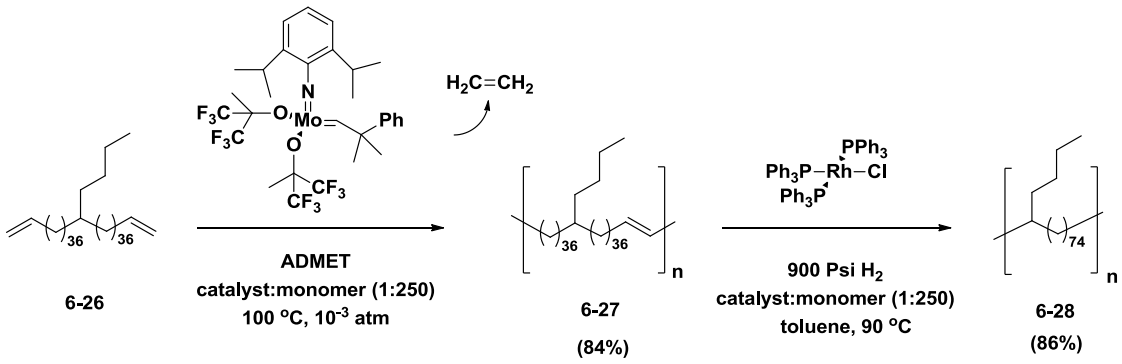

Figure 6-6. Synthesis of precision polymers possessing a branch on every 39th carbon.

Due to the oxophilic nature of [Mo] catalysts, all manipulations prior to polymerization and catalyst addition (catalyst to monomer ratio 1:500) were performed in a glove box. Polymerization was initiated by melting the monomer at 77^{o}C, and the temperature was set to 100^{o}C to be able to stir the viscous polymer melt. After 24 hours of reaction, the polymer was cooled to RT, another portion of [Mo] catalyst (catalyst to monomer ratio 1:500) was added in a glove box, and the temperature was returned to 100^{o}C. ADMET polymerization proceeded smoothly to give the desired unsaturated linear polymer **6-27** with no detectable side reactions. Disappearance of terminal olefin

signals in the ^{1}H NMR spectrum (Figure 6-7) proved the complete conversion, which is necessary for any step-growth polymerization. Unsaturated polymer **6-27** was hydrogenated utilizing Wilkinson`s catalyst (catalyst to monomer ratio 1:250) to yield the precision polyethylene (polymer **6-28**) having a butyl branch on every 75th carbon.

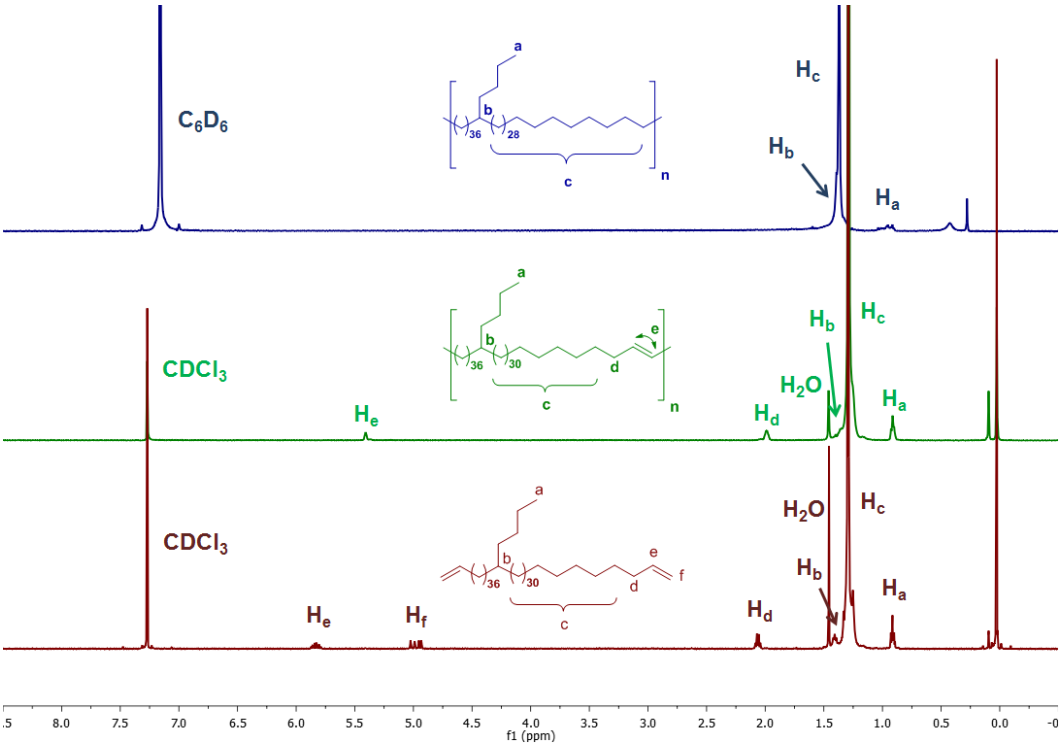

Figure 6-7. ^{1}H NMR spectra of monomer (**6-26**), unsaturated (**6-27**) and saturated (**6-28**) polymers.

The polymerization and hydrogenation steps were followed by ^{1}H NMR spectroscopy. Figure 6-7 shows the ^{1}H NMR spectra of butyl branched polymer, **6-28**, and its precursors. ADMET polymerization of monomer **6-26** yielded the unsaturated polymer, **6-27**. Formation of the ADMET polymer was evidenced by loss of the terminal olefin signals (5.0 and 5.8 ppm) and the appearance of the internal olefin resonance at 5.4 ppm (Figure 6-7). Exhaustive hydrogenation of the internal olefins with Wilkinson`s catalyst generated **6-28**, corresponding to polyethylene with butyl branches on every 75th carbon, with complete loss of the olefinic signals in the ^{1}H NMR spectrum.

After the hydrogenation, the solution of saturated polymer was concentrated and precipitated over methanol. It is important to note that the solubility characteristics of polymer **6-28** (soluble in toluene, dichlorobenzene, trichlorobenzene, etc. at high temperatures) are similar to those of polyethylenes prepared by chain polymerization.

Table 6-2. Molecular weight data for polymers **6-23** and **6-24**

Polymer	$\overline{M}_n$ (kg/mol)[a]	$\overline{M}w$ (kg/mol)[a]	PDI
6-27	16.3	46.7	2.86
6-28	17.7	50.2	2.83

[a]Molecular weight data were collected by GPC in 1,2,4-trichlorobenzene at 135°C relative to polystyrene standards. [b]PDI, polydispersity index $\overline{M}w/\overline{M}_n$.

Molecular weight data were obtained using high temperature gel permeation chromatography (GPC) in 1,2,4-trichlorobenzene at 135°C relative to polystyrene standards. Table 6-2 presents the molecular weight data for precisely butyl branched unsaturated **6-27** and saturated **6-28** polymers.

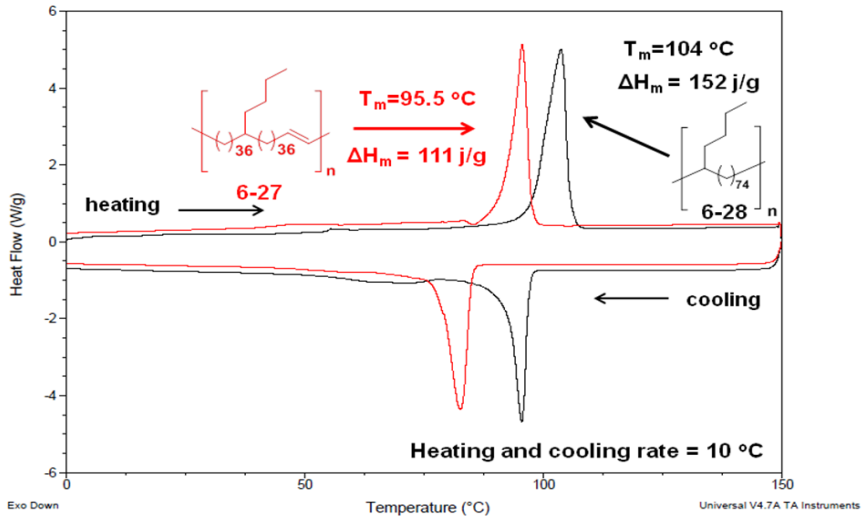

Figure 6-8. DSC exotherms (down) and endotherms (up) for unsaturated (**6-27**) and saturated (**6-28**) polymers.

Figure 6-8 shows the DSC thermograms of the unsaturated **6-27** and saturated **6-28** polymers in both the heating and cooling cycles. The polymers are semicrystalline,

having the melting transitions at 95.5 and 104^{o}C, and as expected, saturation increases both the melting points and the heat of fusion values. The melting transitions of both polymers are sharper than those for chain-polymerized poly(ethylene-*co*-hexene) and other ethylene/α-olefin copolymers, illustrating the importance of precision placement of the branches[209,210].Thermal data for polymer **6-28** and other previously reported precision polyethylenes with more frequent butyl branches[6] (Table 6-3) clearly demonstrate the effect of precision run length in these materials. As the run length increases between two consecutive branch points, the melting point gradually increases, approaching that of ADMET PE (linear PE without branches, T_m=134^{o}C).

Table 6-3. DSC data for precision polyethylenes possessing butyl branch.

Butyl branch on every *n*th carbon, *n*	Butyl branches per 1000 carbon atoms	T_m (^{o}C)	ΔH_m (J/g)
ADMET PE	0	134	204
75	13	104	152
39	26	75.0	66.0
21	48	14.0	47.0
15	67	-33.0	13.0
5	200	amorphous	---

To compare the experimental data for butyl branched precision polymers with theoretical predictions for infinitely long polyethylene interpreted by Flory[211], a plot of melting point vs number of butyl branches per 1000 carbons as shown in Figure 6-9. The plot shows good linearity, an indication of the similarity in thermal behavior between ADMET PE and infinitely long PE.

Morphological examination by WAXD is illustrated in Figure 6-10 for polymer **6-28**, **ADMET PE** and commercial **HDPE** made with Mulheim catalyst. The similarity of polymer **6-28** to **ADMET PE** and **HDPE** is obvious: All three polymers exhibit the typical orthorhombic unit cell structure with two characteristic crystalline peaks observed at

21.5° and 24.0°, corresponding to reflection planes (110) and (200), respectively. Unlike the precision polymer **4-29e-(butyl)** (Figure 5-9 in Chapter 5), the X-ray diffractogram of polymer **6-28** does not display the crystalline peak at the amorphous halo region, confirming the absence of the metastable phase formation.

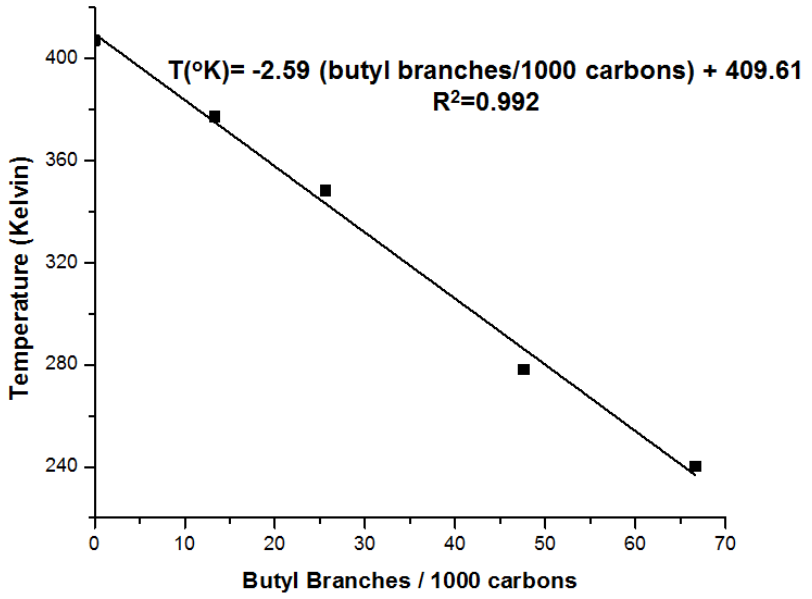

Figure 6-9. Plot of melting temperature vs butyl branch frequency in precision polyethylenes.

Increasing the distance between the two consecutive branches from 38 carbons (5.26 mole% branch concentration) to 74 carbons (2.70 mole% branch concentration) fully expels the butyl branches from the crystal lattice to the amorphous phase. Precision polymer **6-28** represents the first realistic model of commercial LLDPE reported so far in precision polyolefin research.

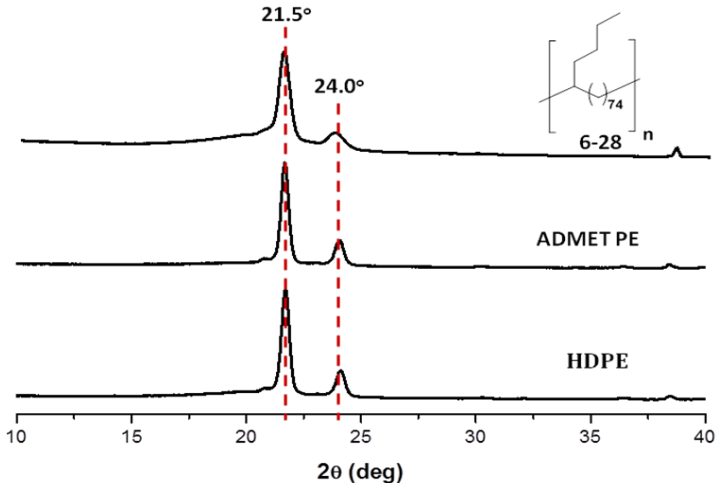

Figure 6-10. WAXD diffractograms of precision polymer **6-28**, ADMET PE, and commercially available High Density Polyethylene (HDPE) prepared with Mulheim catalyst. Data were collected at RT for all polymer samples.

6.3 Experimental Section

6.3.1 Instrumentation

All ^{1}H NMR (300 MHz) and ^{13}C NMR (75 MHz) spectra were recorded in $CDCl_3$ unless otherwise stated. Chemical shifts were referenced to signals from $CDCl_3$ (7.24 ppm for ^{1}H, 77.23 ppm for ^{13}C) with 0.03% v/v TMS and from C_6D_6 (7.16 ppm for ^{1}H, 128.62 ppm for ^{13}C) as an internal reference. For all the NMR work the solvents were chloroform-*d* or benzene-*d* and the temperature was 25 or 75^{o}C. High-resolution mass spectrometry (HRMS) was carried out using a Agilent 6210 TOF-MS mass spectrometer in the direct analysis in real-time (DART) mode with an IonSense DART Source. Thin layer chromatography (TLC) was used to monitor all reactions and was performed on glass plates coated with silica gel (250 μm thickness). Column chromatography was

performed using ultrapure silica gel (40-63 μm, 60 Å pore size). For the purification of 38-bromooctatriacont-1-ene (8), ultrapure silica gel (5-20 µm, 60 Å pore size) was purchased from SiliCycle®. Gel permeation chromatography (GPC) was performed using an Alliance GPC 2000 with an internal differential refractive index detector (DRI), internal differential viscosity detector (DP), and a precision angle light scattering detector (LS). The light scattering signal was collected at a 15° angle, and the three in-line detectors were operated in series in the order LS-DRI-DP. The chromatography was performed at 135°C using a PLgel MIXED-B column (10 μm PD, 8.0 mm ID, 300 mm total length) with HPLC grade 1,2,4-trichlorobenzene as the mobile phase at a flow rate of 1.0 mL/min. Injections were made at 0.05-0.07% w/v sample concentration using a 322.5 μL injection volume. In the case of universal calibration, retention times were calibrated versus narrow-range molecular weight polystyrene standards (purchased from Polymer Standard Service PSS in Mainz, Germany).

Differential scanning calorimetry (DSC) was performed using a TA Instruments DSC Q1000 equipped with a controlled cooling accessory at a heating rate of 10°C/min, unless otherwise specified. Calibrations were made using indium and freshly distilled *n*-octane as the standards for peak temperature transitions and indium for the enthalpy standard. Wide-angle X-ray (WAXS) powder diffraction data were collected on a Mar345 Image Plate Detector with plate diameter of 345 mm and outside dimensions (515 mm * 398 mm * 350 mm). The Cu Kα radiation (λ = 0.15417 nm) produced by a generator operating at 40 kV and 150 mA. Diffraction patterns were recorded for 2θ-values ranging 10° to 40°.

6.3.2 Materials

Chemicals were purchased from the Aldrich Chemical Co. and used as received unless otherwise noted. Grubbs` first generation catalyst, bis(tricyclohexylphosphine)benzylidineruthenium(IV) dichloride, was kindly provided by Materia, Inc. Schrock`s molybdenum metathesis catalyst, $[(CF_3)_2CH_3CO]_2$(N-2,6-C_6H_3-*i*-Pr_2)Mo=CHC$(CH_3)_2$Ph, and Wilkinson's rhodium hydrogenation catalyst, $RhCl(PPh_3)_3$, were purchased from Strem Chemical. Ruthenium and molybdenum catalysts were stored in an argon-filled glovebox prior to use. Tetrahydrofuran (THF) and toluene were freshly used from Butler Polymer Research Laboratories anhydrous solvent preparation unit. HPLC grade 1,2,4-trichlorobenzene was purchased from the Applichem GmbH. HDPE is kindly provided by BASF (M_n=34000 g/mol and PDI=7.43). All the nitriles and alkenyl bromide starting materials, as well as hexamethylphosphoramide and diisopropyl amine were distilled over CaH_2. All reactions were carried out in flame-dried glassware under argon unless otherwise stated.

6.3.3 Procedures

Synthesis of 1,38-dibromooctatriacont-18-ene (6-20). Compound **6-19**, 20-bromo-eicos-1-ene, (4.252g, 1.18 mmol) was placed in a flame-dried reaction tube under vacuum (10^{-3}atm) for 2 hours at 75^{o}C. Grubbs 1st generation catalyst (0.004 g, 4.85×10^{-3}) was added, and the mixture was left at 75^{o}C under vacuum (10^{-3}atm) for 24 hours. The reaction was quenched with 5 mL ethyl vinyl ether and dissolved in 15 mL toluene. The toluene solution was concentrated and the product was precipitated by pouring into 1.0 L of methanol. Crystals were filtered and dried under vacuum overnight. 3.818 g of compound **6-20** was recovered as white crystals. (Yield=94%) ^{1}H NMR ($CDCl_3$): δ (ppm), 1.20-1.38 (br, 64H, CH_2), 2.01-2.08 (q, 4H, allyl CH_2), 3.42 (t, 4H, CH_2Br), 5.39

(m, 2H, vinyl CH) ; ^{13}C NMR ($CDCl_3$) : δ (ppm) 28.3, 29.4, 29.6, 29.8, 32.8, 33.1, 34.7, 130.125 (vinyl CH, *cis*), 130.58 (vinyl CH, *trans*).; DART/HRMS: $[M]^+$ calculated for $C_{38}H_{74}{}^{79}Br_2$: 688.8422, found: 688.4157. Calculated for $C_{38}H_{74}{}^{81}Br_2$: 6692.9042, found: 6692.4304. Elemental analysis calculated for $C_{38}H_{74}Br_2$: 66.07 C, 10.80 H; found: 65.35 C, 10.75 H.

Synthesis of 1,38-dibromooctatriacontane (6-21). Compound **6-20**, 1,38-dibromooctatriacont-18-ene, (3.818g, 0.553 mmol) was dissolved in 50 mL degassed toluene, placed in a Parr bomb with 0.55 mg, 0.85×10^{-3} mmol Wilkinson`s catalyst and left to react at 90^{o}C under 900 psi of hydrogen for 36 hours. The toluene solution was concentrated and the product was precipitated by pouring into 0.5 L of methanol. Crystals were filtered and dried under vacuum overnight. 3.605 g of compound **6-21** was recovered as white crystals. (Yield = 94%) ^{1}H NMR ($CDCl_3$): δ (ppm), 1.30-1.45 (br, 72H, CH_2), 3.42 (t, 4H, CH_2Br); ^{13}C NMR ($CDCl_3$) : δ (ppm) 28.5, 29.0, 29.7, 29.9, 33.2, 34.0 DART/HRMS: $[M]^+$ calculated for $C_{38}H_{76}Br_2$: 690.4314, found: 690.4261. Elemental analysis calculated for $C_{38}H_{76}Br_2$: 66.07 C, 10.79 H; found: 64.84 C, 10.75 H.

Synthesis of 38-bromooctatriacont-1-ene (6-22). In a 250 mL round bottomed flask, compound **6-21** (3.324g, 0.481 mmol) was dissolved in a 2:1 toluene/THF (150 mL/75 mL) mixture. The mixture was warmed to 40^{o}C and potassium *tert*-butoxide (0.086g, 0.771 mmol) was added under argon flow. The reaction mixture was stirred at 40^{o}C for 24 hours. Solvents were evaporated and the crude product was purified by column chromatography using hexane as the eluent and SiliCycle® silica gel with 5-20 µm particle size. 0.923 g of compound **6-22** was recovered after purification. (Yield= 31%). ^{1}H NMR ($CDCl_3$): δ (ppm), 1.30-1.45 (br, 68H, CH_2), 2.01-2.08 (q, 4H, allyl CH_2),

3.42 (t, 4H, CH_2Br), 4.91-5.04 (m, 4H, vinyl CH_2), 5.78-5.87 (m, 2H, vinyl CH); ^{13}C NMR ($CDCl_3$) : δ (ppm) 27.1, 29.2, 29.3, 29.9, 30.4, 33.8, 36.3, 114.3, 139.4; DART/HRMS: $[M]^+$ calculated for $C_{38}H_{75}Br$: 609.4974, found: 609.4981. Elemental analysis calculated for $C_{38}H_{75}Br$: 74.59 C, 12.35 H; found: 74.22 C, 11.94 H.

Synthesis of 2-butyl-2-(octatriacont-37-en-1-yl)tetracont-39-enenitrile (6-25). Compound **6-22**, (1.290g, 0.210 mmol) was placed in a flame-dried 25 mL reaction tube and stirred under vacuum for 2 hour at 85^{o}C. In a separate flame-dried 50 mL 2-neck round bottomed flask, diisopropyl amine (0.22g, 2.10 mmol) was dissolved in 5 mL of anhydrous THF. A 1.4 mL sample of 1.5 M (freshly distilled) n-BuLi (2.10 mmol) was added slowly at -78^{o}C for 5 minutes under argon flow. The LDA solution was warmed to 0^{o}C and stirred for 30 minutes, then cooled to -78^{o}C prior to adding 0.11g hexanenitrile **6-24** (1.13 mmol) over 5 minutes. The reaction mixture was warmed to 0^{o}C and stirred for 30 minutes. This solution was slowly transferred via cannula to the reaction flask for the alkylation reaction in one portion at RT (alkylating agent **6-22** was not soluble at RT in THF). The reaction temperature was increased to 50^{o}C to dissolve compound **6-22** and stirred for 12 hours under argon flow. The solvents were evaporated and the crude product was purified by column chromatography using (hexane/toluene, 9:1) as eluent. 0.292g, 0.025 mmol, of compound **6-25** was recovered as a white solid. (Yield= 24%). ^1H NMR ($CDCl_3$): δ (ppm), 0.94 (t, 3H, CH_3), 1.22-1.34 (br, 146H, CH_2), 2.01-2.08 (q, 4H, allyl CH_2), 4.90-5.03 (m, 4H, vinyl CH_2), 5.76-5.88 (m, 2H, vinyl CH); ^{13}C NMR ($CDCl_3$) : δ (ppm) 14.1, 23.1, 24.5, 26.7, 29.1, 29.4, 29.7, 29.9, 34.1, 36.1, 36.4, 40.9, 114.3, 124.8, 139.5; DART/HRMS: $[M]^+$ calculated for $C_{82}H_{159}N$: 1159.2545, found:

1159.2538. Elemental analysis calculated for $C_{82}H_{159}N$: 84.97 C, 13.83 H, 1.21 N; found: 85.06 C, 13.66 H, 1.23 N.

Synthesis of 39-butylheptaheptaconta-1,76-diene (6-26). Potassium metal (0.340g, 8.69 mmol), HMPA (0.9mL, 4.87 mmol), and anhydrous THF (45 mL) were transferred to a 100 mL flame dried 3-necked round bottomed flask equipped with a stir barr. Compound **6-25** (0.292g, 0.025 mmol) was added to the slurry in one portion at RT under argon flow. The temperature was raised to 40^{o}C to dissolve compound **6-25** and 0.45 mL of *t*-BuOH (7.78 mmol) was added. The reaction mixture was stirred for 24 hours and then quenched with isopropanol (10 mL). The solvents were evaporated and the crude product was purified by column chromatography using hexane as the eluent. 0.253g, 0.022 mmol, of compound **6-26** was recovered as a white solid. (Yield=88%). ^{1}H NMR ($CDCl_3$): δ (ppm), 0.90 (t, 3H, CH_3), 1.24-1.32 (br, 146H, CH_2), 1.35-1.41 (m, 1H, CH), 2.01-2.08 (q, 4H, allyl CH_2), 4.90-5.03 (m, 4H, vinyl CH_2), 5.76-5.88 (m, 2H, vinyl CH); ^{13}C NMR ($CDCl_3$) : δ (ppm) 14.3, 23.4, 27.1, 29.2, 29.4, 29.8, 29.9, 30.4, 32.1, 33.9, 34.0, 34.2, 37.8, 114.3, 139.5; Elemental analysis calculated for $C_{81}H_{160}$: 85.78 C, 14.22 H; found: 85.52 C, 14.36 H.

Polymerization of 39-butylheptaheptaconta-1,76-diene (6-27). Compound **6-26** (0.155g, 0.137 mmol) was placed in a 25 mL reaction tube and left under vacuum for 2 hours at 90^{o}C. The reaction tube was cooled to RT and placed into the glove box. Schrock`s catalyst (0.09g) was added, and the reaction tube was placed under vacuum again. Polymerization was started by raising the temperature to 100^{o}C, and the mixture was left under vacuum for 24 hours. Polymerization was quenched by opening the tube to the air and dissolving the contents in 10 mL of toluene. After precipitation over 0.5 L

of methanol and filtration, 0.130 g of polymer **6-27** was recovered as a white solid. (Yield=84%) ^{1}H NMR ($CDCl_3$): δ (ppm) 0.91 (t, CH_3), 1.21-1.36 (m, CH_2), 1.98 (q, allyl CH_2), 5.40 (m, vinyl CH); ^{13}C NMR ($CDCl_3$) : δ (ppm) 14.26, 23.36, 27.05, 29.46, 29.99, 30.43, 32.77, 33.81, 34.22, 37.83, 130.53.

Synthesis of polymer (6-28). In a 125 mL Parr bomb glass sleeve, unsaturated polymer **6-27** (0.110 g) was dissolved in 50 mL of degassed toluene. Wilkinson`s hydrogenation catalyst (0.7 mg, 7.6×10^{-4} mmol) was added, and the bomb was charged with 900 psi of hydrogen. The reaction was allowed to proceed for three days at 90^{o}C. The polymer solution was concentrated and precipitated in 0.5 L of methanol. The precipitate was filtered and dried under vacuum overnight. 0.95 g of polymer **6-28** was recovered as a white solid. (Yield=86%). ^{1}H NMR (C_6D_6): δ (ppm) 0.91 (d, CH_3), 1.21-1.47 (m, CH_2), 1.56 (m, CH); ^{13}C NMR (C_6D_6) : δ (ppm) 14.27, 29.99.

CHAPTER 7
SUMMARY AND OUTLOOK

Metathesis polycondensation chemistry has been employed to control the crystalline morphology of Linear Low Density Polyethylene (LLDPE) by precisely introducing alkyl branches along the polymer backbone. These polymers, while structurally akin to copolymers made via chain copolymerization of ethylene and vinyl comonomers, have unique properties, because use of symmetrical α, ω diene monomers ensures precise spacing of the chain branches. An important limitation in this work was synthesis of the symmetrical diene monomers required in this chemistry. Spacing in the symmetrical monomer directly determines the precision run lengths in the polymer: Prior monomer synthetic schemes have limited the maximum run lengths between branch points along the polymer to 20 methylene carbons (ie, a branch placed on each and every 21st carbon).

The present work described the systematic increase of precision run lengths to 38 and 74 methylene carbons. Successful preparation of symmetrical α,ω-dienes for both run lengths was presented. For the case of 38 run lengths, the synthesis and characterization of precisely sequenced polyethylenes containing thirteen different branches allowed systematic examination of the effect of branching on polyethylene properties. A clear change in morphology was observed for these polymers from a situation where the methyl branch is included in the polymer's unit cell, to one where branches of greater mass are partially expelled from the unit cell to form metastable crystalline morphologies. The precision LLDPE model polymers were characterized with Differential Scanning Calorimetry (DSC), Infrared Spectroscopy, Solid State Nuclear

Magnetic Resonance Spectroscopy, Wide Angle X-ray Scattering (WAXS) and Transmission Electron Microscopy (TEM).

Precision polymer with butyl branches on every 75th carbon was successfully prepared and X-ray investigation of this polymer displayed an orthorhombic unit cell structure with the absence of metastable phase formation. Increasing the distance between the two consecutive branches from 38 carbons (5.26 mole% branch concentration) to 74 carbons (2.70 mole% branch concentration) fully expels the butyl branches from the crystal lattice to the amorphous phase. This precision polymer with butyl branches on every 75th carbon represents the first realistic model of commercial LLDPE reported so far in precision polyolefin research.

Characterization of these precisely branched polymers should be continued to include temperature dependent WAXD, SS NMR and TEM analysis of all the precision polymers described in this document.

With the present level of advancement in precision polyolefin research, study of the effect of long chain branching in polyethylene is now possible. In the future, the model polymers should be prepared to mirror the commercial metallocene systems.

APPENDIX
DSC PROFILES OF PRECISION POLYMERS

DSC profiles of precision polymers with a branch on every 39th carbon. 2nd heating and 2nd cooling curves are shown (heating and cooling rate= 10^{o}C/min).

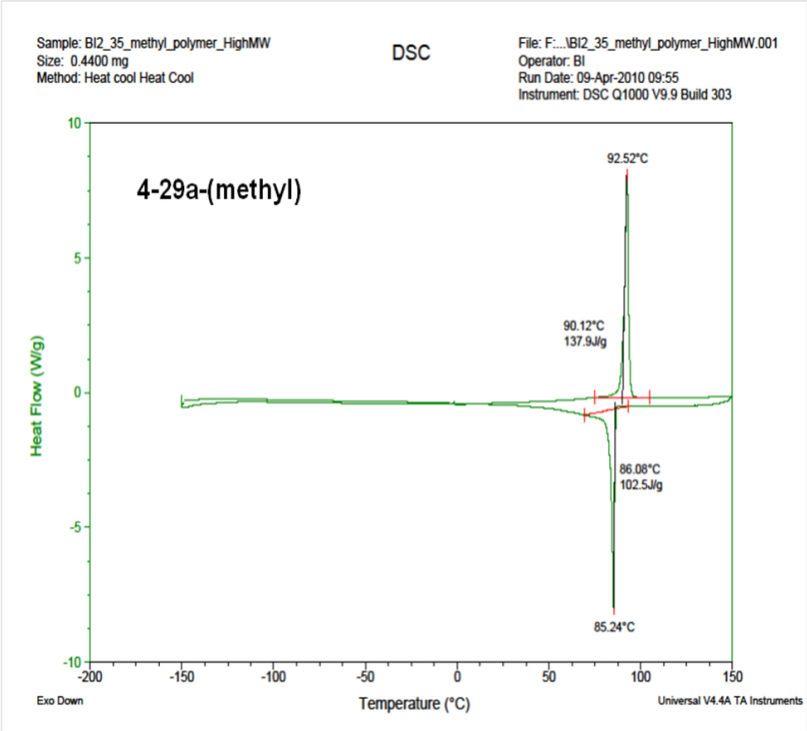

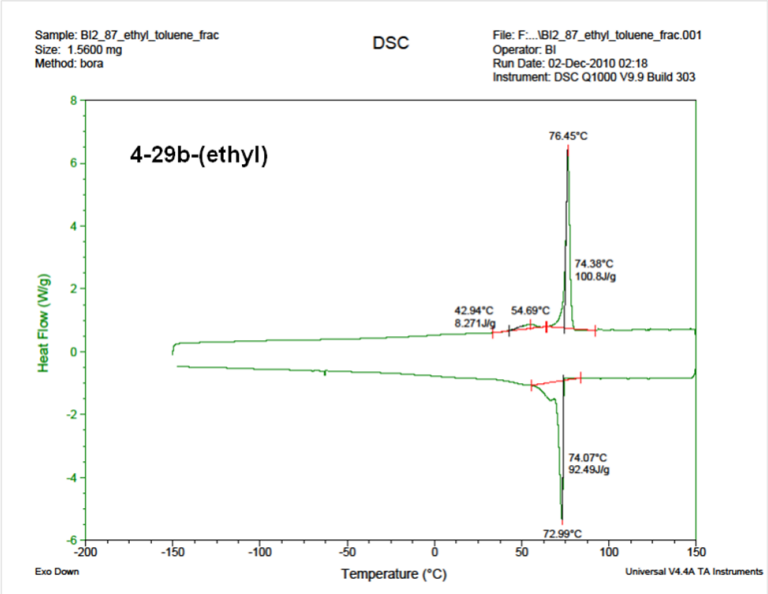

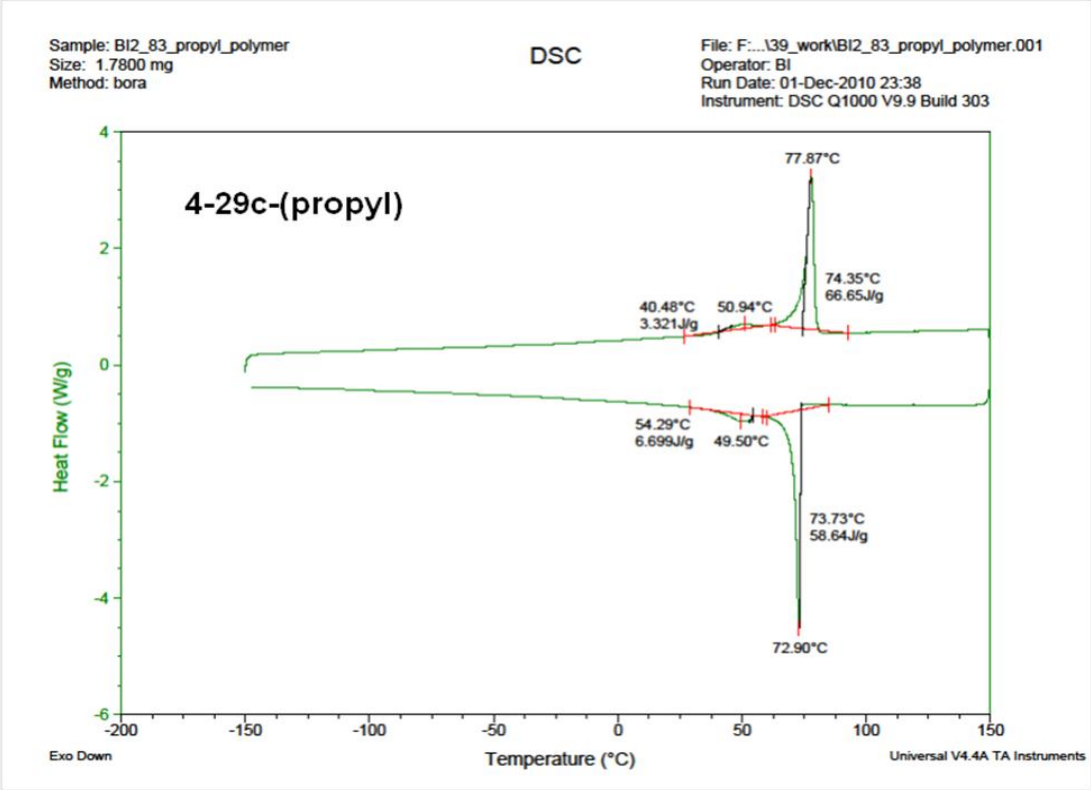
Sample: BI2_83_propyl_polymer
Size: 1.7800 mg
Method: bora
DSC
File: F:...\39_work\BI2_83_propyl_polymer.001
Operator: BI
Run Date: 01-Dec-2010 23:38
Instrument: DSC Q1000 V9.9 Build 303
4-29c-(propyl)
77.87°C
74.35°C
66.65J/g
40.48°C
3.321J/g
50.94°C
54.29°C
6.699J/g
49.50°C
73.73°C
58.64J/g
72.90°C
Heat Flow (W/g)
Exo Down
Temperature (°C)
Universal V4.4A TA Instruments

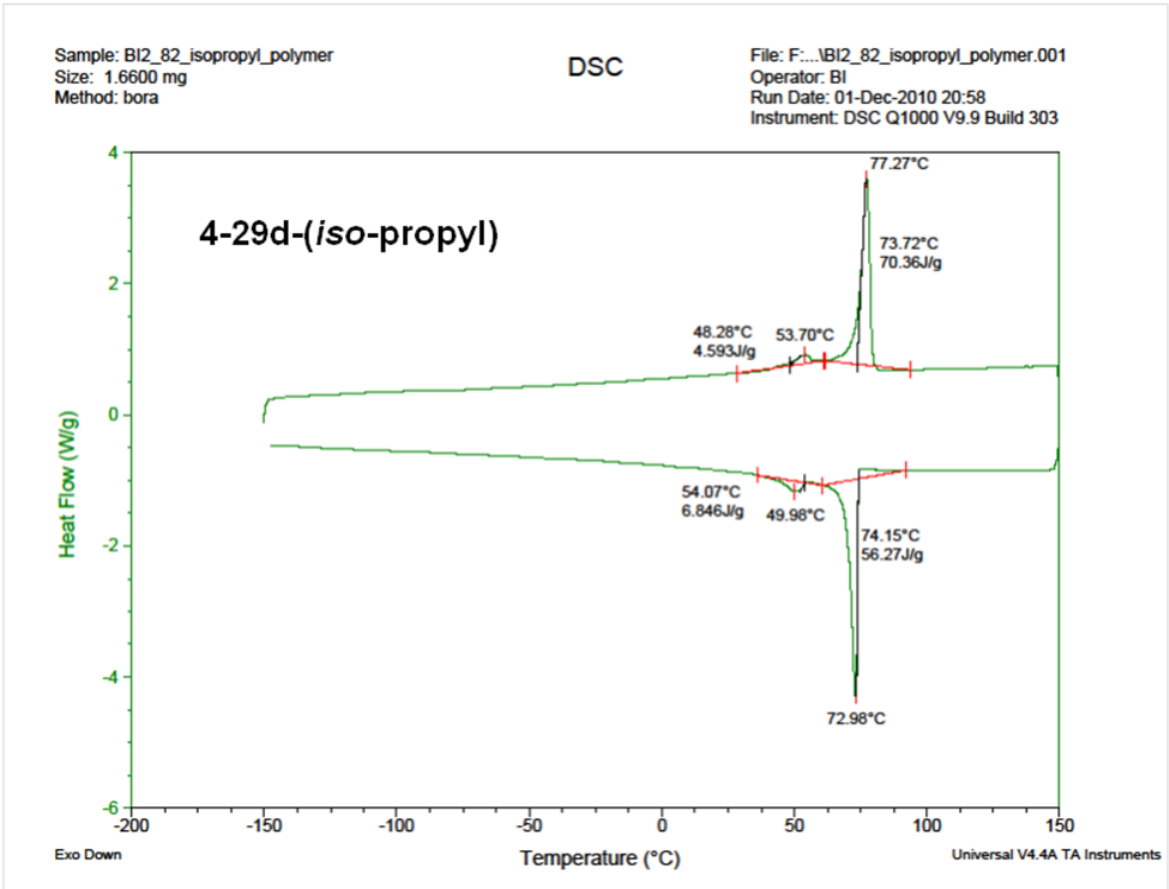
Sample: BI2_82_isopropyl_polymer
Size: 1.6600 mg
Method: bora
DSC
File: F:...\BI2_82_isopropyl_polymer.001
Operator: BI
Run Date: 01-Dec-2010 20:58
Instrument: DSC Q1000 V9.9 Build 303
4-29d-(iso-propyl)
77.27°C
73.72°C
70.36J/g
48.28°C
4.593J/g
53.70°C
54.07°C
6.846J/g
49.98°C
74.15°C
56.27J/g
72.98°C
Heat Flow (W/g)
Exo Down
Temperature (°C)
Universal V4.4A TA Instruments

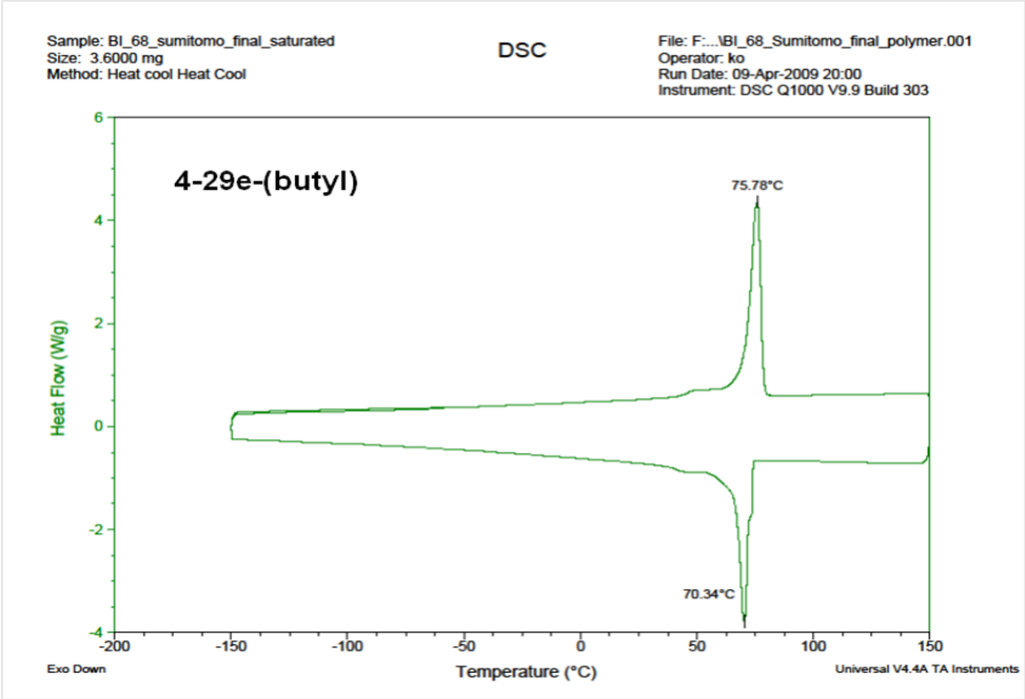
Sample: BI_68_sumitomo_final_saturated
Size: 3.6000 mg
Method: Heat cool Heat Cool
DSC
File: F:...\BI_68_Sumitomo_final_polymer.001
Operator: ko
Run Date: 09-Apr-2009 20:00
Instrument: DSC Q1000 V9.9 Build 303
4-29e-(butyl)
75.78°C
70.34°C
Heat Flow (W/g)
Temperature (°C)
Exo Down
Universal V4.4A TA Instruments

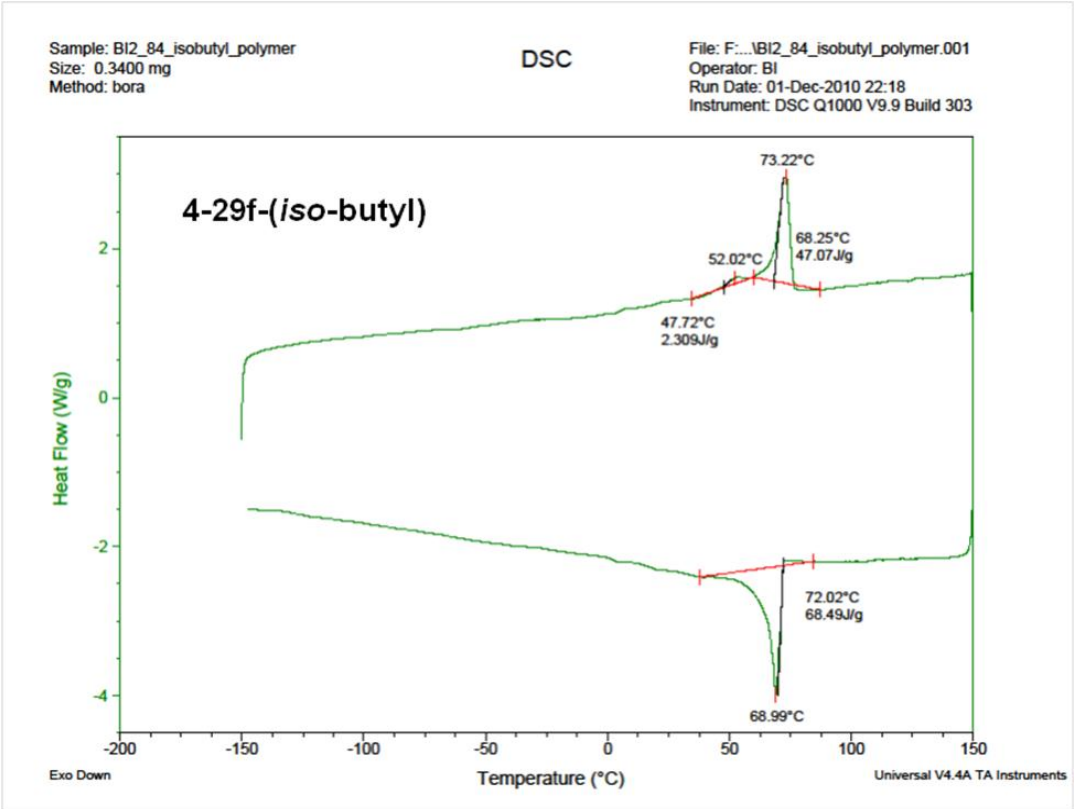
Sample: BI2_84_isobutyl_polymer
Size: 0.3400 mg
Method: bora
DSC
File: F:...\BI2_84_isobutyl_polymer.001
Operator: BI
Run Date: 01-Dec-2010 22:18
Instrument: DSC Q1000 V9.9 Build 303
4-29f-(iso-butyl)
73.22°C
68.25°C
47.07J/g
52.02°C
47.72°C
2.309J/g
72.02°C
68.49J/g
68.99°C
Heat Flow (W/g)
Temperature (°C)
Exo Down
Universal V4.4A TA Instruments

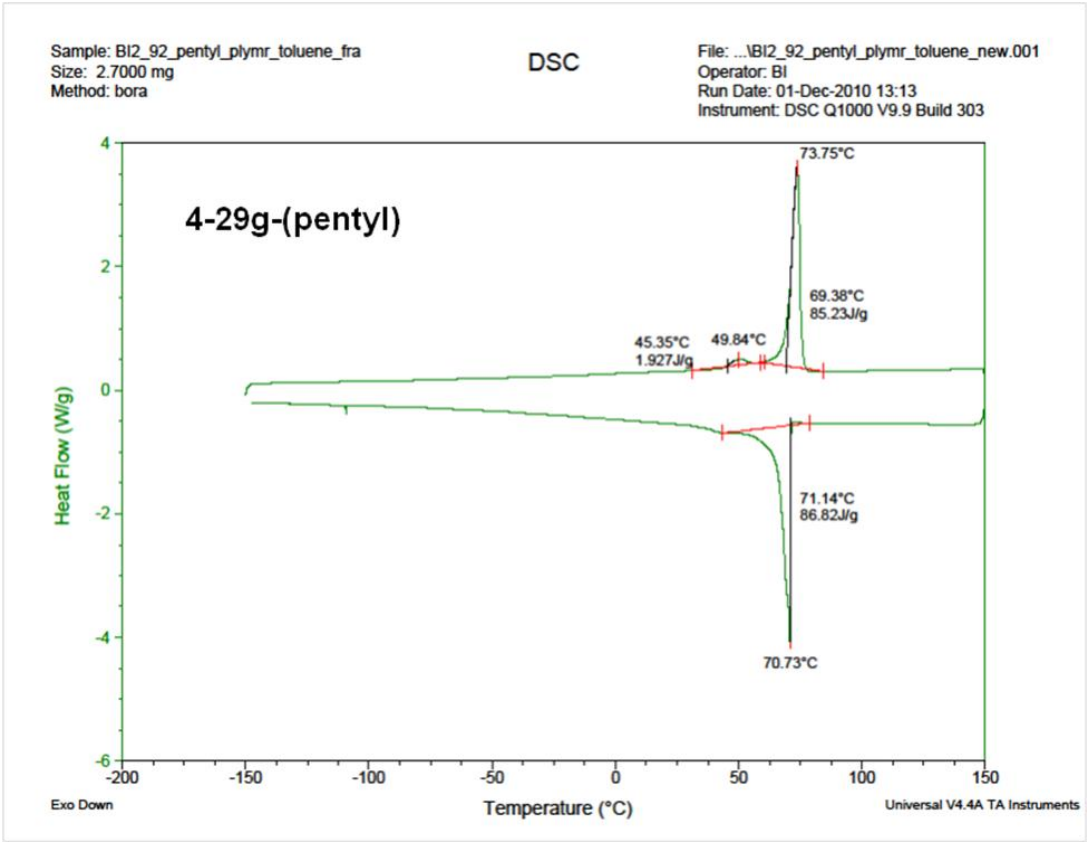
Sample: BI2_92_pentyl_plymr_toluene_fra
Size: 2.7000 mg
Method: bora
DSC
File: ...\BI2_92_pentyl_plymr_toluene_new.001
Operator: BI
Run Date: 01-Dec-2010 13:13
Instrument: DSC Q1000 V9.9 Build 303
4-29g-(pentyl)
73.75°C
69.38°C
85.23J/g
45.35°C
1.927J/g
49.84°C
71.14°C
86.82J/g
70.73°C
Heat Flow (W/g)
Temperature (°C)
Exo Down
Universal V4.4A TA Instruments

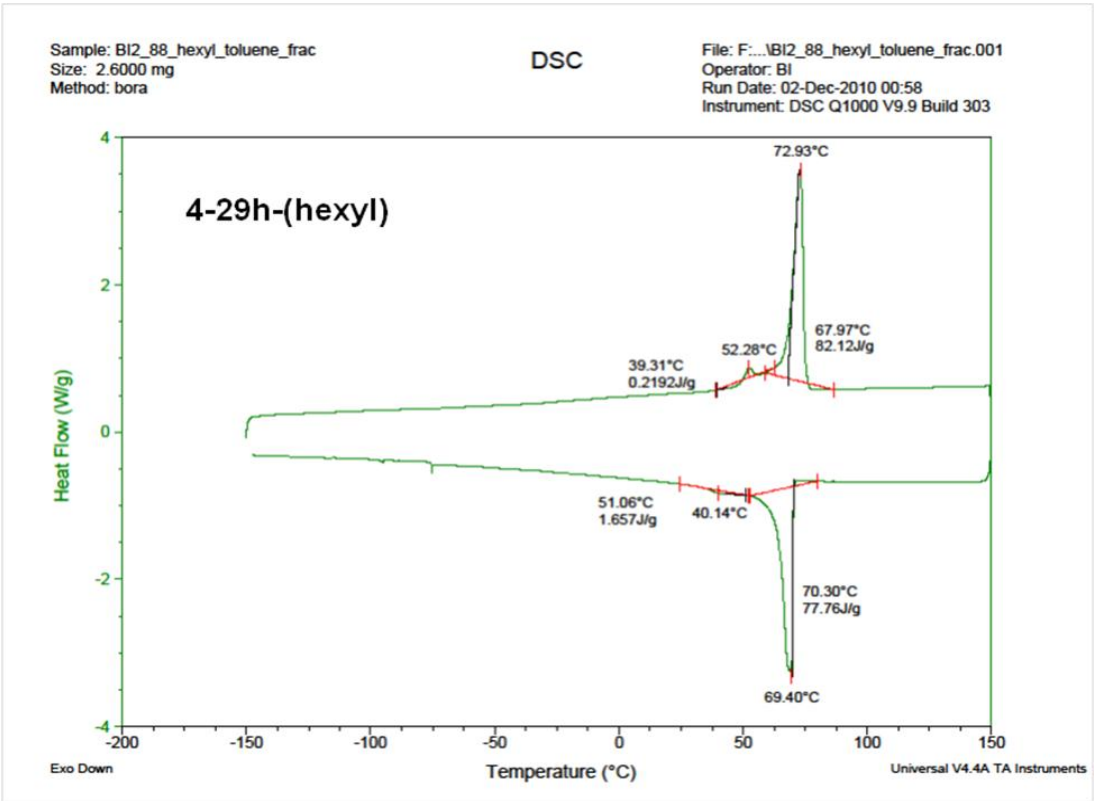
Sample: BI2_88_hexyl_toluene_frac
Size: 2.6000 mg
Method: bora
DSC
File: F:...\BI2_88_hexyl_toluene_frac.001
Operator: BI
Run Date: 02-Dec-2010 00:58
Instrument: DSC Q1000 V9.9 Build 303
4-29h-(hexyl)
72.93°C
67.97°C
82.12J/g
52.28°C
39.31°C
0.2192J/g
51.06°C
1.657J/g
40.14°C
70.30°C
77.76J/g
69.40°C
Heat Flow (W/g)
Temperature (°C)
Exo Down
Universal V4.4A TA Instruments

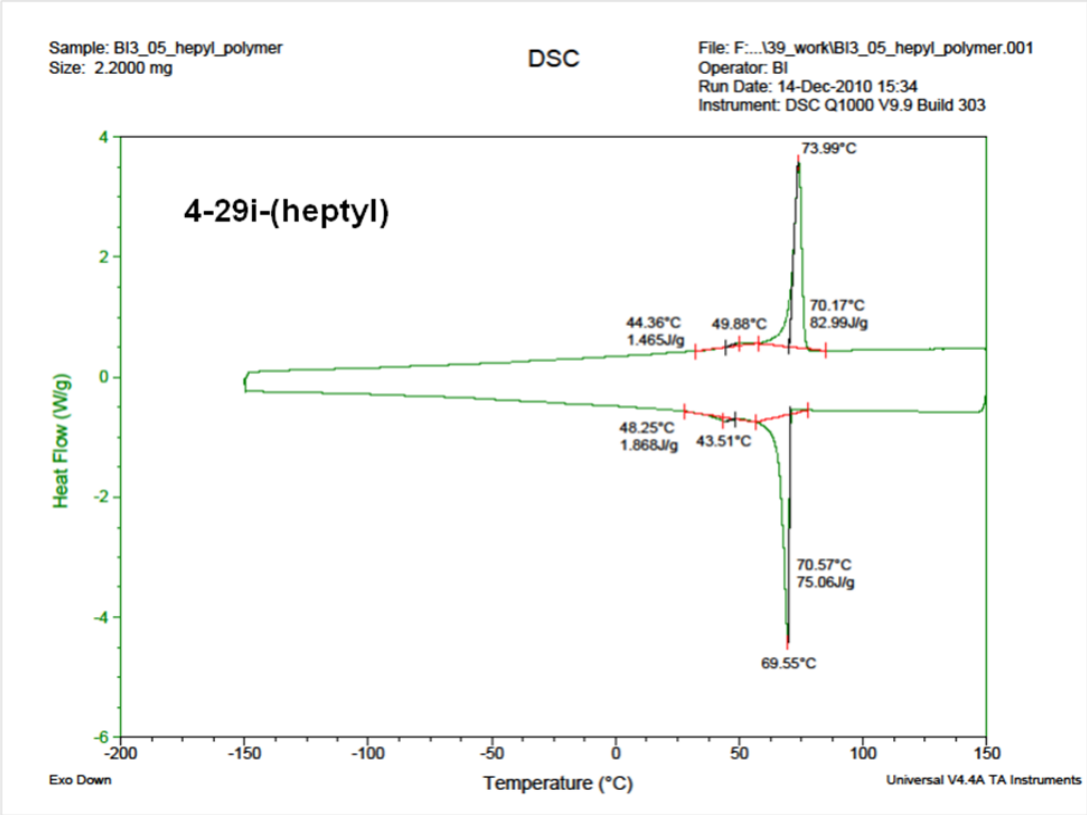
Sample: BI3_05_hepyl_polymer
Size: 2.2000 mg
DSC
File: F:...\39_work\BI3_05_hepyl_polymer.001
Operator: BI
Run Date: 14-Dec-2010 15:34
Instrument: DSC Q1000 V9.9 Build 303
4-29i-(heptyl)
73.99°C
70.17°C
82.99J/g
44.36°C
1.465J/g
49.88°C
48.25°C
1.868J/g
43.51°C
70.57°C
75.06J/g
69.55°C
Heat Flow (W/g)
Exo Down
Temperature (°C)
Universal V4.4A TA Instruments

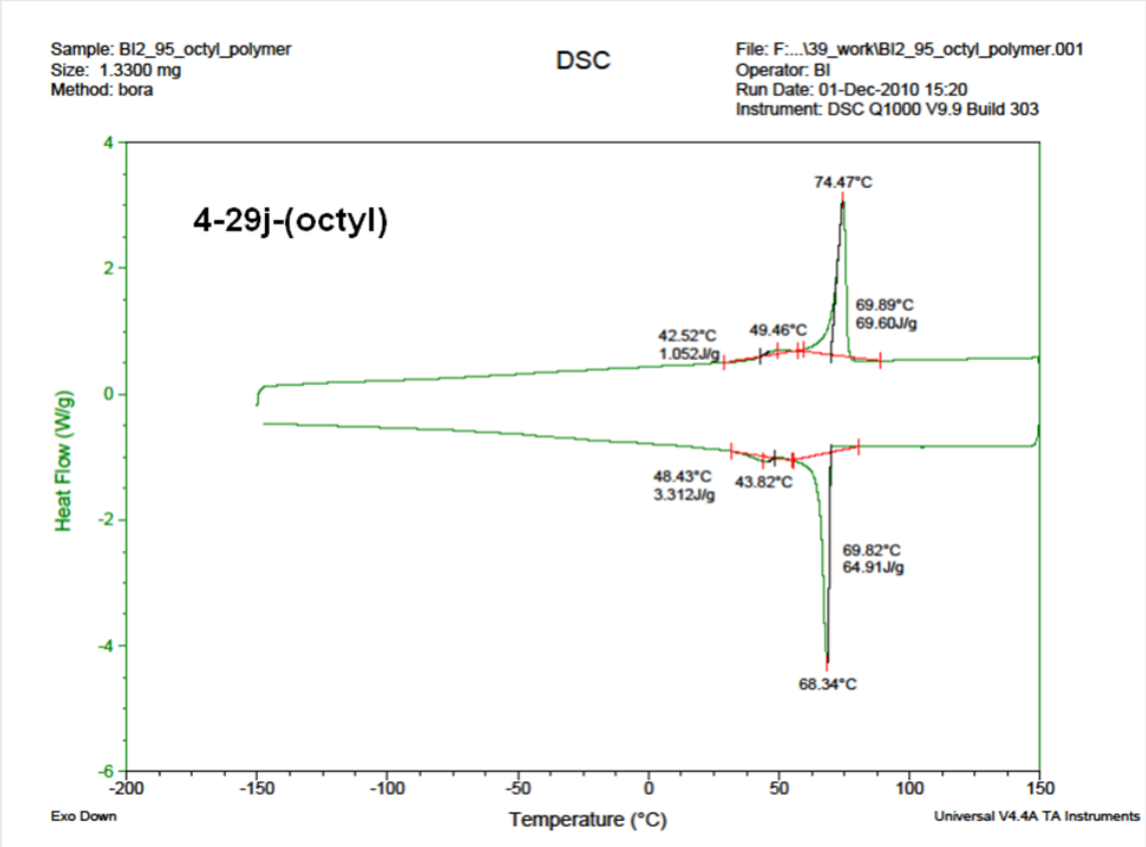
Sample: BI2_95_octyl_polymer
Size: 1.3300 mg
Method: bora
DSC
File: F:...\39_work\BI2_95_octyl_polymer.001
Operator: BI
Run Date: 01-Dec-2010 15:20
Instrument: DSC Q1000 V9.9 Build 303
4-29j-(octyl)
74.47°C
69.89°C
69.60J/g
42.52°C
1.052J/g
49.46°C
48.43°C
3.312J/g
43.82°C
69.82°C
64.91J/g
68.34°C
Heat Flow (W/g)
Exo Down
Temperature (°C)
Universal V4.4A TA Instruments

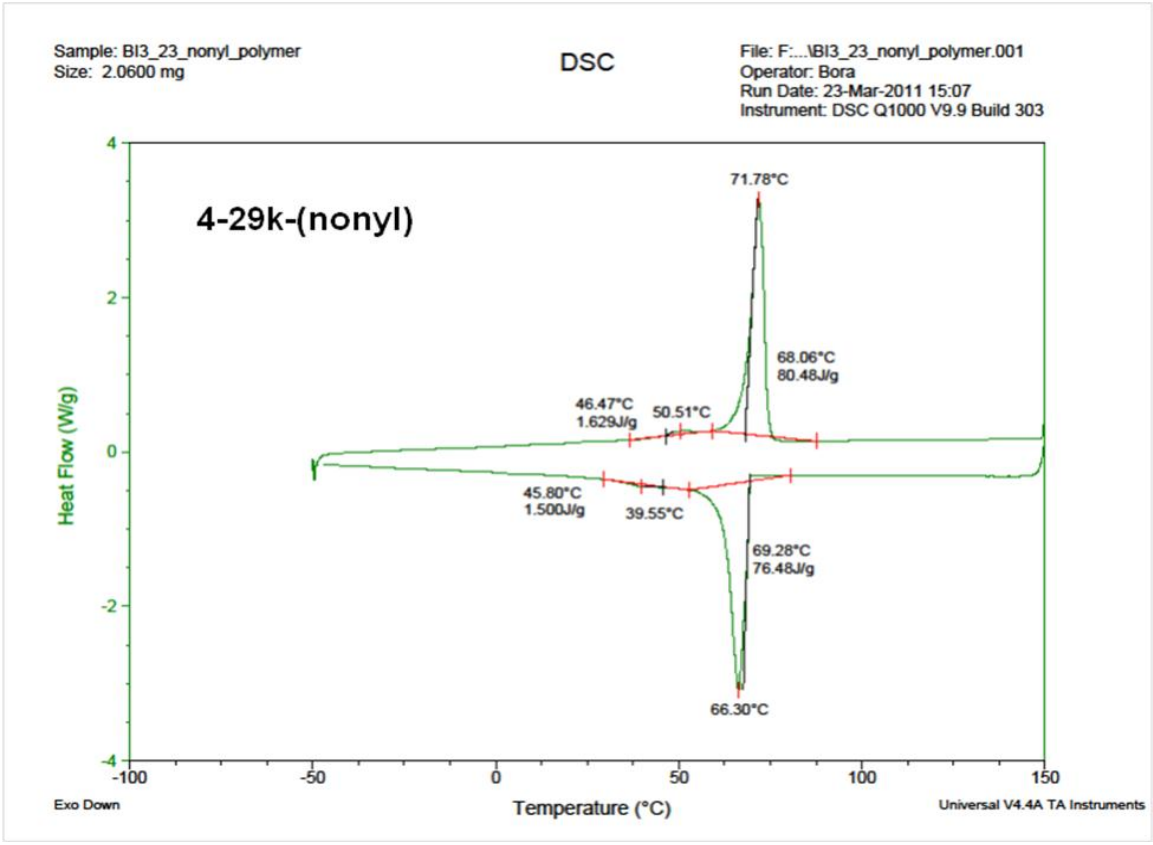
Sample: BI3_23_nonyl_polymer
Size: 2.0600 mg
DSC
File: F:...\BI3_23_nonyl_polymer.001
Operator: Bora
Run Date: 23-Mar-2011 15:07
Instrument: DSC Q1000 V9.9 Build 303
4-29k-(nonyl)
71.78°C
68.06°C
80.48J/g
46.47°C
1.629J/g
50.51°C
45.80°C
1.500J/g
39.55°C
69.28°C
76.48J/g
66.30°C
Heat Flow (W/g)
Exo Down
Temperature (°C)
Universal V4.4A TA Instruments

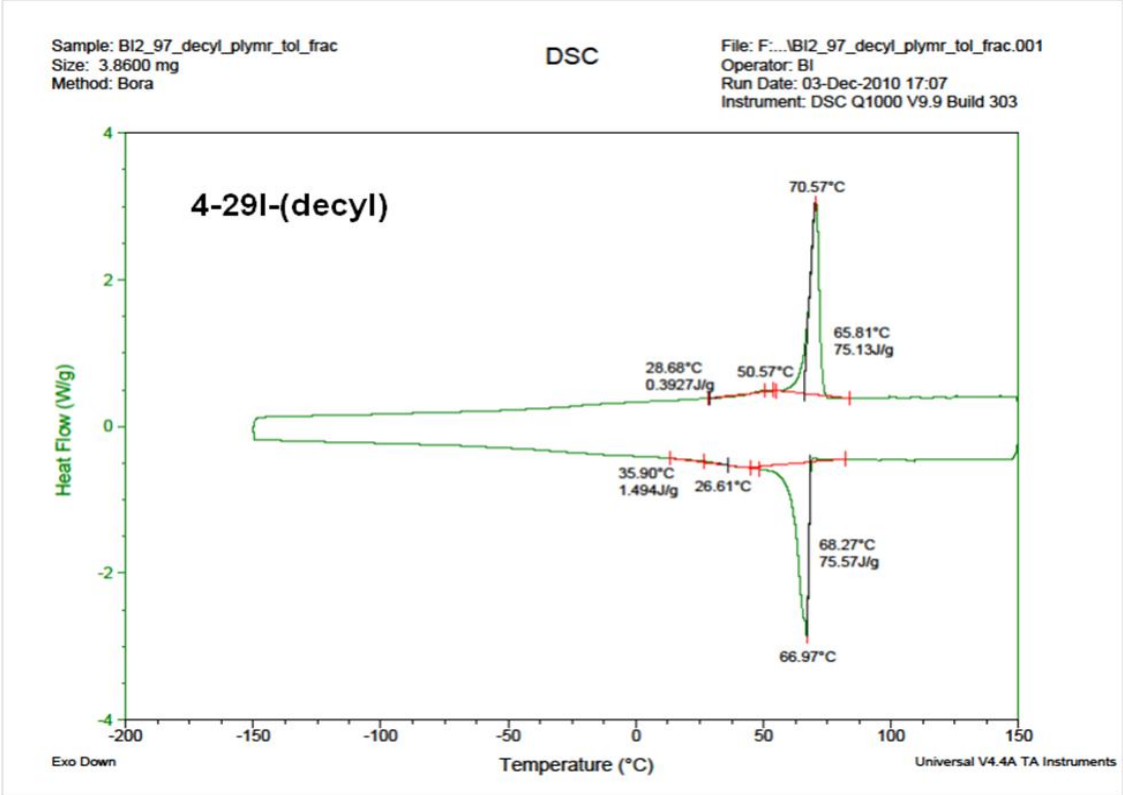
Sample: BI2_97_decyl_plymr_tol_frac
Size: 3.8600 mg
Method: Bora
DSC
File: F:...\BI2_97_decyl_plymr_tol_frac.001
Operator: BI
Run Date: 03-Dec-2010 17:07
Instrument: DSC Q1000 V9.9 Build 303
4-29l-(decyl)
70.57°C
65.81°C
75.13J/g
28.68°C
0.3927J/g
50.57°C
35.90°C
1.494J/g
26.61°C
68.27°C
75.57J/g
66.97°C
Heat Flow (W/g)
Exo Down
Temperature (°C)
Universal V4.4A TA Instruments

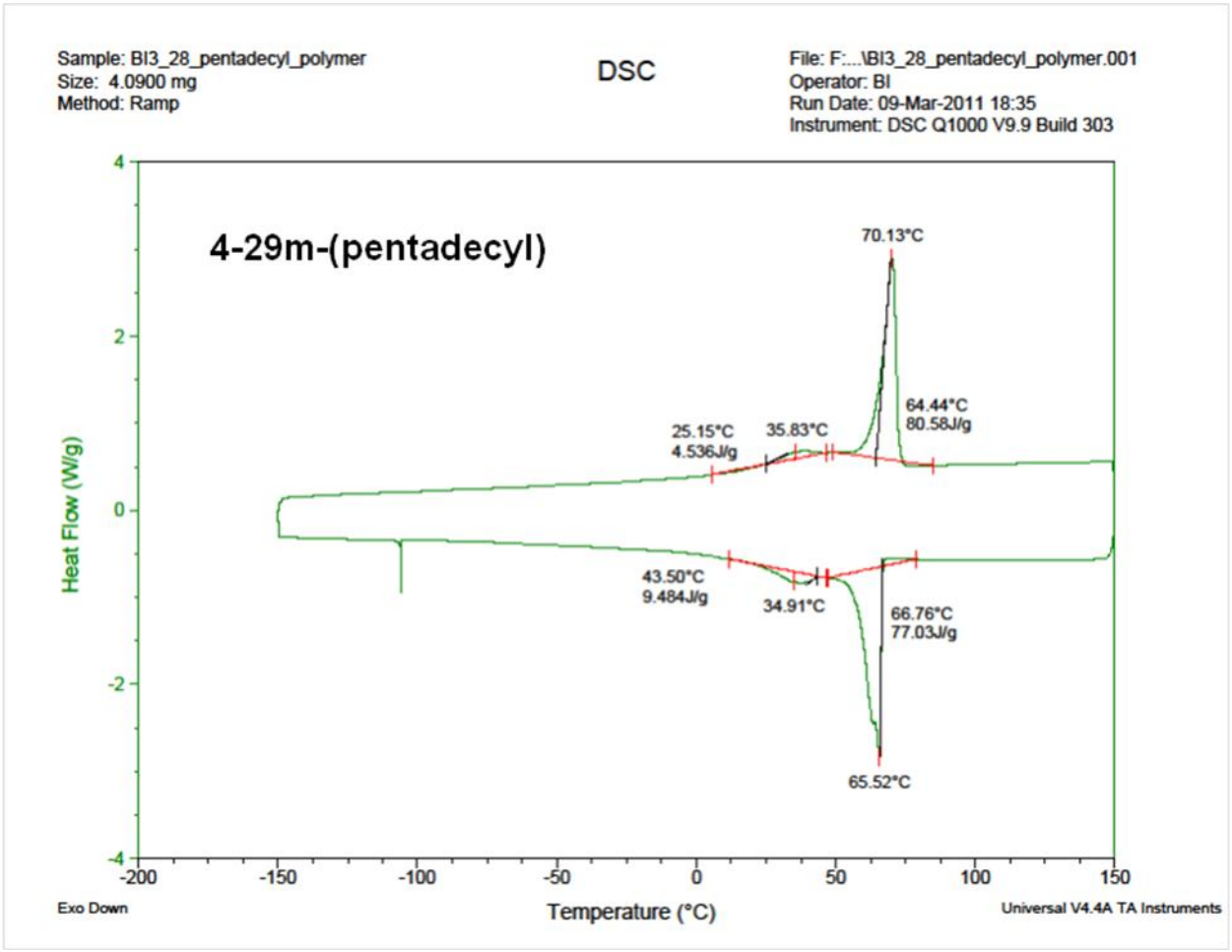
Sample: BI3_28_pentadecyl_polymer
Size: 4.0900 mg
Method: Ramp
DSC
File: F:...\BI3_28_pentadecyl_polymer.001
Operator: BI
Run Date: 09-Mar-2011 18:35
Instrument: DSC Q1000 V9.9 Build 303
4-29m-(pentadecyl)
70.13°C
64.44°C
80.58J/g
25.15°C
4.536J/g
35.83°C
43.50°C
9.484J/g
34.91°C
66.76°C
77.03J/g
65.52°C
Heat Flow (W/g)
Exo Down
Temperature (°C)
Universal V4.4A TA Instruments

LIST OF REFERENCES

(1) Semour, R.; Cheng, T. *History of Polyolefins*; Reidel Publishing Company: Dordrecht, Holland, 1986.

(2) Peacock, A. *Handbook of polyethylene: Structures, properties and applications*; Marcel Dekker: New York USA, 2000.

(3) Bamberger, E.; Tschirner, F. *Berichte Der Deutschen Chemischen Gesellschaft* **1900**, *33*, 955.

(4) Friedrich, M.; Marvel, C. *Journal of the American Chemical Society* **1930**, *52*, 376.

(5) Carothers, W.; Hill, J.; Kirby, J.; Jacobson, R. *Journal of the American Chemical Society* **1930**, *52*, 5279.

(6) Fawcett, E.; Gibson, R.; Perrin, M.; Patton, J.; Williams, E.; Patent, B., Ed.; International Chemical Industries: Great Britain, 1937.

(7) Ziegler, K.; Thielmann, F. *Berichte Der Deutschen Chemischen Gesellschaft* **1923**, *56*, 1740.

(8) Ziegler, K.; Bahr, K. *Berichte Der Deutschen Chemischen Gesellschaft* **1928**, *61*, 253.

(9) Ziegler, K.; Crossmann, F.; Kleiner, H.; Schafer, O. *Justus Liebigs Annalen Der Chemie* **1929**, *473*, 1.

(10) Ziegler, K.; Kleiner, H. *Justus Liebigs Annalen Der Chemie* **1929**, *473*, 57.

(11) Ziegler, K.; Gellert, H. *Annalen Der Chemie-Justus Liebig* **1950**, *567*, 179.

(12) Ziegler, K.; Gellert, H.; Martin, H.; Nagel, K.; Schneider, J. *Annalen Der Chemie-Justus Liebig* **1954**, *589*, 91.

(13) Ziegler, K.; Gellert, H.; Zosel, K.; Lehmkuhl, W.; Pfohl, W. *Angewandte Chemie-International Edition* **1955**, *67*, 424.

(14) Ziegler, K.; Holzkamp, E.; Breil, H.; Martin, H. *Angewandte Chemie-International Edition* **1955**, *67*, 426.

(15) Ziegler, K. *Angewandte Chemie-International Edition* **1959**, *71*, 623.

(16) Ziegler, K.; Holzkamp, E.; Breil, H.; Martin, H. *Angewandte Chemie-International Edition* **1955**, *67*, 541.

(17) Allegra, G. *Makromolekulare Chemie* **1971**, *145*, 235.

(18) Arlman, E.; Cossee, P. *Journal of Catalysis* **1964**, *3*, 99.

(19) Venditto, V.; Guerra, G.; Corradini, P.; Fusco, R. *Polymer* **1990**, *31*, 530.

(20) Patat, F.; Sinn, H. *Naturwissenschaften* **1958**, *45*, 312.

(21) Sinn, H.; Patat, F. *Angewandte Chemie-International Edition* **1964**, *3*, 93.

(22) Rodrigue, L.A.; Vanlooy, H.; Gabant, J. *Journal of Polymer Science Part a-1-Polymer Chemistry* **1966**, *4*, 1917.

(23) Rodrigue, L.A.; Vanlooy, H.; Gabant, J. *Journal of Polymer Science Part a-1-Polymer Chemistry* **1966**, *4*, 1905.

(24) Vanlooy, H.; Rodrigue, L.A.; Gabant, J. *Journal of Polymer Science Part a-1-Polymer Chemistry* **1966**, *4*, 1927.

(25) Tait, P. *Chemtech* **1975**, *5*, 688.

(26) Ziegler, K. German Patent, 878 560, 1953.

(27) Ziegler, K.; Holzkamp,E.; Breil, H.; Martin, H., US Patent, 3 392 162, 1954.

(28) Sinn, H.; Kamisky, W.; Vollmer, H.; Woldt, R. *Angewandte Chemie-International Edition in English* **1980**, *19*, 390.

(29) Kaminsky, W.; Miri, M.; Sinn, H.; Woldt, R. *Makromolekulare Chemie-Rapid Communications* **1983**, *4*, 417.

(30) Brintzinger, H.; Fischer, D.; Mulhaupt, R.; Rieger, B.; Waymouth, R. *Angewandte Chemie-International Edition in English* **1995**, *34*, 1143.

(31) McKnight, A.; Waymouth, R. *Chemical Reviews* **1998**, *98*, 2587.

(32) Coates, G. *Chemical Reviews* **2000**, *100*, 1223.

(33) Alt, H.; Koppl, A. *Chemical Reviews* **2000**, *100*, 1205.

(34) Alt, H.; Milius, W.; Palackal, S. *Journal of Organometallic Chemistry* **1994**, *472*, 113.

(35) Johnson, L.; Tempel, D.; Brookhart, M. *Abstracts of Papers of the American Chemical Society* **1995**, *210*, 244.

(36) Johnson, L.; Killian, C.; Brookhart, M. *Journal of the American Chemical Society* **1995**, *117*, 6414.

(37) Johnson, L.; Mecking, S.; Brookhart, M. *Journal of the American Chemical Society* **1996**, *118*, 267.

(38) Killian, C.; Tempel, D.; Johnson, L.; Brookhart, M. *Journal of the American Chemical Society* **1996**, *118*, 11664.

(39) Killian, C.; Johnson, L.; Brookhart, M. *Organometallics* **1997**, *16*, 2005.

(40) Mecking, S.; Johnson, L.; Wang, L.; Brookhart, M. *Journal of the American Chemical Society* **1998**, *120*, 888.

(41) Svejda, S.; Johnson, L.; Brookhart, M. *Journal of the American Chemical Society* **1999**, *121*, 10634.

(42) Tempel, D.; Johnson, L.; Huff, R.; White, P.; Brookhart, M. *Journal of the American Chemical Society* **2000**, *122*, 6686.

(43) Gates, D.; Svejda, S.; Onate, E.; Killian, C.; Johnson, L.; White, P.; Brookhart, M. *Macromolecules* **2000**, *33*, 2320.

(44) Ittel, S.; Johnson, L.; Brookhart, M. *Chemical Reviews* **2000**, *100*, 1169.

(45) Leatherman, M.; Svejda, S.; Johnson, L.; Brookhart, M. *Journal of the American Chemical Society* **2003**, *125*, 3068.

(46) Brookhart, M. S.; Johnson, L.; Killian, C.; Arthur, S.; Feldman, J.; McCord, E.; McLain, S.; Kreutzer, K.; Bennett, A.; Coughlin, E.; Ittel, S.; Parthasarathy, A.; Tempel, D.; DuPont, Ed. 1995, p 9623010.

(47) Emert, J.; Rossi, A.; Gindelberger, D.; Stanat, J.; Stokes, J.; Sim, J.; Exxon, Ed. 1997 p9803617.

(48) Geprags, M.; Mulhaupt, R.; Heinemann, J.; Aktiengesellschaft, B., Ed. March 19, 1998. , p 9947569

(49) Mecking, S.; Johnson, L.; Brookhart, M. *Abstracts of Papers of the American Chemical Society* **1996**, *211*, 114.

(50) Brown, K.; Kesti, M., US Patent, 9 748 739, 1996.

(51) Brown, K.; Kesti, M.; Stewart, E.; McGrath, J., US Patent, 9 748 740, 1996.

(52) Brown, K.; Stewart, E.; Swanson, P.; Christopher, S., US Patent, 9 748 777, 1996.

(53) Kitano, K.; Sugawara, M.; Matsuura, M. *Macromolecular Symposia* **2003**, *201*, 309.

(54) Till, P. *Journal of Polymer Science* **1957**, *24*, 301.

(55) Fischer, E. *Zeitschrift Fur Naturforschung Part a-Astrophysik Physik Und Physikalische Chemie* **1957**, *12*, 753.

(56) Keller, A. *Philosophical Magazine* **1957**, *2*, 1171.

(57) Keller, A.; Oconnor, A. *Nature* **1957**, *180*, 1289.

(58) Herrmann, K.; Gerngross, O.; Abitz, W. *Zeitschrift Fur Physikalische Chemie-Abteilung B-Chemie Der Elementarprozesse Aufbau Der Materie* **1930**, *10*, 371.

(59) Storks, K.; Germer, L. *Journal of Chemical Physics* **1937**, *5*, 131.

(60) Storks, K. *Journal of the American Chemical Society* **1938**, *60*, 1753.

(61) Gedde, U.; Mattozzi, A. *Long-Term Properties of Polyolefins* **2004**, *169*, 29.

(62) Bidd, I.; Whiting, M. *Journal of the Chemical Society-Chemical Communications* **1985**, 543.

(63) Lee, K.; Wegner, G. *Makromolekulare Chemie-Rapid Communications* **1985**, *6*, 203.

(64) Ungar, G.; Stejny, J.; Keller, A.; Bidd, I.; Whiting, M. *Science* **1985**, *229*, 386.

(65) Muller, A. *Proceedings of the Royal Society of London Series a-Containing Papers of a Mathematical and Physical Character* **1928**, *120*, 437.

(66) Smith, A. *Journal of Chemical Physics* **1953**, *21*, 2229.

(67) Shearer, H.; Vand, V. *Acta Crystallographica* **1956**, *9*, 379.

(68) Piesczek, W.; Strobl, G.; Malzahn, K. *Acta Crystallographica Section B-Structural Science* **1974**, *30*, 1278.

(69) Dawson, I.; Vand, V. *Proceedings of the Royal Society of London Series a-Mathematical and Physical Sciences* **1951**, *206*, 555.

(70) Dawson, I. *Proceedings of the Royal Society of London Series a-Mathematical and Physical Sciences* **1952**, *214*, 72.

(71) Flory, P.; Vrij, A. *Journal of the American Chemical Society* **1963**, *85*, 3548.

(72) Wunderlich, B.; Czornyj, G. *Macromolecules* **1977**, *10*, 906.

(73) Ando, I.; Sorita, T.; Yamanobe, T.; Komoto, T.; Sato, H.; Deguchi, K.; Imanari, M. *Makromolekulare Chemie-Rapid Communications* **1985**, *6*, 349.

(74) Ando, I.; Sorita, T.; Yamanobe, T.; Komoto, T.; Sato, H.; Deguchi, K.; IMANARI, M. *Polymer* **1985**, *26*, 1864.

(75) Yamanobe, T.; Sorita, T.; Ando, I.; Sato, H. *Makromolekulare Chemie-Macromolecular Chemistry and Physics* **1985**, *186*, 2071.

(76) Broadhurst, M. *Journal of Research of the National Bureau of Standards Section a-Physics and Chemistry* **1962**, *66*, 241.

(77) Broadhurst, M. *Journal of Chemical Physics* **1962**, *36*, 2578.

(78) Bunn, C. *Transactions of the Faraday Society* **1939**, *35*, 0482.

(79) Busing, W. *Macromolecules* **1990**, *23*, 4608.

(80) Teare, P.; Holmes, D. *Journal of Polymer Science* **1957**, *24*, 496.

(81) Seto, T.; Hara, T.; Tanaka, K. *Japanese Journal of Applied Physics* **1968**, *7*, 31.

(82) Shirayam, K; Watabe, H.; Kita, S. *Makromolekulare Chemie* **1972**, *151*, 97.

(83) Bassett, D.; Block, S.; Piermari, G. J. *Journal of Applied Physics* **1974**, *45*, 4146.

(84) Hu, W.; Srinivas, S.; Sirota, E. *Macromolecules* **2002**, *35*, 5013.

(85) Odian, G. *Principles of Polymerization*; John Wiley & Sons, Inc.: Hokoben, New Jersey, 2004.

(86) Axelson, D.; Levy, G.; Mandelkern, L. *Macromolecules* **1979**, *12*, 41.

(87) Melillo, G.; Izzo, L.; Zinna, M.; Tedesco, C.; Oliva, L. *Macromolecules* **2002**, *35*, 9256.

(88) Galland, G.; de Souza, R.; Mauler, R.; Nunes, F. *Macromolecules* **1999**, *32*, 1620.

(89) Roedel, M. *Journal of the American Chemical Society* **1953**, *75*, 6110.

(90) Billmayer, F. *Journal of the American Chemical Society* **1953**, *75*, 6118.

(91) Jacovic, M.; Pollock, D.; Porter, R. *Journal of Applied Polymer Science* **1979**, *23*, 517.

(92) White, W.; Randall, J.; Leigh, C. *Chemical Engineering Communications* **1983**, *24*, 139.

(93) Mendelson, R. *Polymer Engineering and Science* **1983**, *23*, 79.

(94) Mendelson, R.A.; Finger, F. *Journal of Applied Polymer Science* **1973**, *17*, 797.

(95) Ghijsels, A.; Ente, J. *International Polymer Processing* **1992**, *7*, 44.

(96) Fetters, L.; Lohse, D.; Milner, S.; Graessley, W. *Macromolecules* **1999**, *32*, 6847.

(97) Seppala, J.; Lofgren, B.; Lehmus, P.; Malmberg, A. *Macromolecular Symposia* **2001**, *173*, 227.

(98) Piel, C.; Starck, P.; Seppala, J.; Kaminsky, W. *Journal of Polymer Science Part a-Polymer Chemistry* **2006**, *44*, 1600.

(99) Lai, Y.; Wilson, J.; Knight, G.; Stevens, J.; Chum, P. In *US Patent*; Chemicals, D., Ed. US, 1993; Vol. 5272236.

(100) Lai, Y.; Wilson, J.; Knight, G.; Stevens, J. In *US Patent*; Dow, Ed. 1997; Vol. 5665800.

(101) Usami, T.; Gotoh, Y.; Takayama, S. *Macromolecules* **1986**, *19*, 2722.

(102) Usami, T.; Gotoh, Y.; Takayama, S.; Ohtani, H.; Tsuge, S. *Macromolecules* **1987**, *20*, 1557.

(103) Hosoda, S. *Polymer Journal* **1988**, *20*, 383.

(104) Litvinov, V.; Mathot, V. *Solid State Nuclear Magnetic Resonance* **2002**, *22*, 218.

(105) Adriaensens, P.; Karssenberg, F.; Gelan, J.; Mathot, V. *Polymer* **2003**, *44*, 3483.

(106) Wild, L.; Chang, S.; Shankernarayanan, M. *Abstracts of Papers of the American Chemical Society* **1990**, *199*, 161.

(107) Bovey, F. *Pure and Applied Chemistry* **1982**, *54*, 559.

(108) Mirabelle, F.; Ford, E. *Journal of Polymer Science Part B-Polymer Physics* **1987**, *25*, 777.

(109) Wild, L.; Blatz, C. *Abstracts of Papers of the American Chemical Society* **1992**, *204*, 84.

(110) Soares, J.; Hamielec, A. *Polymer* **1995**, *36*, 1639.

(111) Ramachandran, R.; Beaucage, G.; McFaddin, D.; Merrick-Mack, J.; Galiatsatos, V.; Mirabella, F. *Polymer* **2011**, *52*, 2661.

(112) Smith, J.; Brzezinska, K.; Valenti, D.; Wagener, K. *Macromolecules* **2000**, *33*, 3781.

(113) Wagener, K.; Valenti, D.; Hahn, S. *Macromolecules* **1997**, *30*, 6688.

(114) Sworen, J.; Smith, J.; Wagener, K.; Baugh, L.; Rucker, S. *Journal of the American Chemical Society* **2003**, *125*, 2228.

(115) Lieser, G.; Wegner, G.; Smith, J.; Wagener, K. *Colloid and Polymer Science* **2004**, *282*, 773.

(116) Sworen, J.; Smith, J.; Berg, J.; Wagener, K. *Journal of the American Chemical Society* **2004**, *126*, 11238.

(117) Baughman, T.; Sworen, J.; Wagener, K. *Macromolecules* **2006**, *39*, 5028.

(118) Sworen, J.; Wagener, K. *Macromolecules* **2007**, *40*, 4414.

(119) Rojas, G.; Berda, E.; Wagener, K. *Polymer* **2008**, *49*, 2985.

(120) Rojast, G.; Wagener, K. *Macromolecules* **2009**, *42*, 1934.

(121) Lindmarkhamberg, M.; Wagener, K. B. *Macromolecules* **1987**, *20*, 2949.

(122) Wagener, K.; Nel, J.; Konzelman, J.; Boncella, J. *Macromolecules* **1990**, *23*, 5155.

(123) Boz, E.; Wagener, K.; Ghosal, A.; Fu, R.; Alamo, R. *Macromolecules* **2006**, *39*, 4437.

(124) Boz, E.; Nemeth, A.; Alamo, R.; Wagener, K. *Advanced Synthesis & Catalysis* **2007**, *349*, 137.

(125) Boz, E.; Nemeth, A.; Ghiviriga, I.; Jeon, K.; Alamo, R.; Wagener, K. *Macromolecules* **2007**, *40*, 6545.

(126) Boz, E.; Ghiviriga, I.; Nemeth, A.; Jeon, K.; Alamo, R.; Wagener, K. *Macromolecules* **2008**, *41*, 25.

(127) Boz, E.; Nemeth, A.; Wagener, K.; Jeon, K.; Smith, R.; Nazirov, F.; Bockstaller, M.; Alamo, R. *Macromolecules* **2008**, *41*, 1647.

(128) Boz, E.; Wagener, K. *Polymer Reviews* **2007**, *47*, 511.

(129) Baughman, T.; Chan, C.; Winey, K.; Wagener, K. *Macromolecules* **2007**, *40*, 6564.

(130) Seitz, M.; Chan, C.; Opper, K.; Baughman, T.; Wagener, K.; Winey, K. *Journal of the American Chemical Society* **2010**, *132*, 8165.

(131) Opper, K.; Fassbender, B.; Brunklaus, G.; Spiess, H.; Wagener, K. *Macromolecules* **2009**, *42*, 4407.

(132) Opper, K.; Wagener, K. *Macromolecular Rapid Communications* **2009**, *30*, 915.

(133) Opper, K.; Markova, D.; Klapper, M.; Mullen, K.; Wagener, K. *Macromolecules* **2010**, *43*, 3690.

(134) Matloka, P.; Sworen, J.; Zuluaga, F.; Wagener, K. *Macromolecular Chemistry and Physics* **2005**, *206*, 218.

(135) Matloka, P.; Wagener, K. *Journal of Molecular Catalysis a-Chemical* **2006**, *257*, 89.

(136) Matloka, P.; Kean, Z.; Greenfield, M.; Wagener, K. *Journal of Polymer Science Part a-Polymer Chemistry* **2008**, *46*, 3992.

(137) Matloka, P.; Kean, Z.; Wagener, K. *Journal of Polymer Science Part a-Polymer Chemistry* **2010**, *48*, 1866.

(138) Hopkins, T.; Pawlow, J.; Koren, D.; Deters, K.; Solivan, S.; Davis, J.; Gomez, F.; Wagener, K. *Macromolecules* **2001**, *34*, 7920.

(139) Hopkins, T.; Wagener, K. *Advanced Materials* **2002**, *14*, 1703.

(140) Hopkins, T.; Wagener, K. *Macromolecules* **2003**, *36*, 2206.

(141) Hopkins, T.; Wagener, K. *Advanced Materials* **2003**, *15*, 478.

(142) Hopkins, T.; Wagener, K. *Macromolecules* **2004**, *37*, 1180.

(143) Hopkins, T.; Wagener, K. *Journal of Molecular Catalysis a-Chemical* **2004**, *213*, 93.

(144) Leonard, J.; Hopkins, T.; Chaffin, K.; Wagener, K. *Macromolecular Chemistry and Physics* **2008**, *209*, 1485.

(145) Baughman, T.; Wagener, K. *Metathesis Polymerization* **2005**, *176*, 1.

(146) Opper, K.; Wagener, K. *Journal of Polymer Science Part a-Polymer Chemistry* **2011**, *49*, 821.

(147) Mutlu, H.; de Espinosa, L.; Meier, M. *Chemical Society Reviews* **2011**, *40*, 1404.

(148) Kim, M.; Phillips, P. *Journal of Applied Polymer Science* **1998**, *70*, 1893.

(149) Zhang, M.; Lynch, D.; Wanke, S. *Polymer* **2001**, *42*, 3067.

(150) Crist, B.; Williams, D. *Journal of Macromolecular Science-Physics* **2000**, *B39*, 1.

(151) Krigas, T.; Carella, J.; Struglinski, M.; Crist, B.; Graessley, W.; SCHILLING, F. *Journal of Polymer Science Part B-Polymer Physics* **1985**, *23*, 509.

(152) Mirabella, F. *Journal of Polymer Science Part B-Polymer Physics* **2001**, *39*, 2800.

(153) Mathot, V.; Pijpers, M. *Journal of Applied Polymer Science* **1990**, *39*, 979.

(154) Mathot, V.; Scherrenberg, R.; Pijpers, M.; Bras, W. *Journal of Thermal Analysis* **1996**, *46*, 681.

(155) Goderis, B.; Peeters, M.; Mathot, V.; Koch, M.; Bras, W.; Ryan, A.; Reynaers, H. *Journal of Polymer Science Part B-Polymer Physics* **2000**, *38*, 1975.

(156) Rojas, G.; Baughman, T.; Wagener, K. *Synthetic Communications* **2007**, *37*, 3923.

(157) Rojas, G.; Wagener, K. *Journal of Organic Chemistry* **2008**, *73*, 4962.

(158) Rojas, G.; Inci, B.; Wei, Y. Y.; Wagener, K. B. *Journal of the American Chemical Society* **2009**, *131*, 17376.

(159) Ulman, M.; Grubbs, R. *Journal of Organic Chemistry* **1999**, *64*, 7202.

(160) Hong, S.; Day, M.; Grubbs, R. *Journal of the American Chemical Society* **2004**, *126*, 7414.

(161) Hong, S.; Wenzel, A.; Salguero, T.; Day, M.; Grubbs, R. *Journal of the American Chemical Society* **2007**, *129*, 7961.

(162) Courchay, F.; Sworen, J.; Ghiviriga, I.; Abboud, K.; Wagener, K. *Organometallics* **2006**, *25*, 6074.

(163) Fokou, P.; Meier, M. *Journal of the American Chemical Society* **2009**, *131*, 1664.

(164) Randall, J. *Journal of Macromolecular Science-Reviews in Macromolecular Chemistry and Physics* **1989**, *C29*, 201.

(165) Grant, D.; Paul, E. *Journal of the American Chemical Society* **1964**, *86*, 2984.

(166) Liu, W.; Ray, D.; Rinaldi, P. *Macromolecules* **1999**, *32*, 3817.

(167) Kuroda, N.; Nishikitani, Y.; Matsuura, K.; Ikegami, N. *Macromolecules* **1992**, *25*, 2820.

(168) Rossi, A.; Zhang, J.; Odian, G. *Macromolecules* **1996**, *29*, 2331.

(169) Luruli, N.; Heinz, L.; Grumel, V.; Brull, R.; Pasch, H.; Raubenheimer, H. *Polymer* **2006**, *47*, 56.

(170) Randall, J. C. *Journal of Polymer Science Part B - Polymer Physics* **1973**, *11*, 275.

(171) Striegel, A. M.; Krejsa, M. R. *Journal of Polymer Science Part B-Polymer Physics* **2000**, *38*, 3120.

(172) Baughman, T.; Sworen, J.; Wagener, K. *Tetrahedron* **2004**, *60*, 10943.

(173) Starck, P. *Polymer International* **1996**, *40*, 111.

(174) Starck, P.; Malmberg, A.; Lofgren, B. *Journal of Applied Polymer Science* **2002**, *83*, 1140.

(175) Starck, P.; Lofgren, B. *Journal of Macromolecular Science-Physics* **2002**, *B41*, 579.

(176) Starck, P.; Rajanen, K.; Lofgren, B. *Thermochimica Acta* **2003**, *395*, 169.

(177) Wilfong, D.; Knight, G. *Journal of Polymer Science Part B-Polymer Physics* **1990**, *28*, 861.

(178) Hosoda, S.; Nomura, H.; Gotoh, Y.; Kihara, H. *Polymer* **1990**, *31*, 1999.

(179) Perez, E.; Vanderhart, D.; Crist, B.; Howard, P. *Macromolecules* **1987**, *20*, 78.

(180) Vanden Eynde, S.; Mathot, V.; Koch, M.; Reynaers, H. *Polymer* **2000**, *41*, 4889.

(181) Vanden Eynde, S.; Mathot, V.; Hohne, G.; Schawe, J.; Reynaers, H. *Polymer* **2000**, *41*, 3411.

(182) Hosoda, S.; Nozue, Y.; Kawashima, Y.; Suita, K.; Seno, S.; Nagamatsu, T.; Wagener, K.; Inci, B.; Zuluaga, F.; Rojas, G.; Leonard, J. *Macromolecules* **2011**, *44*, 313.

(183) Tashiro, K.; Sasaki, S.; Kobayashi, M. *Macromolecules* **1996**, *29*, 7460.

(184) Schmidt-Rohr, K.; Spiess, H. W. *Multidimensional Solid-State NMR and Polymers*; Academic Press: London, 1994.

(185) Blumich, B. *NMR Basic Principles and Progress. Solid-State NMR III Organic Matter*; SpringlerVerlag: Berlin, 1994.

(186) Tycho, R. *Nuclear Magnetic Resonance Probes of Molecular Dynamics*; Kluwer Academic Publishers: Dordrecht, The Netherlands, 1994.

(187) Kitamaru, R.; Horii, F.; Murayama, K. *Macromolecules* **1986**, *19*, 636.

(188) Kitamaru, R.; Horii, F.; Zhu, Q.; Bassett, D.; Olley, R. *Polymer* **1994**, *35*, 1171.

(189) Nakaoki, T.; Ohira, Y.; Hayashi, H.; Horii, F. *Macromolecules* **1998**, *31*, 2705.

(190) Kuwabara, K.; Horii, F. *Macromolecules* **1999**, *32*, 5600.

(191) Kuwabara, K.; Kaji, H.; Horii, F.; Bassett, D.; Olley, R. *Macromolecules* **1997**, *30*, 7516.

(192) Keith, H. *Journal of Applied Physics* **1964**, *35*, 3115.

(193) Bassett, D.; Keller, A.; Frank, F. *Philosophical Magazine* **1963**, *8*, 1753.

(194) Kawai, T.; Keller, A. *Philosophical Magazine* **1965**, *11*, 1165.

(195) Organ, S.; Keller, A. *Journal of Materials Science* **1985**, *20*, 1571.

(196) Organ, S.; Keller, A. *Journal of Materials Science* **1985**, *20*, 1586.

(197) Organ, S.; Keller, A. *Journal of Materials Science* **1985**, *20*, 1602.

(198) Iakoubovskii, K.; Mitsuishi, K.; Nakayama, Y.; Furuya, K. *Microscopy Research and Technique* **2008**, *71*, 626.

(199) Werschkun, B.; Thiem, J. *Angewandte Chemie-International Edition* **1997**, *36*, 2793.

(200) Wang, W.; Zhang, Y.; Zhou, H.; Bleriot, Y.; Sinay, P. *European Journal of Organic Chemistry* **2001**, 1053.

(201) Sato, K.; Sakuma, S.; Nakamura, Y.; Yoshimura, J.; Hashimoto, H. *Chemistry Letters* **1991**, 17.

(202) Sato, K.; Kubo, N.; Takada, R.; Sakuma, S. *Bulletin of the Chemical Society of Japan* **1993**, *66*, 1156.

(203) Posner, G.; Whitten, C.; Sterling, J. *Journal of the American Chemical Society* **1973**, *95*, 7788.

(204) Bertz, S.; Eriksson, M.; Miao, G.; Snyder, J. *Journal of the American Chemical Society* **1996**, *118*, 10906.

(205) Johnson, C.; Dutra, G. *Journal of the American Chemical Society* **1973**, *95*, 7777.

(206) Johnson, C.; Dutra, G. *Journal of the American Chemical Society* **1973**, *95*, 7783.

(207) Dieter, R.; Silks, L.; Fishpaugh, J.; Kastner, M. *Journal of the American Chemical Society* **1985**, *107*, 4679.

(208) Burns, D.; Miller, J.; Chan, H.; Delaney, M. *Journal of the American Chemical Society* **1997**, *119*, 2125.

(209) Alamo, R.; Mandelkern, L. *Macromolecules* **1989**, *22*, 1273.

(210) Mirabella, F. *Journal of Polymer Science Part B-Polymer Physics* **2006**, *44*, 2369.

(211) Flory, P. *Transactions of the Faraday Society* **1955**, *51*, 848.

BIOGRAPHICAL SKETCH

Bora Inci was born in Aydin, Turkey in 1982. He is a son of Fikriye Inci and Sezgin Inci. After finishing Bursa Ali Osman Sonmez Science High School, he enrolled in Bilkent University chemistry department. During his last two years of undergraduate studies he worked with Professor Sefik Suzer on X-ray photoelectron spectroscopy analysis of rough surfaces. He received his B.S. in 2005 and joined to Koc University, Istanbul, Turkey for his M.S. degree in the material science and engineering program. He worked under the guidance of Professor Iskender Yılgor on the synthesis and characterization of segmented polyurethanes. Bora moved to the University of Florida and joined the Wagener group in the fall of 2007. While at Florida, he was able to expand and develop the ongoing modeling polyethylene project. Part of his graduate studies, he joined the Prof. Katharina Landfester`s Research Group at Max-Planck-Institute for Polymer Research at Mainz, Germany as a visiting scientist for the period of three months. He is recipient of 2009 Proctor & Gamble Research Excellence and 2010 Butler Polymer Research Awards. He likes playing soccer and is the captain of the chemistry soccer team “Isotopes” at University of Florida.